Climate Dynamics:
Physics and Dynamics of the Ocean

*Riccardo Farneti*
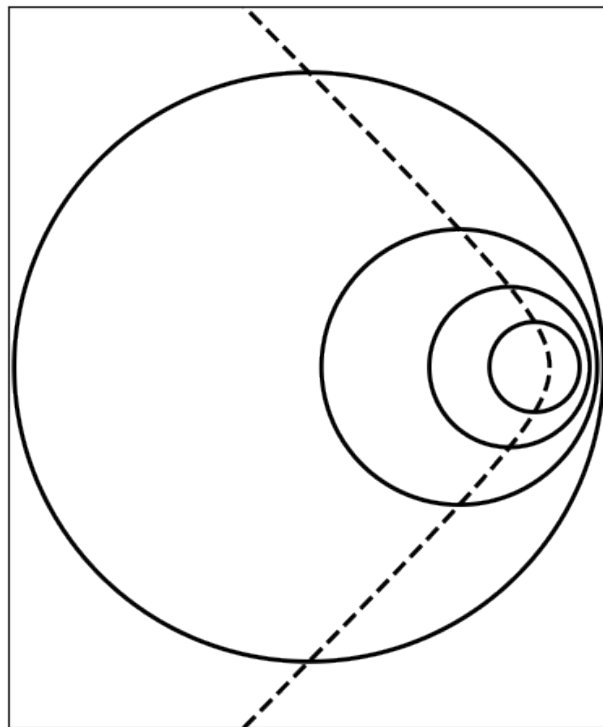
LAUREA MAGISTRALE IN FISICA
2023-2024

These notes form the basis for the first part of the *Climate Dynamics* Course at the Laurea Magistrale in Fisica, University of Trieste.

Most of the material on these notes is *borrowed* from *Vallis* (2006); *Talley et al.* (2011); *Olbers et al.* (2012); *Vallis* (2019). Students are encouraged to supplement these notes with readings of those and more textbooks.

The notes will grow in time, and comments and suggestions are highly appreciated.

This is the version from October 5, 2023.

Riccardo Farneti
(rfarneti@ictp.it)
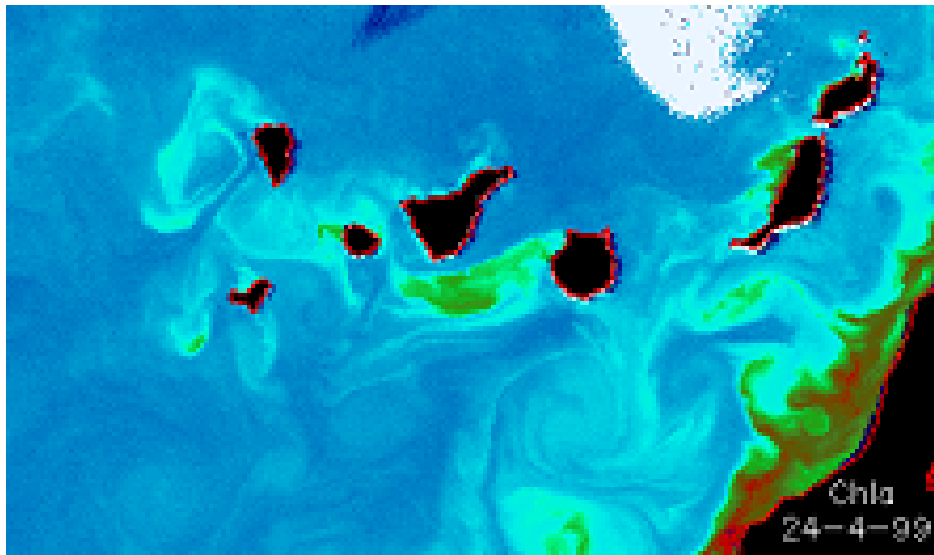
Cover photo: Satellite image from SeaWIFS showing surface Chl-a concentration on the north-west coast of Africa around the Canary Islands. Notice the downstream cyclonic and anticyclonic eddies formed by the interaction of the Canary Current with the islands and the coastal upwelling shedding filaments and eddies.

Contents

Chapter 1

Introduction

We shall discuss the basic principles and dynamics setting up the large-scale ocean circulation. We will make use of all concepts we have developed in our previous courses (Geophysical Fluid Dynamics, Physics of the Ocean) and we will probably see some topics that have been mentioned in other courses (e.g., Atmospheric dynamics). But, *repetita iuvant!*. And those same principles will be applied here to ocean dynamics, perhaps in a revised way.

The large-scale ocean circulation can be broadly divided into two different kinds, a *horizontal surface wind-driven circulation* and a *meridional deep buoyancy- and wind-driven circulation*, although the distinction is only a bad approximation as they are intimately connected. This is particularly so for the meridional overturning which is driven both by buoyancy and wind at the surface.

Ocean circulation theory is based on the very same principles that drive atmospheric circulation, and many theories have been borrowed from the meteorological and atmospheric fields. Of course, the ocean is just another geophysical fluid, and as such it is governed by all GFD conservation principles, forces and instabilities you have been exposed already. There are two main differences with respect to the atmosphere that are worth pointing out now.

- First, contrary to the atmosphere, the ocean is heated and cooled from above.

- Second, ocean circulation is often constrained by the presence of continents, and this will alter the structure and dynamics of the flow.

These two peculiarities will explain some of the differences between oceanic
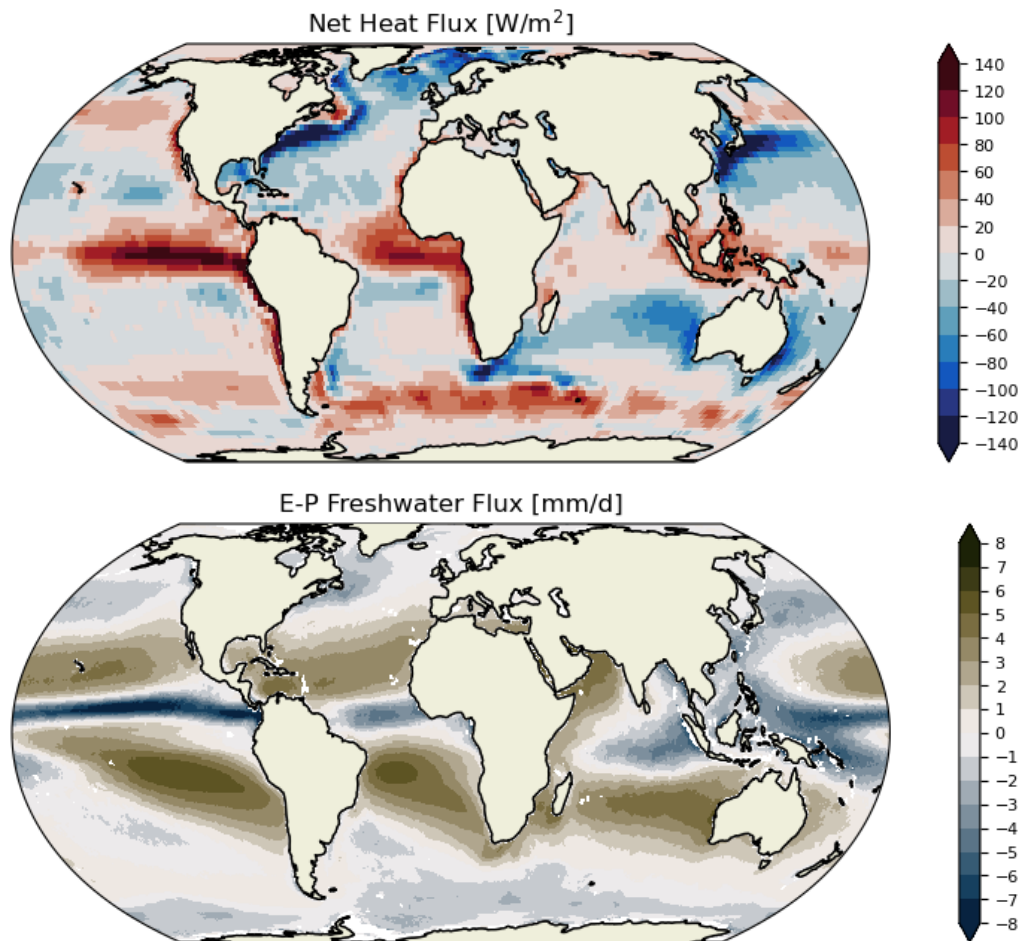
Figure 1.1: Net heat and freshwater fluxes computed from the NCEP/NCAR reanalysis for the period 2010-2019 *Kalnay et al.* (1996).

and atmospheric circulation, as well as some geographical uniqueness in ocean circulation.

The ocean is largely driven by surface wind stress (Fig. 3.6) –actually not the stress but its curl! ... see later–, and common patterns arise in the surface wind-driven large-scale circulation of all different basins (Fig. 1.3). They all have just a few common ingredients, and these will qualitatively explain the main features of the wind-driven gyres. The Southern Ocean is a rather different story, and it will be discussed separately.

However, buoyancy forcing –the sum of surface heat and freshwater fluxes– and the latitudinal extent of the ocean basins, will alter the way the surface of each basin is buoyancy forced, with profound implications for
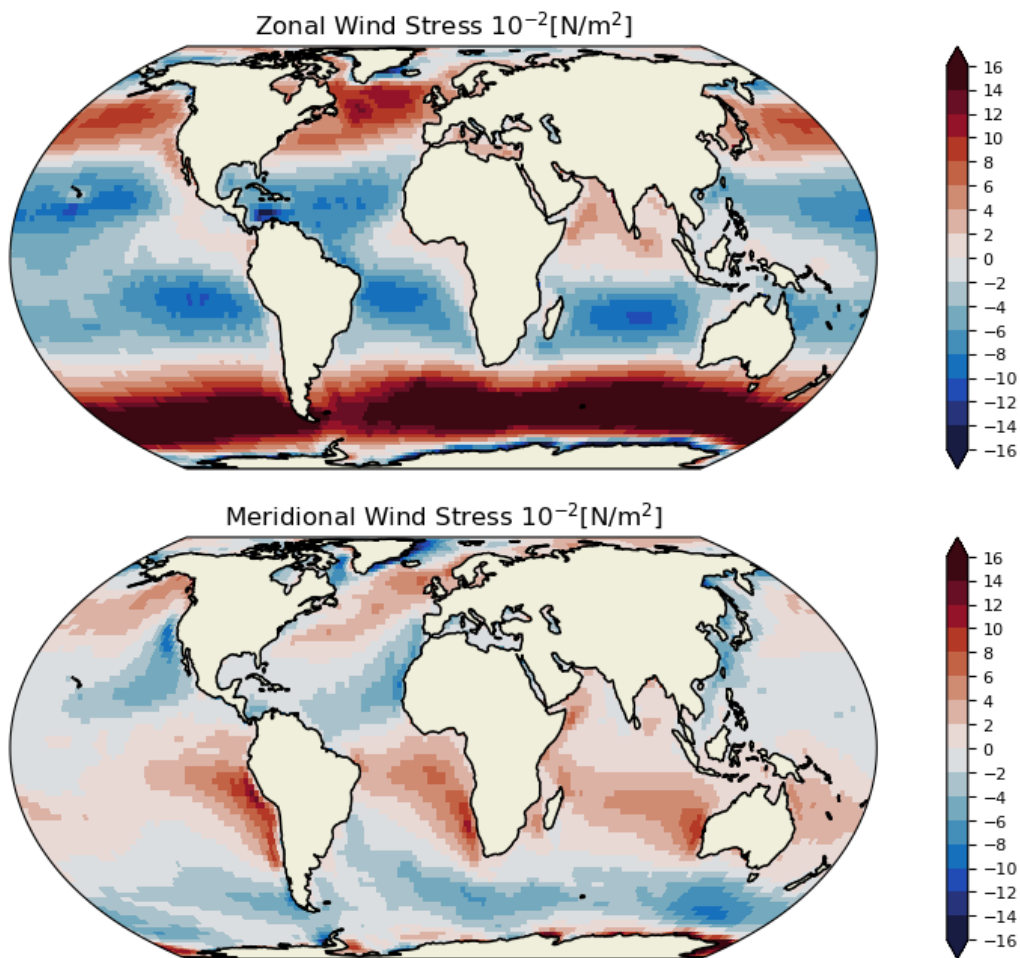
Figure 1.2: Surface zonal and meridional components of the wind stress computed from the NCEP/NCAR reanalysis for the period 2010-2019 *Kalnay et al.* (1996).

the interior temperature and salinity structure as well as deep circulations of the oceans. Once we have highlighted the major circulations and their relations, a clear picture of the interior and meridional circulation will also appear.

There is a good observational and theoretical understanding of the major processes responsible for the Meridional Overturning Circulation (MOC) (Fig. 1.4). This is not the same in each and every basin (Fig. 1.5), and fundamental differences exist giving rise to shallow and deep circulations, responsible for different degrees of meridional energy and mass transports. Our present models capture these features reasonably well
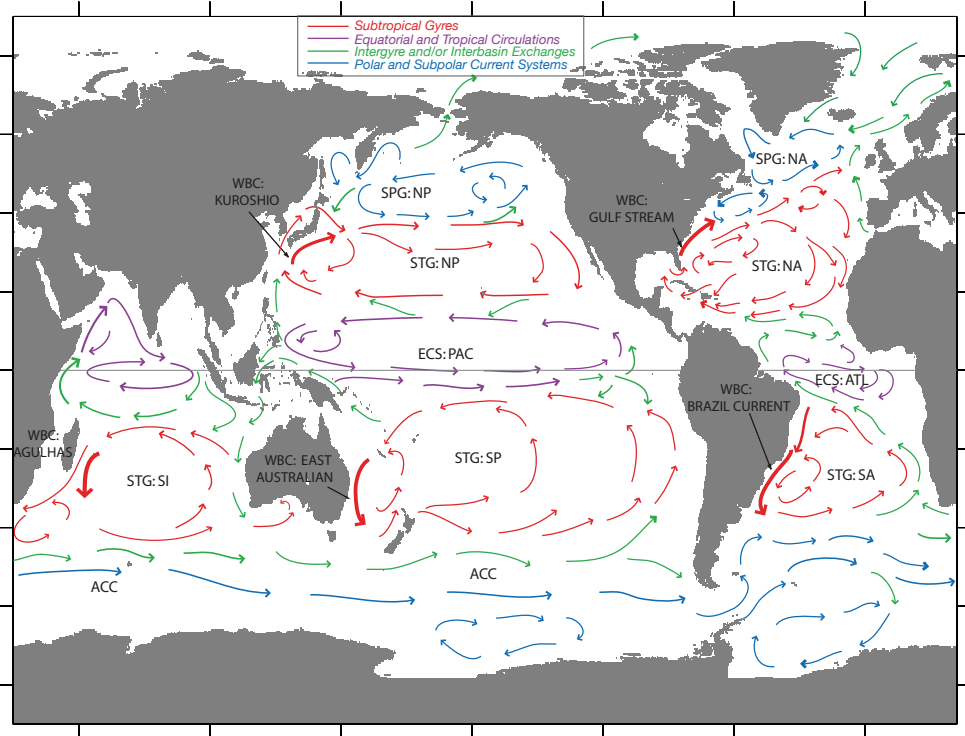
Figure 1.3: A schema of the main currents of the global ocean [from *Vallis* (2006)].

(Fig. 1.6), although many small-scale effects are missing or poorly parameterized, and most importantly the variability of this circulation is not well understood (let alone its future evolution!).
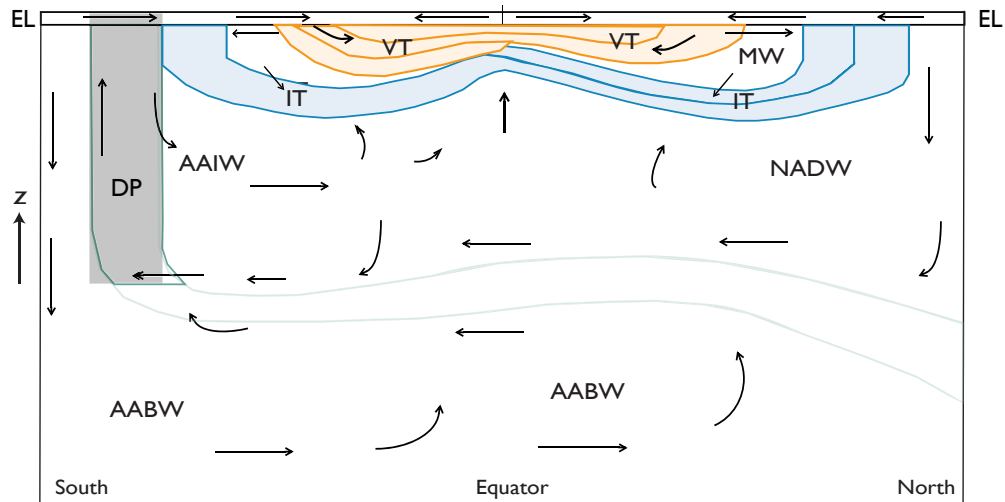
Figure 1.4: A schema of the stratification and overturning circulation. [from *Vallis* (2006)]
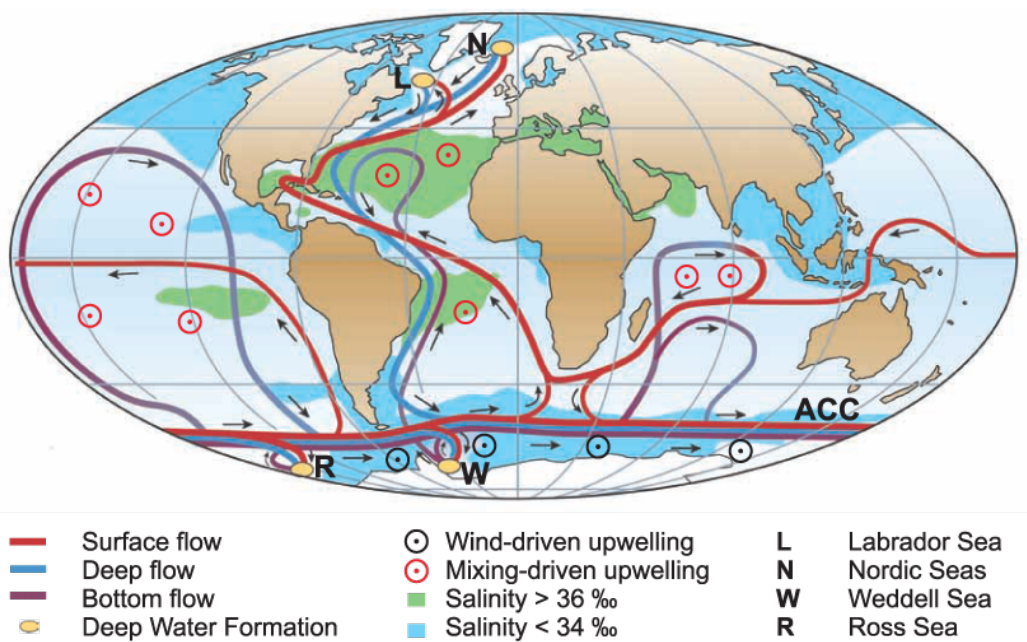
Figure 1.5: A schema of the thermohaline circulation (THC), or the Meridional Overturning Circulation (MOC). [from *Kuhlbrodt et al.* (2007)]
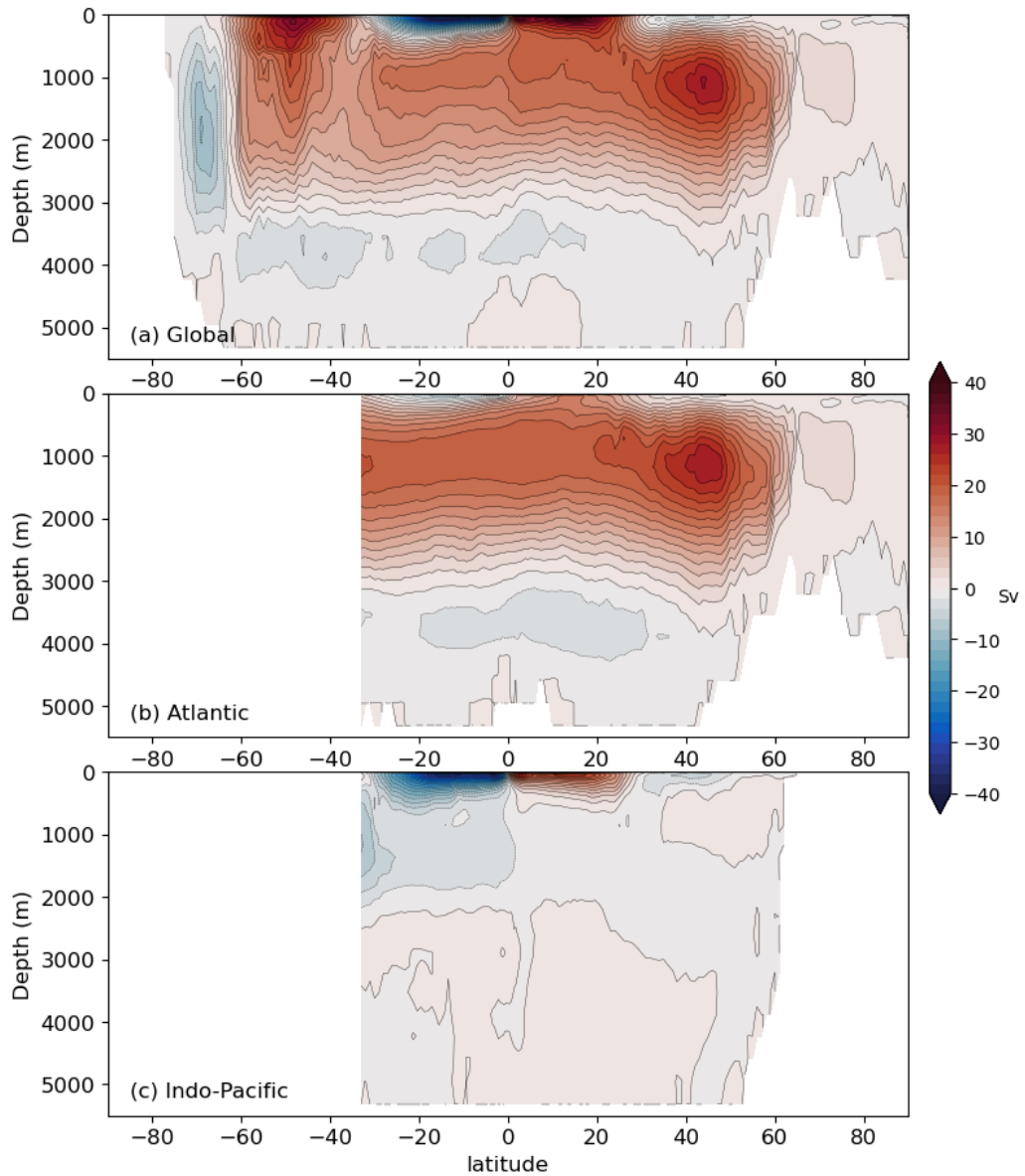
Figure 1.6: The global MOC as computed from a Coupled General Circulation Model (CGCM). We clearly see the presence of the North Atlantic Deep Water cell, the interhemispheric meridional circulation, a locally-circulating deacon Cell, and two SubTropical Cells. Each meridional cell is driven by different dynamics and all together set up the global ocean circulation.

Fundamental tools

We have already discussed the Geostrophic equations, or *geostrophic bal-*
ance, in previous courses (*Geophysical Fluid Dynamics*, and maybe in Physics
of the Atmospheric too), but it is good to restate our assumptions and start-
ing point (*repetita iuvant!*).

2.1 Kinematics

- In the LAGRANGIAN description of motion, one essentially follows
  the history of an individual particle. A flow variable $F(r_0, t)$ and its
  velocity is given by $u_i = \mathrm{d}(r_i)/\mathrm{d}t$

- In the EULERIAN description one focuses on what happens at a spa-
  tial point r, so the flow variable is $F(r, t)$.

- In the Eulerian case, $\mathrm{d}/\mathrm{d}t$ gives the local rate of change of F at each
  point r and is not the total rate of change seen by a fluid particle ...
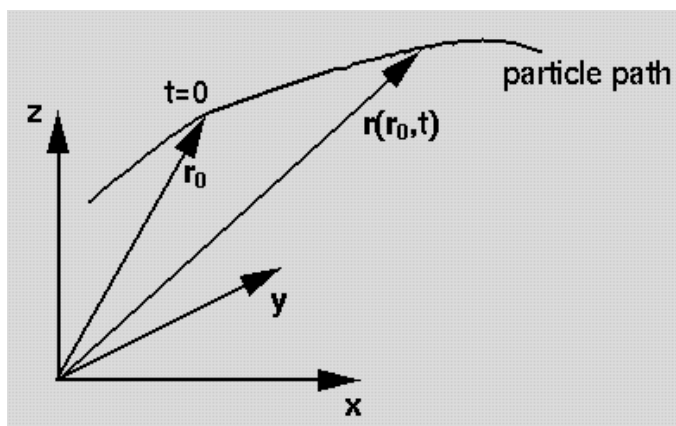
2.1.1 Lagrangian Derivative

We seek to calculate the rate of change of F at each point following a particle of fixed identity.

$$\boxed{\frac{DF}{Dt} = \frac{\partial F}{\partial t} + u_i \frac{\partial F}{\partial x_i}} \tag{2.1}$$

The Lagrangian Derivative $\frac{DF}{Dt}$ is made of (1) the local rate of change at a given point (zero for steady flows...) and (2) the advective derivative.

$\frac{\partial F}{\partial t}$ is the local rate of change of F at a given point.

$u_i \frac{\partial F}{\partial x_i}$ is the advective derivative, it is the change in F as a result of advection of the particle from one location to another where F is different.

2.1.2 Streamlines and streamfunctions

The streamline

- At $t = t_0$, streamlines are curves that are tangent to direction of flow.

- For unsteady flows, streamlines change with time.

Let $ds = (dx, dy, dz)$ be an element of arc length along a streamline, and let $u = (u, v, w)$ be the local velocity vector along that streamline, then $dx/u = dy/v = dz/w$.
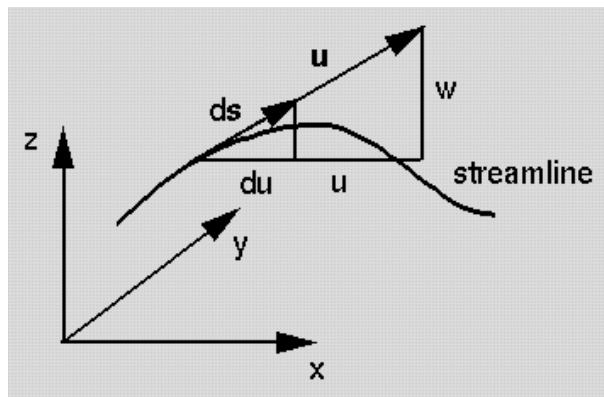
- Close to a solid boundary, streamlines are parallel to that boundary.

- The direction of the streamline is the direction of the fluid velocity.

- Fluid can not cross a streamline.

- Streamlines can not cross each other.

- Any particle starting on one streamline will stay on that same stream-line.

- In unsteady flow, streamlines can change position with time.

- **Streamlines** are a family of curves that are instantaneously tangent to the velocity vector of the flow. These show the direction a fluid element will travel in at any point in time.

- **Pathlines** are the trajectories that individual fluid particles follow. These can be thought of as a "recording" of the path a fluid element in the flow takes over a certain period. The direction the path takes will be determined by the streamlines of the fluid at each moment in time.

- For a steady flow, the two are the same.

The streamfunction

2.1.3 (Gauss') Divergence theorem

The theorem relates a volume integral to a surface integral. Consider a volume V bounded by a closed surface A. Consider an infinitesimal surface element dA whose outward unit normal is **n**. The vector ndA has magnitude dA and direction **n**.
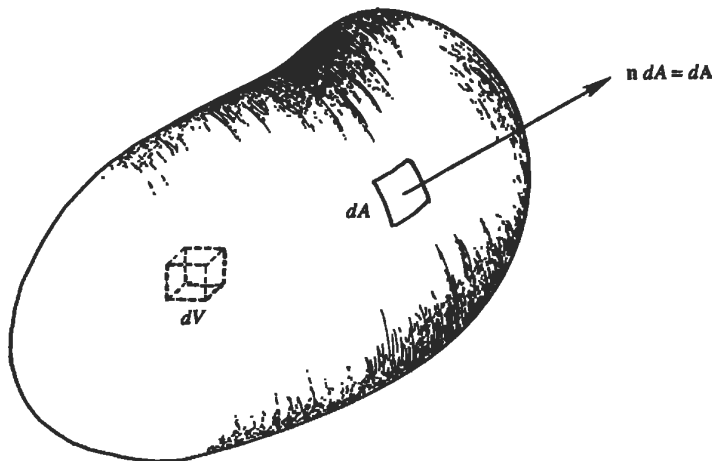
Gauss' theorem states that the volume integral of the divergence of **Q** is equal to the surface integral of the outflow of **Q**.

$$\int_v \frac{\partial Q}{\partial x_i} dV = \int_A dA_i Q \qquad (2.2)$$

For a vector Q:

$$\boxed{\int_v \frac{\partial Q_i}{\partial x_i} dV = \int_A dA_i Q},$$ (2.3)

which is now called the Divergence Theorem. In vector notation

$$\int_v \nabla \cdot \mathbf{Q} \, dV = \int_A d\mathbf{A} \cdot \mathbf{Q}$$ (2.4)

2.1.4 Stokes' theorem

The theorem relates a surface over an open surface to a line integral. Consider an open surface A, with bounding curve C. Let $d\mathbf{r}$ be an element of the bounding curve whose direction is that of the tangent.
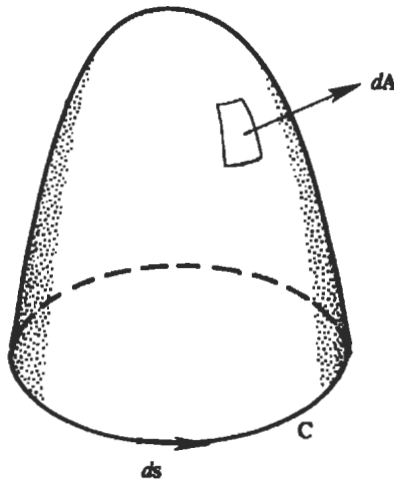
Stokes' theorem states that

$$\boxed{\int_A (\nabla \times \mathbf{F}) \cdot d\mathbf{A} = \int_C \mathbf{F} \cdot d\mathbf{r}}$$ (2.5)

the surface integral of the curl of a vector field $\mathbf{F}$ is equal to the line integral of $\mathbf{F}$ along the bounding curve. The line integral of a vector around a closed curve C is the *circulation of the field about C*.

Prove that $div(curl\,\boldsymbol{u}) = 0$, for any vector $\boldsymbol{u}$.

2.2 The equations of motion

There can be two kind of forces acting on fluids. Body forces, and we will restrict our attention, for now, to gravitational force per unit mass

$$\mathbf{g} = -\nabla(gz) = -\hat{k}\frac{\partial(gz)}{\partial z} = -\hat{k}g \tag{2.6}$$

and surface forces, which can be normal or tangential to the fluid. Normal forces will be relate to pressure, whereas tangential forces will be related to shear stresses.

In order to derive a principle of conservation of momentum we will start by applying Newton's law of motion to an infinitesimal element of fluid. The continuity equation, for an element of fluid of constant density is

$$\frac{\partial \rho}{\partial t} + \nabla \cdot (\rho \mathbf{u}) = 0 \tag{2.7}$$

and we multiply this by $\mathbf{u}$:

$$\frac{\partial(\rho u)}{\partial t} + \frac{\partial(\rho u^2)}{\partial x} + \frac{\partial(\rho uv)}{\partial y} + \frac{\partial(\rho uw)}{\partial z} = f_x \tag{2.8}$$

$$\frac{\partial(\rho v)}{\partial t} + \frac{\partial(\rho vu)}{\partial x} + \frac{\partial(\rho v^2)}{\partial y} + \frac{\partial(\rho vw)}{\partial z} = f_y \tag{2.9}$$

$$\frac{\partial(\rho w)}{\partial t} + \frac{\partial(\rho wu)}{\partial x} + \frac{\partial(\rho wv)}{\partial y} + \frac{\partial(\rho w^2)}{\partial z} = f_z \tag{2.10}$$

$$\tag{2.11}$$

which for a constant density reduces to

$$\rho \left(\frac{\partial}{\partial t} + \mathbf{u} \cdot \nabla \right) \mathbf{u} = \mathbf{f} \tag{2.12}$$

If we express our body force per unit volume $\rho\mathbf{g}$, we arrive to the Cauchy equation of motion

$$\rho \frac{\mathrm{D} u_i}{\mathrm{D} t} = \rho g_i + \frac{\partial \tau_{ij}}{\partial x_j} \tag{2.13}$$

where the stress tensor τ_{ij} includes all surface forces. Using the constitutive equation for a Newtonian fluid, we now arrive to the Navier-Stokes equation

$$\rho \frac{\mathrm{D} u_i}{\mathrm{D} t} = \rho \mathbf{g} - \nabla p + \mu \nabla^2 \mathbf{u} \tag{2.14}$$

which reduces to the Euler equation under the assumption of frictionless flow

$$\rho \frac{\mathrm{D}\, u_i}{\mathrm{D}\, t} = \rho \mathbf{g} - \nabla p \tag{2.15}$$

2.2.1 Motion in a rotating frame of reference

Eq.2.28 is valid for an inertial or fixed frame of reference. But in GFD we measure positions and velocities relative to a frame of reference fixed on the surface of the Earth, which rotates w.r.t. to a frame inertial.

Let's have a frame of reference (x_1, x_2, x_3) rotating at a uniform angular velocity $\mathbf{\Omega}$ w.r.t. a fixed frame (X_1, X_2, X_3). Any vector $\mathbf{P}$ is represented by

$$\mathbf{P} = P_1 i_1 + P_2 i_2 + P_3 i_3 \tag{2.16}$$

For a fixed observer, the directions of the rotating unit vectors (i_1, i_2, i_3) change with time. The time derivatives of $\mathbf{P}$ is thus

$$\left(\frac{d\mathbf{P}}{dt} \right)_F = \frac{d}{dt}(P_1 i_1 + P_2 i_2 + P_3 i_3) =$$
$$i_1 \frac{dP1}{dt} + i_2 \frac{dP2}{dt} + i_3 \frac{dP3}{dt} + P_1 \frac{di_1}{dt} + P_2 \frac{di_2}{dt} + P_3 \frac{di_3}{dt} \tag{2.17}$$
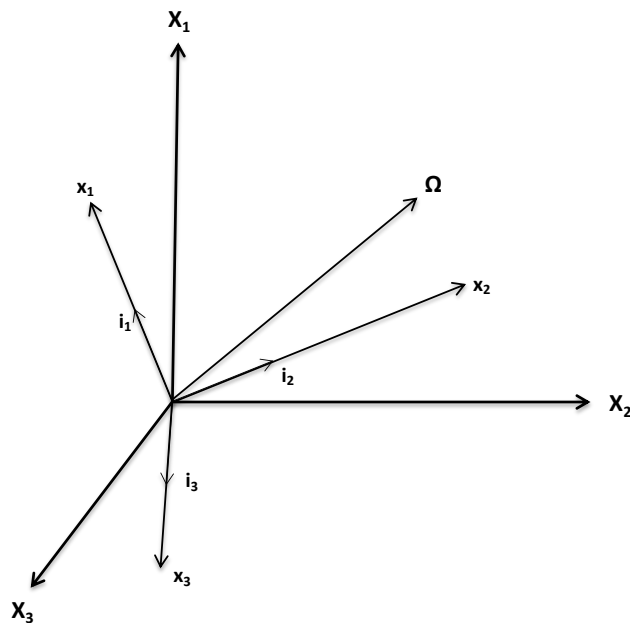
Figure 2.1: *Coordinate frame (x_1, x_2, x_3) rotating at angular velocity Ω with respect to a fixed frame (X_1, X_2, X_3).*

For an observer rotating with (x_1, x_2, x_3) the rate of change of $\mathbf{P}$ is equal to the first three terms in Eq.2.17, and so

$$\left(\frac{d\mathbf{P}}{dt}\right)_F = \left(\frac{d\mathbf{P}}{dt}\right)_R + P_1\frac{di_1}{dt} + P_2\frac{di_2}{dt} + P_3\frac{di_3}{dt} \tag{2.18}$$

Each unit vector i traces a cone with radius $\sin\alpha$, where α is a constant angle. i changes in time dt as $di = \sin\alpha d\theta$ which is the length travelled by the top of i. The rate fo change is thus

$$\frac{di}{dt} = \sin\alpha\left(\frac{d\theta}{dt}\right) = \sin\alpha\Omega \tag{2.19}$$

The direction of the rate of change is thus perpendicular to the plane $(\Omega, \mathbf{i})$, hence

$$\frac{d\mathbf{i}}{dt} = \Omega \times \mathbf{i} \tag{2.20}$$

for any rotating vector $\mathbf{i}$, giving us

$$\left(\frac{d\mathbf{P}}{dt}\right)_F = \left(\frac{d\mathbf{P}}{dt}\right)_R + \mathbf{P} \times \Omega \tag{2.21}$$

Applying this rule to the position vector $\mathbf{r}$

$$\left(\frac{d\mathbf{r}}{dt}\right)_F = \left(\frac{d\mathbf{r}}{dt}\right)_R + \mathbf{r} \times \Omega \tag{2.22}$$

or

$$\mathbf{u}_F = \mathbf{u}_R + \mathbf{r} \times \Omega \tag{2.23}$$

Applying this rule to the velocities

$$\left(\frac{d\mathbf{u_F}}{dt}\right)_F = \left(\frac{d\mathbf{u_F}}{dt}\right)_R + \mathbf{u_F} \times \Omega \tag{2.24}$$

$$\left(\frac{d\mathbf{u_F}}{dt}\right)_F = \frac{d}{dt}(\mathbf{u}_R + \mathbf{r} \times \Omega)_R + \Omega \times (\mathbf{u}_R + \mathbf{r} \times \Omega) \tag{2.25}$$

Hence, accelerations in the two frames are relates as

$$\mathbf{a}_F = \mathbf{a}_R + 2\Omega \times \mathbf{u}_R - \Omega^2\mathbf{r} \tag{2.26}$$

The second term of the r.h.s is the Coriolis acceleration and the last term the centripetal acceleration. This last term is added to the Newtonian gravity as an effective gravity

$$\mathbf{g} = \mathbf{g_n} + \Omega^2\mathbf{r} \tag{2.27}$$

The apparent force $\Omega^2 \mathbf{r}$ will be zero at the poles.

The momentum equations are now

$$\frac{D\mathbf{u}}{Dt} = \mathbf{g} - \frac{1}{\rho}\nabla p + \nu\nabla^2\mathbf{u} - (2\mathbf{\Omega} \times \mathbf{u}) \qquad (2.28)$$

It is clear that the Coriolis force $(-2\mathbf{\Omega} \times \mathbf{u})$ will deflect a particle to the right of its direction in the northern hemisphere (right-hand rule). As the Coriolis force constantly acts normal to the fluid path, it will not accelerate the particle (in fact, Coriolis does not play any role in the conservation of mechanical energy ...).

2.2.2 Thin shell approximation

A scale analysis of the continuity equation reveals that, for typical length scales much larger than typical vertical scales, $L \gg H$, horizontal velocities must be much larger than the vertical ones, $U \gg W$.

Now, decomposing the angular velocity vector into its three components (Fig.2.2), we have

$$\begin{aligned}
\Omega_x &= 0 \\
\Omega_y &= \Omega\cos\theta \\
\Omega_z &= \Omega\sin\theta
\end{aligned}$$

The Coriolis term, assuming $U \gg W$, has the following components

$$2\mathbf{\Omega} \times \mathbf{u} = 2\Omega\left[(-v\sin\theta)\hat{i} + (u\sin\theta)\hat{j} - (u\cos\theta)\hat{k}\right] \qquad (2.29)$$

and defining the Coriolis parameter as $f = 2\Omega\sin\theta$, which is now clearly twice the angular velocity and hence a (planetary) vorticity

$$2\mathbf{\Omega} \times \mathbf{u} = (-fv)\hat{i} + (fu)\hat{j} - (2\Omega u\cos\theta)\hat{k} \qquad (2.30)$$

But the vertical component of the Coriolis force, $2\Omega u\cos\theta$, is negligible compared to the dominant terms in the vertical equation of motion, namely the pressure gradient and the gravitational acceleration. Our final set of momentum equations reduces to

$$\frac{Du}{Dt} - fv = -\frac{1}{\rho}\frac{\partial p}{\partial x} + \nu\nabla^2 u \qquad (2.31)$$

$$\frac{Dv}{Dt} + fu = -\frac{1}{\rho}\frac{\partial p}{\partial y} + \nu\nabla^2 v \qquad (2.32)$$

$$\frac{Dw}{Dt} = -\frac{1}{\rho}\frac{\partial p}{\partial z} - g + \nu\nabla^2 w \qquad (2.33)$$
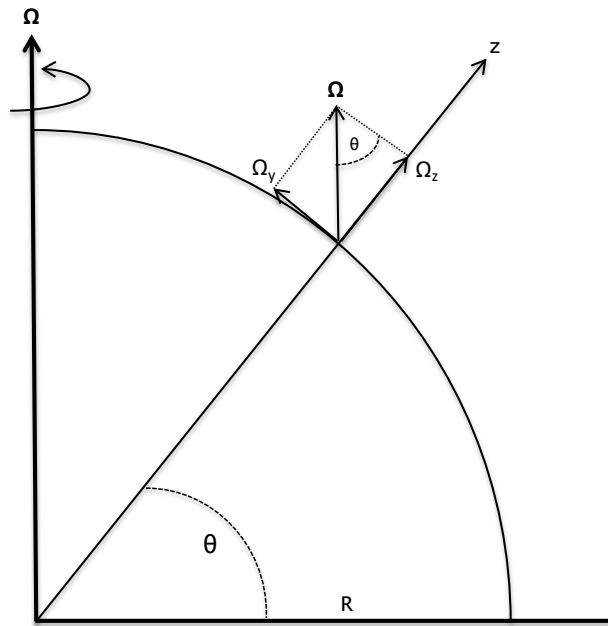
Figure 2.2: *Components of the angular velocity vector for a point on the sphere.*

Or

$$\boxed{\frac{D\mathbf{u}}{Dt} + 2\mathbf{\Omega} \times \mathbf{u} = -\frac{1}{\rho}\nabla p - \mathbf{g} + \nu\nabla^2\mathbf{u}}$$ (2.34)

where $\nu = \mu/\rho$ is the kinematic viscosity.

2.2.3 The β-plane

A first approximation is to set the Coriolis parameter, f, to a constant value. This approximation, denoted the f-plane, is useful in some very idealized studies when the westward propagation of disturbances is not of interest or it is purposely neglected. But for large-scale dynamics it is not appropriate, when flows occurring over large horizontal scales are of interest. Rossby waves depend on variations of f, it is their restoring mechanism, for example, and the large-scale dynamics of the ocean will this be affected by latitudinal variations in the Coriolis parameter. An approximation can be done, however, to make equations more tractable, and it consists of considering a cartesian plane over which f does vary, so neglecting spherical coordinates.

The β-plane approximation is useful to avoid the sphericity and staying in a cartesian plane, yet retaining the dynamical effects of sphericity itself.
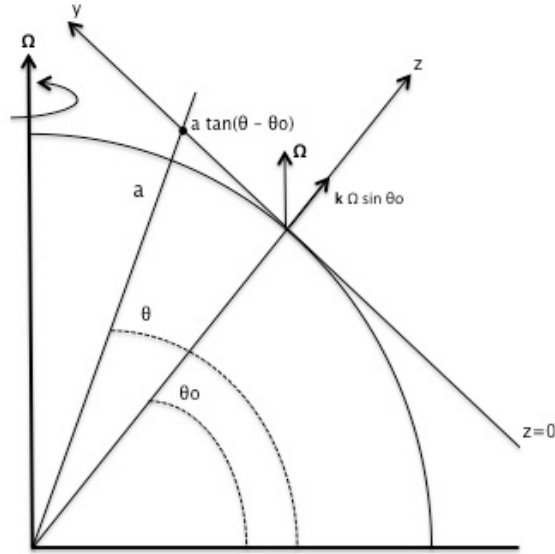
Figure 2.3: *A cartesian reference system (x,y,z) and its associated spherical system (r, θ, φ) around the point (a, θ₀, φ₀). The plane z = 0 (or β-plane) is tangent to the sphere around the point (a, θ₀, φ₀). The approximation $tan(\theta - \theta_0) \approx (\theta - \theta_0)$ is well justified for small variations in latitude. On the β-plane, the rotation vector is $k\Omega\,sin\theta$, where $sin\theta \approx sin\theta_0 + (y/a)cos\theta_0$.*

The plane $z = 0$, what will be called the β-plane is tangent to the sphere in (a, θ_0, ϕ_0). For small variations in latitude we can approximate $tan(\theta - \theta_0) \approx \theta - \theta_0$. hence, our meridional cartesian coordinate is

$$
\begin{aligned}
y &= a(\theta - \theta_0) \\
z &= r - a \\
x &= (\phi - \phi_0)a\,cos\theta_0,
\end{aligned}
$$

where r is the distance of the fluid from the center of the sphere, θ is the latitude, ϕ the longitude, and a is the radius of the Earth.

Hence, latitude θ is a linear function of y

$$
\theta = \theta_0 + \frac{y}{a}. \tag{2.35}
$$

Now, for small variations in latitude we have:

$$
sin\theta \approx sin\theta_0 + cos\theta_0\frac{y}{a}, \tag{2.36}
$$

as a truncated series around θ_0. And we can express f as the following:

$$
f = 2\Omega sin\theta = 2\Omega sin\theta_0 + \frac{2\Omega}{a}cos\theta_0\,y = f_0 + \beta\,y. \tag{2.37}
$$

Where we have introduced $\beta = \frac{2\Omega}{a}cos\theta_0$.

But what is β? We have gone from $f = 2\Omega sin\theta$ to $f = f_0 + \beta y$. The dependence of f on latitude is conserved because of the linear relationship between f and y. This is an important result: **we are not working on spherical coordinates but the dynamical effects of sphericity are retained.**

β is called the gradient of planetary vorticity given that:

$$\frac{\partial f}{\partial y}(\theta = \theta_0) = \frac{1}{a}\frac{\partial f}{\partial \theta}(\theta = \theta_0) = \frac{2\Omega}{a}cos\theta_0 = \beta. \qquad (2.38)$$

Typical mid-latitude values for f and β are 10^{-4} s^{-1} and 10^{-11} m^{-1}s^{-1} (Fig. 2.4).

In conclusion, we have the β-plane approximation as

$$\boxed{f = f_0 + \beta y} \qquad (2.39)$$

For relatively large areas, with θ varying over a few tens of degrees, between mid-latitudes and the equator, the tangent plane approximation is called β-plane. This approximation is only valid if

$$\beta y \ll f_0 \quad or \quad \frac{\beta y}{f_0} \ll 1. \qquad (2.40)$$

For even smaller variations in θ the f-plane is used, where

$$f = f_0 = 2\Omega\,sin\theta_0. \qquad (2.41)$$
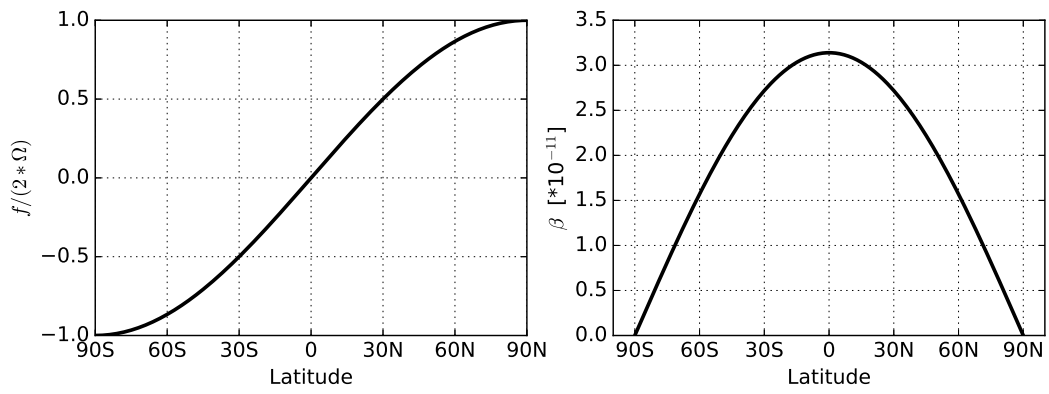
Figure 2.4: *The Coriolis parameter f and its meridional gradient β as a function of latitude.*

2.3 Kinematical and dynamical approximations

2.3.1 Hydrostatic balance

The vertical component (the component parallel to the gravitational force, $\mathbf{g}$) of the momentum equation is

$$\frac{\mathrm{D}w}{\mathrm{D}t} = -\frac{1}{\rho}\frac{\partial p}{\partial z} - g, \tag{2.42}$$

where w is the vertical component of the velocity and $\mathbf{g} = -g\mathbf{k}$. If the fluid is static the gravitational term is balanced by the pressure term and we have

$$\frac{\partial p}{\partial z} = -\rho g, \tag{2.43}$$

which is called the *hydrostatic balance*, or hydrostasy. Scaling analysis shows that the hydrostatic balance is the dominant balance within the vertical momentum equation , so long as the vertical length scales of motion are much smaller than the horizontal length scales. Such scales are relevant for large-scale ocean climate modeling, and global ocean models typically assume a hydrostatic balance, and this constitutes a basic assumption of the primitive equations. Integrating the hydrostatic balance vertically from the ocean surface η determines the pressure at a point in the ocean column

$$p(z) = p_a + g \int_z^\eta \mathrm{d}z' \rho(z'), \tag{2.44}$$

where p_a is the sea surface pressure resulting from external forcing (e.g., atmospheric loading, sea ice, ...).

Scaling and aspect ratio

For a Boussinesq fluid, the momentum equations are

$$\frac{\mathrm{D}\mathbf{u}}{\mathrm{D}t} + \mathbf{f} \times \mathbf{u} = -\nabla\phi \tag{2.45}$$

$$\frac{\mathrm{D}w}{\mathrm{D}t} = -\frac{\partial\phi}{\partial z} + b, \tag{2.46}$$

where $\phi = p/\rho_0$ and buoyancy $b = -g\rho/\rho_0$. In the case of $f = 0$ the horizontal momentum equation reduces to

$$\frac{\mathrm{D}\mathbf{u}}{\mathrm{D}t} = -\nabla\phi \tag{2.47}$$

and a scaling for the horizontal equation is

$$\frac{U}{T} \sim \frac{\Phi}{L}, or \frac{LU}{T} \sim \Phi, or U^2 \sim \Phi. \tag{2.48}$$

Using mass conservation to scale vertical velocities we obtain

$$\nabla_z \cdot \mathbf{u} + \frac{\partial w}{\partial z} = 0. \tag{2.49}$$

A scaling of this equation is

$$\frac{U}{L} + \frac{W}{H} = 0 \tag{2.50}$$

$$W = \frac{H}{L}U = \alpha U \tag{2.51}$$

where $\alpha \equiv \frac{H}{L}$ is the aspect ratio between the typical horizontal and vertical scales. The advective terms in the vertical momentum equation scale as

$$\frac{\mathrm{D}w}{\mathrm{D}t} \sim \frac{W}{T} = \frac{U}{L}W = \frac{U}{L}(\frac{H}{L}U) = \frac{U^2 H}{L^2}. \tag{2.52}$$

Now we can use the scaling for the horizontal and vertical motions, together with the aspect ratio of their typical scales, to reveal the condition for hydrostasy.

For hydrostatic balance to hold, the ratio of advective terms to the pressure gradient term in (2.46) must be

$$\frac{|\frac{\mathrm{D}w}{\mathrm{D}t}|}{|\frac{\partial \phi}{\partial z}|} \ll 1 \tag{2.53}$$

This implies that

$$\frac{|\frac{\mathrm{D}w}{\mathrm{D}t}|}{|\frac{\partial \phi}{\partial z}|} \sim \frac{U^2 H/L^2}{U^2/H} \sim \left(\frac{H}{L}\right)^2 \ll 1. \tag{2.54}$$

In other words, the aspect ratio should be

$$\alpha^2 \equiv \left(\frac{H}{L}\right)^2 \ll 1 \tag{2.55}$$

for the advective terms in the vertical momentum to be neglected. The hydrostatic balance is then a *small aspect ratio approximation*.

2.3.2   Hydrostatic approximation

2.3.3   Shallow water approximation

2.3.4   Boussinesq approximation

2.3.5   Rigid lid approximation

2.4   Rossby number

We consider the dynamical balance in the horizontal components of the momentum equation. In the horizontal plane (along geopotential surfaces) we find that the Coriolis term is much larger than the advective terms and the dominant balance is between Coriolis and the horizontal pressure force. The balance is called *geostrophic balance*, and it occurs when the Rossby number is small.

The horizontal momentum equation is

$$
\frac{\partial \mathbf{u}}{\partial \mathbf{t}} + (\mathbf{v} \cdot \nabla)\mathbf{u} + \mathbf{f} \times \mathbf{u} = -\frac{1}{\rho}\nabla_z p, \tag{2.56}
$$

where $\mathbf{v} = (u, v, w)$ and $\mathbf{u} = (u, v, 0)$. A scaling analysis of the second (U^2/L) and third (fU) terms, where U is the approximate magnitude of the horizontal velocities and L is a typical length scale over which that velocity varies, reveals the importance of rotation. The ratio of the sizes of the advective and Coriolis terms defines the Rossby number:

$$
\boxed{Ro \equiv \frac{U}{fL}} \tag{2.57}
$$

The Rossby number characterizes the importance of rotation in a fluid. It is the ratio of the magnitude of the relative acceleration to the Coriolis acceleration, and it is of fundamental importance in geophysical fluid dynamics.

2.5   Geostrophic and Thermal Wind Balance

If the Rossby number is sufficiently small, then the rotation term dominates the nonlinear advection term, and if the time period of the motion scales advectively (or there are no accelerations) then the rotation term also
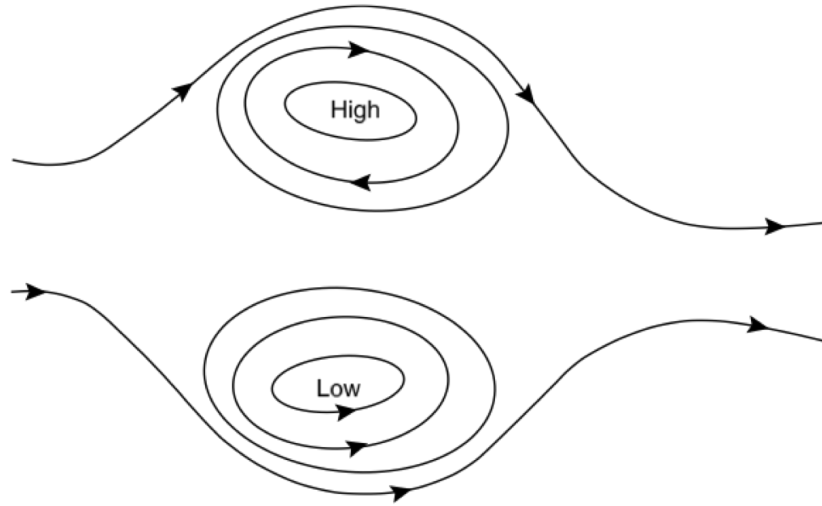
Figure 2.5: Schematic of a geostrophically balanced flow with a positive value of the Coriolis parameter f. Flow is parallel to the lines of constant pressure. Cyclonic flow is anticlockwise around a low pressure region. [from *Vallis* (2006)]

dominates the local time derivative. The only term that can then balance the rotation term is the pressure term, leaving us with

$$fv \approx \frac{1}{\rho}\frac{\partial p}{\partial x} \tag{2.58}$$

$$fu \approx -\frac{1}{\rho}\frac{\partial p}{\partial y}. \tag{2.59}$$

This balance is known as *geostrophic balance*, and is one of the pillars of geophysical fluid dynamics. We can now define geostrophic velocities as

$$fu_g = -\frac{1}{\rho}\frac{\partial p}{\partial y} \qquad fv_g = \frac{1}{\rho}\frac{\partial p}{\partial x} \tag{2.60}$$

and for flows with a low Rossby numbers, $u \approx u_g$ and $v \approx v_g$.

A geostrophic flow is parallel to lines of constant pressure (isobars). If $f > 0$, after a pressure gradient is initiated somehow, the fluid starts to move down the gradient. Then, the fluid experiences the Coriolis force to the right and therefore swings to the right. The fluid eventually moves along isobars (along the slope, not down it), with the pressure force down

the slope balanced by the Coriolis force up the slope. In the northern hemisphere, the flow is anticlockwise round a region of low pressure and clockwise around a region of high pressure.

Consider now a plane horizontal flow in which density does not vary along the fluid path (the Boussinesq approximation). In this case the continuity equation reduces to

$$\frac{\partial u}{\partial x} + \frac{\partial v}{\partial y} = 0. \tag{2.61}$$

We can now define a function $\psi(x, y, t)$ such that

$$u \equiv -\frac{\partial \psi}{\partial y}, \tag{2.62}$$

$$v \equiv \frac{\partial \psi}{\partial x}, \tag{2.63}$$

and Eq.2.61 is thus satisfied, and this is called a *streamfunction*.

Returning to our geostrophic balance, if the Coriolis force is constant and if density does not vary in the horizontal, the geostrophic flow is horizontally non-divergent

$$\nabla_z \cdot \mathbf{u_g} = \frac{\partial u_g}{\partial x} + \frac{\partial v_g}{\partial y} = 0, \tag{2.64}$$

and we may define a geostrophic streamfunction, ψ_g, by $\psi_g \equiv \frac{p}{f\rho}$, and

$$u_g \equiv -\frac{\partial \psi}{\partial y}, \quad v_g \equiv \frac{\partial \psi}{\partial x}. \tag{2.65}$$

Thermal wind

Thermal wind balance arises when combining the geostrophic and hydrostatic approximations. They are useful in elucidating how temperature differences in the horizontal can lead to vertical variations in geostrophic velocities, hence the term *thermal wind equations*.

Taking the vertical derivative of the geostrophic equations for a Boussinesq fluid

$$\rho_0 f \partial_z u = -\partial_z \frac{\partial p}{\partial y} \tag{2.66}$$

$$\rho_0 f \partial_z v = \partial_z \frac{\partial p}{\partial x}. \tag{2.67}$$
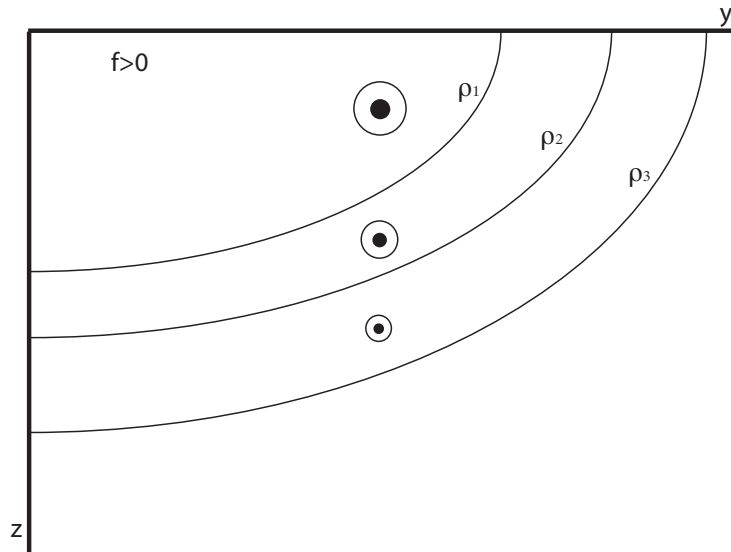
Figure 2.6: Schematic of thermal wind balance in the northern hemisphere. Shown are surfaces of constant density, or isopycnals. Density increases with depth and latitude, $\rho_3 > \rho_2 > \rho_1$. The termal wind associated with this density field is eastward, or out of the page, and decreases with depth. The same eastward thermal wind velocity would have resulted in the southern hemisphere, with $\rho_y < 0$ and $f < 0$.

Combining these with the hydrostatic balance, $\partial_z p = -\rho g$, and changing the order of differentiation for p, gives

$$\rho_0 f \, \partial_z u = g \, \partial_y \rho \tag{2.68}$$
$$\rho_0 f \, \partial_z v = -g \, \partial_x \rho. \tag{2.69}$$

These equations represent the *thermal wind balance*, and the vertical derivative of the geostrophic wind is the 'thermal wind'. Thermal wind balance says that **the geostrophic velocity has a vertical *thermal wind shear* in case where density has a horizontal gradient**.

In general, zonally averaged ocean temperature decrease poleward due to the differential heating received from solar radiation. Neglecting salinity effects on density, this poleward reduction in temperature corresponds to a poleward increase in density. Also, for a stably stratified fluid, density increases with depth. In a zonally-averaged flow, $\partial_x \rho = 0$, and so thermal wind reduces to

$$\partial_z u = \frac{g}{\rho_0 f} \partial_y \rho \tag{2.70}$$

This equation is telling us that, if temperature falls in the poleward direc-

tion, $\partial_y \rho > 0$, then the zonally-averaged thermal wind is eastward. Wind shear also increases as we move upward in the ocean, $\partial_z u > 0$, which yields a surface intensified zonal velocity field. Thermal wind, although diagnostic, represents a valid steady state balance of a frictionless rotating fluid. That is, in the presence of rotation, a flow can exist in steady state with nonflat isopycnals. Vertical integration of the thermal wind relation, along with knowledge of the geostrophic velocity at a point along the integration path, allows for determination of the full geostrophic velocity in terms of density. However, the baroclinic density field (with a horizontal gradient) is related to the baroclinic component of the velocity field through thermal wind balance. The barotropic flow component has zero vertical shear.

2.6   The Rossby radius

The Rossby radius of deformation is a length scale of fundamental importance in atmosphere-ocean dynamics. It describes the horizontal scale at which rotation effects become as important as buoyancy effects. For example, in the first stage of an adjustment problem, first the disturbance has a small structure and gravity dominates with a very large pressure gradient. Later, as the perturbation spreads over a larger horizontal scale, Coriolis becomes more important and of similar magnitude as the pressure gradient, and thus rotation causes a response that is much different from a non-rotating case.

Using a geostrophic flow, it is easy to show that the Rossby radius of deformation, L_d, is

$$L_d = c/|f| = (gH)^{1/2}/|f| \tag{2.71}$$

where c is the phase speed of the gravity wave. For the deep ocean, where H= 4 km and c= 200 m/s, the Rossby radius is about 2000 km. Which is much larger than depth, so the hydrostatic approximation is valid. However, the ocean is not only in rotation but also stratified, and so what is more important is not the barotropic radius of deformation but rather the baroclinic ones

$$L_d = c_n/|f| \tag{2.72}$$

where c_n are baroclinic gravity wave phase speeds. So the Rossy radius is directly related to the phase speed of long, baroclinic gravity waves, which is also a very useful parameter in the study of ocean wave dynamics. A global atlas of the first baroclinic gravity-wave phase speed, c, has been

computed on a 1-degree global grid from observations (Fig. 2.7) as follows

$$c_n \sim \frac{1}{n\pi} \int_{-H}^{0} N \, \mathrm{d}z \qquad (2.73)$$

where N is the buoyancy frequency.

Now, the first baroclinic Rossby radius, given that c_1=1-3 m/s, is $L_d \sim$10-30 km with values increasing towards low latitudes (Fig. 2.8). Mesoscale eddies have the size of the first baroclinic Rossby radius, therefore in order to resolve mesoscale eddies and associated fluxes, ideally an ocean model should have at least two grid points within L_d. It is clear from Fig. 2.9 that standard global ocean model can resolve mesoscale fluxes up to $\sim$25°, poleward of that latitude fluxes need to be parameterized. Benefits of having fine-resolution ocean models is illustrated in Fig. 2.10, where eddies and filaments are ubiquitous in the fine-resolution version of the model whereas a laminar ocean is simulated in the (standard!) 1° version.
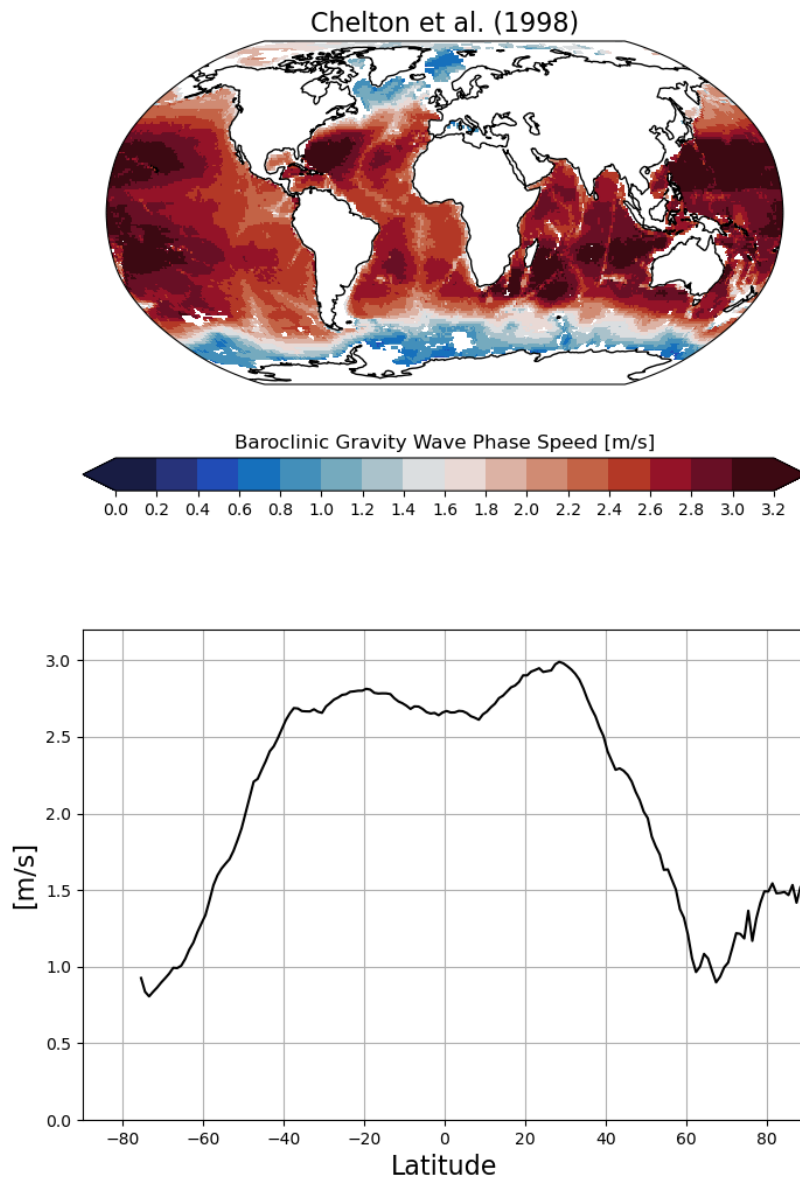
Figure 2.7: A global map of the first baroclinic gravity wave phase speed and its zonal mean. [data from Chelton et al., 1998]
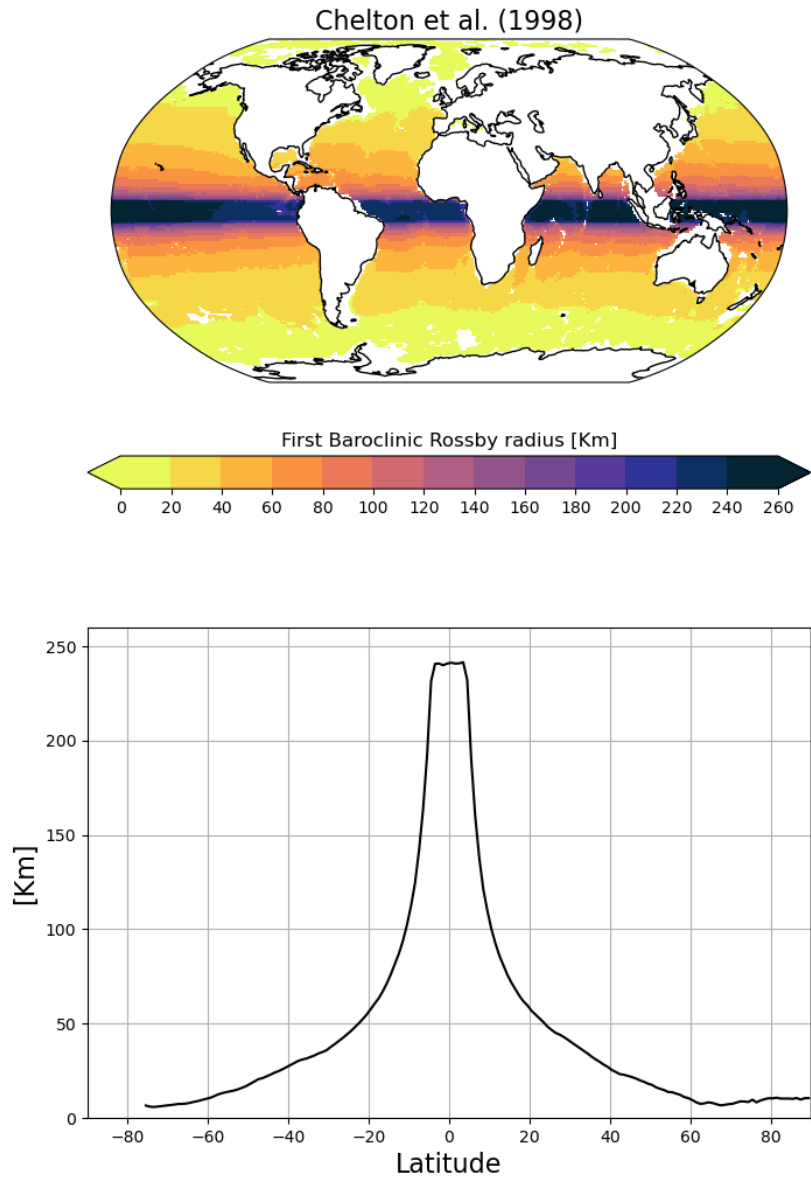
Figure 2.8: A global map of the first baroclinic Rossby radius of deformation and its zonal mean. [data from Chelton et al., 1998]
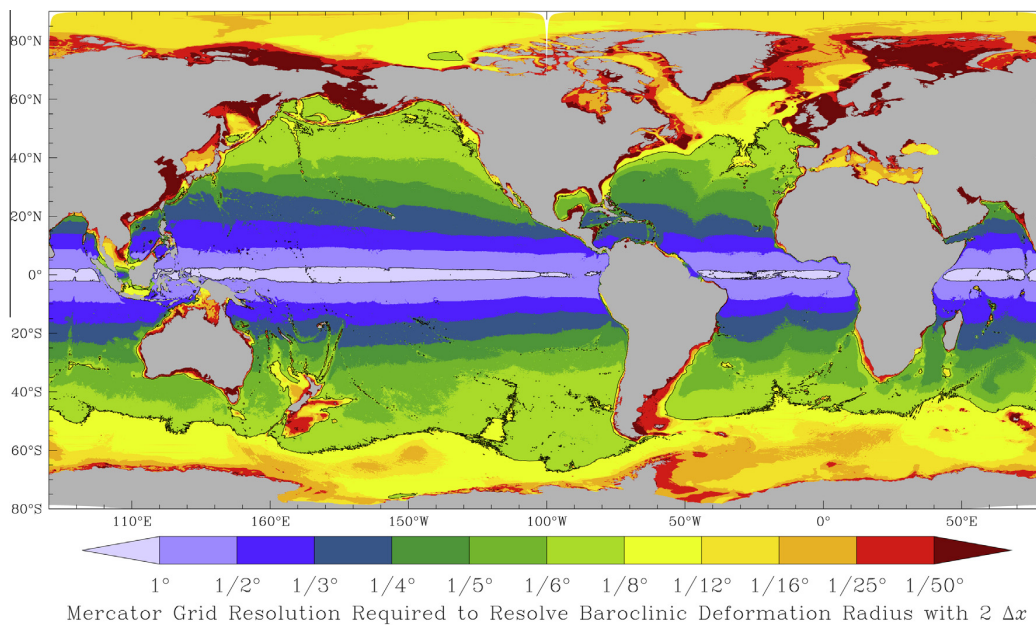
Figure 2.9: The oceanic resolution needed to resolve the Rossby Radius of deformation in an ocean model [from Hallberg et al., 2013].
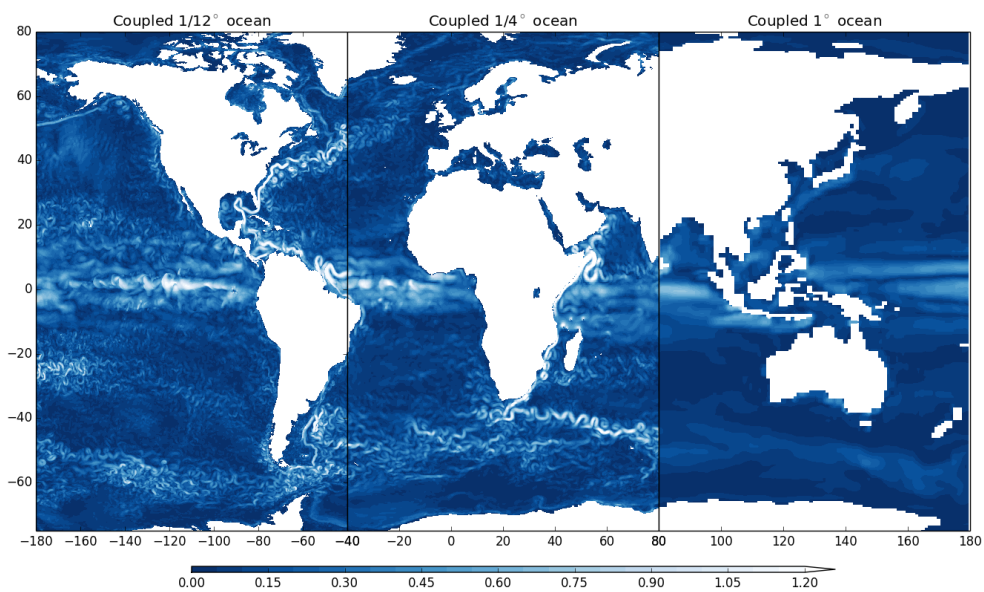
Figure 2.10: The same ocean model at different horizontal resolutions, increasing from right to left.

Let's now go a little ahead of ourselves. Consider that the Coriolis parameter is not constant and is actually a function of latitude $f(y)$. The nondivergent condition $\nabla \cdot (f\mathbf{u}) = 0$ is satisfied by the geostrophically balanced flow. Cross-differentiating Eq.2.60 gives

$$\frac{\partial f}{\partial y}v_g + f\nabla_z \cdot \mathbf{u_g} = 0 \tag{2.74}$$

Using mass continuity leads to

$$\boxed{\beta v_g = f\frac{\partial w}{\partial z}}, \tag{2.75}$$

where $\beta \equiv \frac{\partial f}{\partial y}$. This is a geostrophic vorticity balance, also called *Sverdrup balance*. In a Sverdrup balance, the vertical velocity results from an external agent, most notably wind stress. It states that the vertical shear in the vertical velocity balances a meridional current, with the Coriolis parameter f and the planetary vorticity gradient β determining the sense and strength of the meridional flow. A vertical velocity shear arises when there is a nonzero curl in the wind stress acting on the ocean surface. Vorticity is then transferred to the ocean via frictional effects causing *Ekman pumping or suction*. These effects alter the vertical structure of the vertical velocity and, through Sverdrup balance, induce a meridional flow.

2.7 The shallow-water equations

To describe large-scale oceanic, and atmospheric, motions, where the horizontal scale is much larger than the vertical scale, we can use a set of simplified equations that retain the necessary ingredients of the fluid motion but use some useful approximations. We will thus consider a fluid in hydrostatic balance of constant density and, for simplicity, we will also consider a flat bottom. The necessary condition of the shallow-water equations is that the horizontal length scale must be much larger than the vertical scale over which the fluid develops so that $L >> H$.

If the fluid is in hydrostatic balance

$$\frac{\partial p}{\partial z} = -\rho g. \tag{2.76}$$

Then the total pressure will be

$$p(x, y, z, t) = -\rho g z + p'. \tag{2.77}$$

Pressure must vanish at the surface, so that $p = 0$ at $z = \eta$

$$p = p_0 + p' = 0 \tag{2.78}$$

and at $z = \eta$ we have

$$p' = \rho g \eta \tag{2.79}$$

Our total pressure will then be

$$p(x, y, z, t) = \rho g(\eta(x, y) - z) \tag{2.80}$$

This means that the horizontal gradient of pressure, and the flow, is independent of depth

$$\nabla p = \rho g \nabla \eta \tag{2.81}$$

and the horizontal momentum equations reduce to

$$\frac{D\boldsymbol{u}}{Dt} = -\frac{1}{\rho}\nabla p = -g\nabla \eta \tag{2.82}$$

We can now easily add rotation to our shallow-water momentum equations

$$\boxed{\frac{D\boldsymbol{u}}{Dt} + \boldsymbol{f} \times \boldsymbol{u} = -\frac{1}{\rho}\nabla p = -g\nabla \eta} \tag{2.83}$$

The continuity equation is obtained by the mass balance within an infinitesimal column of fluid. The mass flux passing through a section of the
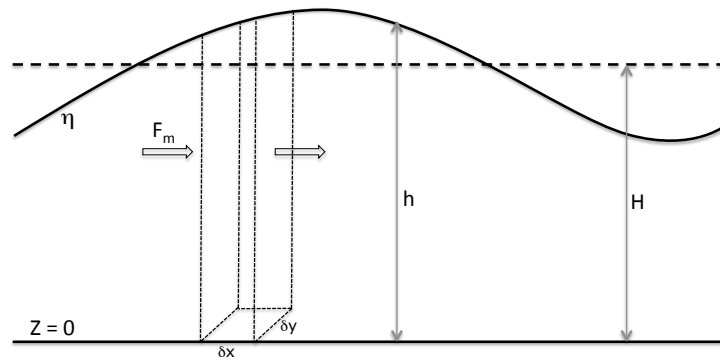
Figure 2.11: Schematic of a flat-bottomed shallow-water system and mass balance within a column of fluid.

column is $F_m = \rho u(H + \eta)\delta y$ and the difference between the fluxes into and out of the section is given by

$$\delta x \delta y \frac{\partial}{\partial x}[\rho u(H + \eta)] \tag{2.84}$$

Considering the total volume, the net rate of change is

$$\frac{\partial h}{\partial t} + \frac{\partial}{\partial x}[u(H + \eta)] + \frac{\partial}{\partial y}[v(H + \eta)] = 0 \tag{2.85}$$

which is the new continuity equation for the shallow-water system

$$\frac{\partial h}{\partial t} + \frac{\partial}{\partial x}(uh) + \frac{\partial}{\partial y}(vh) = 0 \tag{2.86}$$

$$\boxed{\frac{\partial h}{\partial t} + \nabla \cdot (\boldsymbol{u}h) = 0} \tag{2.87}$$

and if the perturbation is small and H is constant, mass continuity reduces to the linear equation

$$\boxed{\frac{\partial \eta}{\partial t} + H\nabla \cdot \boldsymbol{u} = 0} \tag{2.88}$$

If there is flux by advection this is balanced by a net increase in mass and an increase in height, giving rise to a vertical velocity, so that the mass convergence is balanced by the increase in height allowing for a dynamical surface elevation. This will be the basis for the propagation of waves within the rotating shallow-water system.

Exercices

1. Use $\phi = p/\rho_0$ and the definition of buoyancy $b = -g\rho/\rho_0$ to rewrite the hydrostatic balance and thermal wind equations.

2. Where is thermal wind velocity directed in the southern hemisphere, considering a poleward increasing (decreasing) density (temperature)? (see Fig. 2.12)

3. How is thermal wind shear changed as we approach the poles?
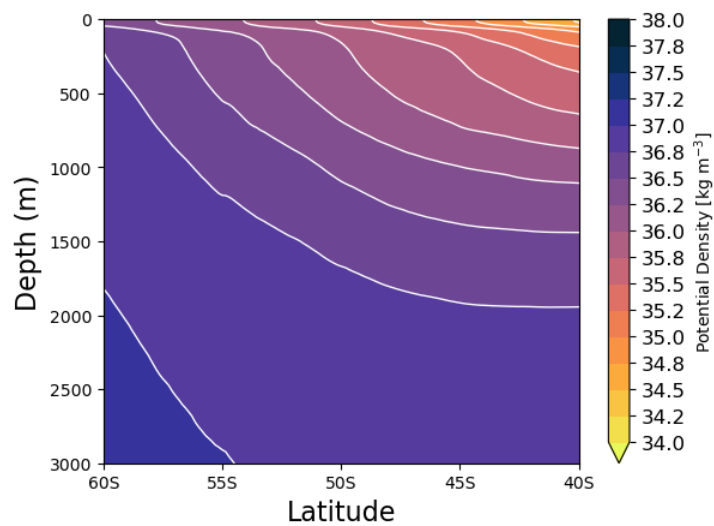
Figure 2.12: Zonal-mean potential density in the latitudes of the Drake Passage.

Chapter 3

Air-Sea interactions

3.1 Air-sea exchange of heat

About half the solar energy reaching Earth is absorbed by the ocean and land, where it is temporarily stored near the surface. Only about a fifth of the available solar energy is directly absorbed by the atmosphere. Of the energy absorbed by the ocean, most is released locally to the atmosphere, mostly by evaporation and infrared radiation. The remainder is transported by currents to other areas especially mid latitudes. Note that heat is the amount of thermal energy transferred from one body to another because of the temperature difference between those bodies.

Heat lost by the tropical ocean is the major source of energy needed to drive the atmospheric circulation. And, solar energy stored in the ocean from summer to winter helps ameliorate Earth's climate. The thermal energy transported by ocean currents is not steady, and significant changes in the transport, particularly in the Atlantic, may have been important for the development of the ice ages. For these reasons, oceanic heat budgets and transports are important for understanding Earth's climate and its short and long term variability.

Changes in energy stored in the upper layers of the ocean result from a local imbalance between input and output of heat through the sea surface. This transfer of heat through the surface is called a heat flux. The flux of heat and water also changes the density of surface waters, and hence their buoyancy. As a result, the sum of the heat and water fluxes is often called the buoyancy flux.

The flux of energy to deeper layers is usually much smaller than the flux through the surface. And, the total flux of energy into and out of the global ocean must be zero, otherwise the ocean as a whole would heat up
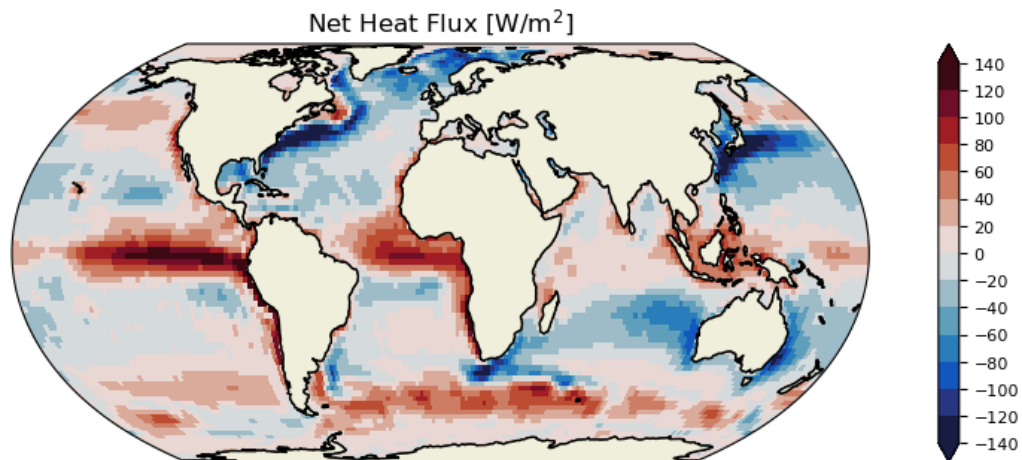
Figure 3.1: *Long-term means of surface net heat flux. Positive values indicate a flux into the ocean. Data from the NCEP/NCAR reanalysis (Kalnay et al., 1996).* *2019 only!*

or cool down. The sum of the heat fluxes into or out of a volume of water is the heat budget.

3.1.1 Heat budget at the surface

The major terms in the budget at the sea surface are:

1. **insolation**, Q_{sw}, the flux of sunlight into the sea. Represents the radiative heat flux from the incoming solar radiation minus that reflected. The average value of incoming solar radiation at the top of Earth's atmosphere is 342 W m^{-2}, although this value varies considerably with latitude and season. Some of the solar radiation is absorbed by the atmosphere or reflected back to space by clouds and aerosols, never reaching the ocean. Furthermore, the ocean doesn't absorb all of the shortwave radiation that reaches its surface; some is also reflected back to space. The albedo α describes how much radiation is absorbed versus reflected. Therefore, the shortwave heating is given by

$$Q_{sw} = (1 - \alpha) Q_{sw}^{inc}. \tag{3.1}$$

The net solar heat input at the sea surface ranges 250 W/m^2 in the tropics to 50 W/m^2 at high latitudes. This differential solar heating over the globe is the powerhouse of the atmosphere and ocean.

2. **Net Infrared Radiation**, $\mathcal{Q}_{lw}$, net flux of infrared radiation from the sea. It is the radiative heat flux over the range of wavelengths emitted from the sea surface, dominated by infrared radiation, so it is negative. Because of its much lower temperature, the earth emits radiation in the longwave (i.e. infrared) band. On a global scale, emission is the main way the planet balances the incoming solar radiation to maintain its thermal equilibrium. The power of emitted radiation is strongly dependent on temperature; specifically, the Stefan-Boltzman law states that

$$\mathcal{Q}_{lw} = -\sigma T^4. \tag{3.2}$$

The fact that $\mathcal{Q}_{lw}$ is negative definite means that longwave emissions acts to cool the ocean.

3. **Sensible Heat Flux**, $\mathcal{Q}_{sh}$, the flux of heat out of the sea due to conduction. Turbulent transfer of heat across the sea surface as a function of the air-sea temperature difference. Radiative fluxes transmit heat energy over long distances, e.g.from the sun to the earth. Sensible heat exchange instead depends on direct molecular contact between air and water. The molecules of the two fluids bump against each other, thereby exchanging heat energy. When the ocean and air temperature are the same, the sensible heat flux is therefore zero. When they differ, heat is exchanged in such as way as to homogenize the temperature. This is analogous to the phenomenon of "Newtonian cooling" commonly studied in introductory physics courses.

The rate of exchange is highly dependent on the sea state, and in particular on the winds, which generate breaking waves and turbulence. It is easy to imagine how breaking waves enhance the exchange of heat: they literally pull air down into the water (bubbles) and splash water up into the air (sea spray). It is much harder to quantify this process mathematically. Nevertheless, laboratory experiments and field campaigns have permitted us to develop empirical formulas to do so:

$$\mathcal{Q}_{sh} = \rho^a C_p^a C_H |\mathbf{u_{10}^a} - \mathbf{u^o}|(T_{10}^a - T^o) \tag{3.3}$$

All of the complexity and difficulty of turbulent air-sea exchange is absorbed into the parameter C_H.

The annual mean contribution of $\mathcal{Q}_{sh}$ to $\mathcal{Q}$ is almost negligible. This is because, on average, the T and T_{10}^a are very close. There is, however, a strong seasonal cycle in sensible heat exchange. Because of the large ocean heat capacity, the ocean is usually colder than the

air in summer and warmer than the air in the winter. This drives important seasonal changes in circulation

4. **Latent Heat Flux**, $\mathcal{Q}_{lh}$, the flux of heat carried by evaporated water. Turbulent transfer of evaporated water, and heat is used to enable the phase change from liquid to vapour. This process requires thermodynamic energy and therefore extracts heat from the ocean. The latent exchange nearly always dominates over the sensible exchange.

$$\mathcal{Q}_{lh} = -L_e E, \tag{3.4}$$

where E is the evaporation rate and L_e is the latent heat of vaporization. The latent heat flux always cools the ocean

5. **Advection** $\mathcal{Q}_{adv}$, heat transported by ocean currents.

Conservation of heat requires:

$$\mathcal{Q} = \mathcal{Q}_{sw} + \mathcal{Q}_{lw} + \mathcal{Q}_{sens} + \mathcal{Q}_{latent} + \mathcal{Q}_{adv} \tag{3.5}$$

where Q is the resultant heat gain or loss. Units for heat fluxes are W/m^2. The product of flux times surface area times time is energy in joules.

There is no local heat balance, instead there is a net heating gain over the tropical regions and a localised loss of heat at high latitudes. To keep the ocean in a steady state, ocean circulation must therefore transport heat from equator to pole ($\mathcal{Q}_{adv}$).
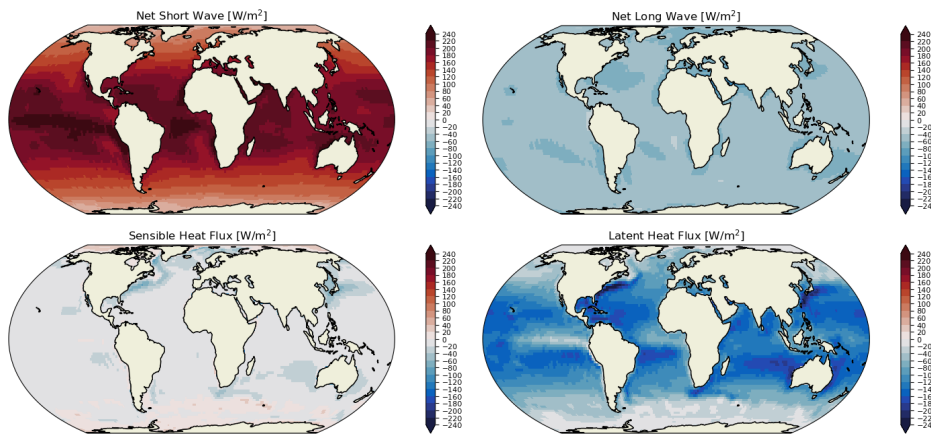
Figure 3.2: *Long-term means of net surface shortwave, net surface longwave radiation, surface sensible and latent heat fluxes. Positive values indicate a flux into the ocean. Data from the NCEP/NCAR reanalysis (Kalnay et al., 1996).2019 only!*
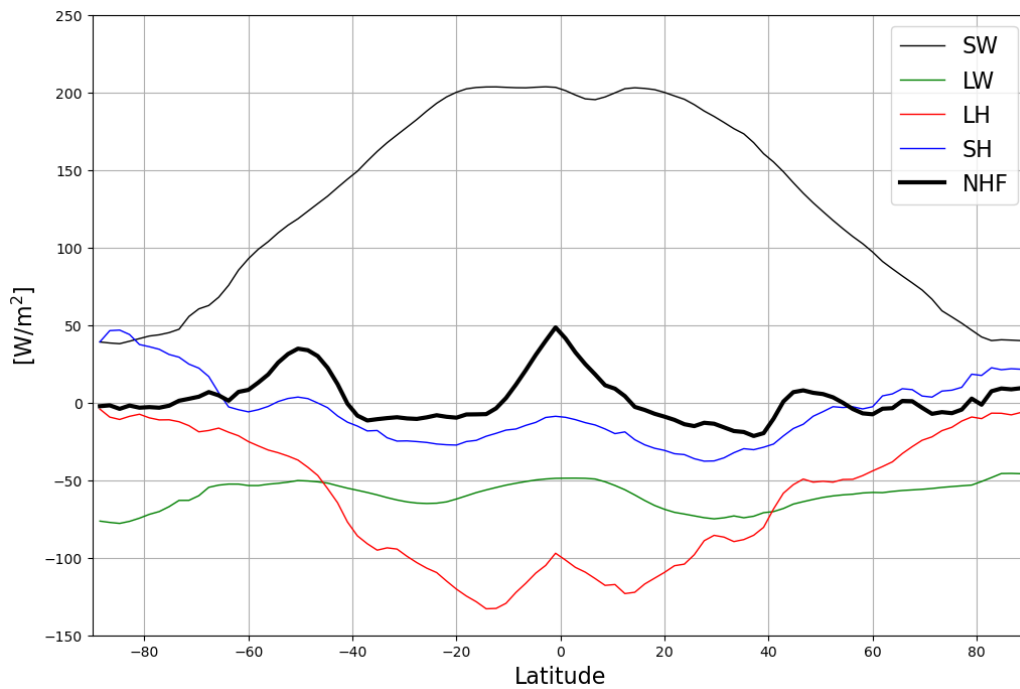

Figure 3.3: *The zonal-mean of net surface shortwave and net surface longwave radiation, surface sensible and latent heat fluxes, and the net heat flux. Positive values indicate a flux into the ocean. Data from the NCEP/NCAR reanalysis (Kalnay et al., 1996).2019 only!*

Mixed layer heat budget equation

In general, two physical processes can cause $\mathcal{H}$ to vary over time within a surface layer of the ocean: an exchange of heat with the atmosphere and advection of heat within the ocean:

$$\frac{\partial \mathcal{H}}{\partial t} = \mathcal{Q} - \mathbf{u} \cdot \nabla \mathcal{H}, \tag{3.6}$$

where $\mathcal{Q} = \mathcal{Q}_{sw} + \mathcal{Q}_{lw} + \mathcal{Q}_{sens} + \mathcal{Q}_{latent}$

The heat content, per unit area, is

$$\mathcal{H} = h\rho C_p T. \tag{3.7}$$

Now considering $\rho \sim \rho_0$ within the mixed layer and h to be constant, these heat fluxes drive a temperature change over a surface mixed layer given by

$$\boxed{\frac{DT}{Dt} = \frac{\mathcal{Q}}{\rho C_p h} - \mathbf{u} \cdot \nabla T} \tag{3.8}$$

Annual gain in heat in the tropics and loss at high latitudes is offset by an ocean heat transport, generally directed poleward, $\mathcal{Q}_{adv}$. Consider the case in which $\mathcal{Q} = 0$, so that temperature advection is the only remaining process causing a change in T in the mixed layer

$$\frac{DT}{Dt} = -\mathbf{u} \cdot \nabla T = -u\frac{\partial T}{\partial x} - v\frac{\partial T}{\partial y} - w\frac{\partial T}{\partial z}. \tag{3.9}$$

So far we have considered h to be a constant, but the thickness of the mixed layer varies in time, mostly through heating and cooling at the surface and turbulent wind mixing. Using Fick's laws of diffusion

$$F_x = -A\frac{\partial C}{\partial x}, \tag{3.10}$$

where F_x is the flux in the x direction, A is a diffusivity coefficient. Also, the time rate of change of a concentration due to diffusive fluxes will be proportional to the second spatial derivative of the concentration

$$\frac{\partial C}{\partial t} = A\frac{\partial^2 C}{\partial x^2}, \tag{3.11}$$

or

$$\frac{\partial C}{\partial t} = A\nabla^2 C. \tag{3.12}$$

This is our starting point for the parameterization of ocean mixing, where C is any physical property and A is the efficiency of turbulent eddies. A local temperature change due to turbulent mixing by eddies is

$$\boxed{\frac{\partial T}{\partial t} = K\nabla^2 T}. \tag{3.13}$$

What is the value of $K = (K_x, K_y, K_z)$? Difficult question, but $K_h >> K_z$ reflecting the fact that the ocean is stably stratified in the vertical, and mixing along isopycnals requires less work than diapycnal mixing. The contribution to the ocean mixed layer heat budget by turbulent mixing is thus

$$\boxed{\frac{\partial T}{\partial t} = K_h\nabla_h^2 T + K_z\frac{\partial T}{\partial z}}. \tag{3.14}$$

Turbulent mixing is important in the upper ocean and can significantly modify the surface temperature. When mixing occurs, for example because of strong winds reaching the depth h, water from below the mixed layer can be entrained into the mixed layer, resulting in deepening of the mixed layer and a change in its temperature. The vertical velocity, called entrainment velocity w_e is

$$w_e = \frac{\partial h}{\partial t} + w_{z=h}, \tag{3.15}$$

representing both deepening of the mixed layer and an upwelling velocity. Hence, both entrainment processes are important in the vertical mixing of temperature. Also, neglecting horizontal components

$$\frac{DT}{Dt} = -w\frac{\partial T}{\partial z} = -w_e\frac{\Delta T}{h}, \tag{3.16}$$

and as the mixed layer gets shallower, small deepening or modest upwelling will result in large temperature tendencies.

The total heat budget for a mixed layer is

$$\boxed{\frac{DT}{Dt} = \frac{\mathcal{Q}}{\rho C_p h} - \mathbf{u}\cdot\nabla T + K_h\nabla_h T + K_z\frac{\partial T}{\partial z}} \tag{3.17}$$

Page 45

(a) The change in temperature ΔT of the water is related to change in energy ΔE through:
$$\Delta E = C_p m \Delta T \tag{3.18}$$
where m is the mass of water being warmed or cooled, and C_p is the specific heat of sea water at constant pressure, $C_p \sim 4.0 \times 10^3 \text{ J kg}^{-1} \text{ K}^{-1}$. Thus, 4,000 Joules of energy are required to heat 1.0 kg of sea water by $1.0°\text{K}$.
Estimate how many Joules are required to heat 1.0 kg of air by $1.0°\text{K}$.

(b) Estimate the thickness of the ocean that holds as much heat as the overlying atmosphere, where the amount of heat $\mathcal{H}$ required to raise the temperature of the atmosphere or ocean by ΔT is given by

$$\mathcal{H} = \rho C_p A D \Delta T, \tag{3.19}$$

where ρ is density, C_p is heat capacity, A is horizontal area and D is the vertical scale. Assume $\rho \sim 1 \text{ Kg m}^{-3}$ for the atmosphere and 10^3 for the ocean, $C_p \sim 1000 \text{ J kg}^{-1} \text{ K}^{-1}$ for the atmosphere and 4000 for the ocean, D of 10 km for the atmosphere, $\Delta T = 1 \text{ K}$ and $A = 1 \text{m}^2$.

3.2 Air-sea freshwater flux and surface salinity

The mass of salt M_s in a volume of seawater, per unit area, is

$$M_s = \rho h S, \tag{3.20}$$

and tendencies in the mass will be expressed as

$$\frac{\partial M_s}{\partial t} = \rho h \frac{\partial S}{\partial t}. \tag{3.21}$$

But the salt itself is not exchanged with the atmosphere, only freshwater, so a mass flux of salt is not very practical nor useful.

Fresh water is exchanged between the atmosphere and ocean mainly via precipitation $\mathcal{P}$ and evaporation $\mathcal{E}$, but also from river runoff $\mathcal{R}$. Units for the freshwater flux are $m\,y^{-1}$ or $mm\,d^{-1}$, from the volume flux of fresh water ($m^3\,y^{-1}$) exchanged per unit area (m^2). Transfer of fresh water from the ocean to the atmosphere will increase the concentration of salts in the surface mixed layer of the ocean.

We define a virtual mass flux of salt as $(E - P)S$

$$\frac{\mathrm{D}\,S}{\mathrm{D}\,t} = \frac{(\mathcal{E} - \mathcal{P})}{\rho h} S - \mathbf{u} \cdot \nabla S. \tag{3.22}$$

Similarly to the heat budget, we can write

$$\boxed{\frac{DS}{Dt} = \frac{(\mathcal{E} - \mathcal{P})}{\rho h} S - u\frac{\partial S}{\partial x} - v\frac{\partial S}{\partial y} - w_e \frac{\Delta S}{h} + K_h \nabla_h S + K_z \frac{\partial S}{\partial z}} \tag{3.23}$$
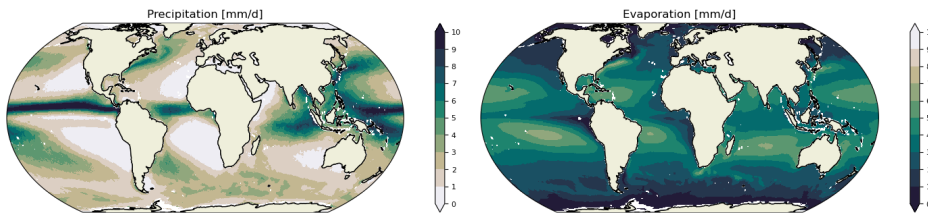

Figure 3.4: Precipitation and Evaporation fluxes computed from the NCEP/NCAR reanalysis for the period 2010-2019 *Kalnay et al.* (1996).

3.3   Air-sea forcing of surface density

The combination of surface heat and freshwater fluxes alters the surface density: warming or freshening will lighten surface waters, while cooling and evaporation will increase surface density. The forcing of surface density is thus

$$\mathcal{D} = -\frac{\alpha_T}{C_p}\mathcal{Q} + \rho\beta_S S(\mathcal{E} - \mathcal{P}) \qquad (3.24)$$

with units of mass per unit area and unit time, and α_T is the density expansion coefficient for temperature, β_S is the density contraction coefficient for salinity, both from the linearized equation of state

$$\frac{\Delta\rho}{\rho} = -\alpha_T\Delta T + \beta_S\Delta_S, \qquad (3.25)$$

with $\alpha_T = -\frac{1}{\rho}\frac{\partial\rho}{\partial T}$ and $\beta_S = \frac{1}{\rho}\frac{\partial\rho}{\partial S}$.

This surface forcing is also a buoyancy flux $-g\mathcal{D}/\rho$, with units of m^2 s^{-3} and perhaps more useful. Which perturbation is more important in generating density changes? Thermal or saline? It depends on the ambient temperature. From the linearised equation of state, the relative contribution of ΔT and ΔS are measured by α_T and β_S, or their ratio α_T/β_S, for given temperature and salinity changes, which depends strongly with temperature (the ratio increases with temperature). Hence, a temperature perturbation will have a larger effect on density in warm waters, and a salinity perturbation becomes more important in controlling density changes in cold waters.
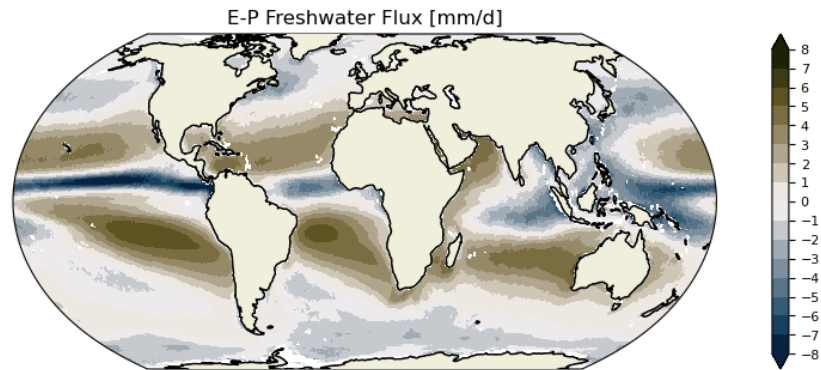
Figure 3.5: Net freshwater fluxes computed from the NCEP/NCAR reanalysis for the period 2010-2019 *Kalnay et al.* (1996).
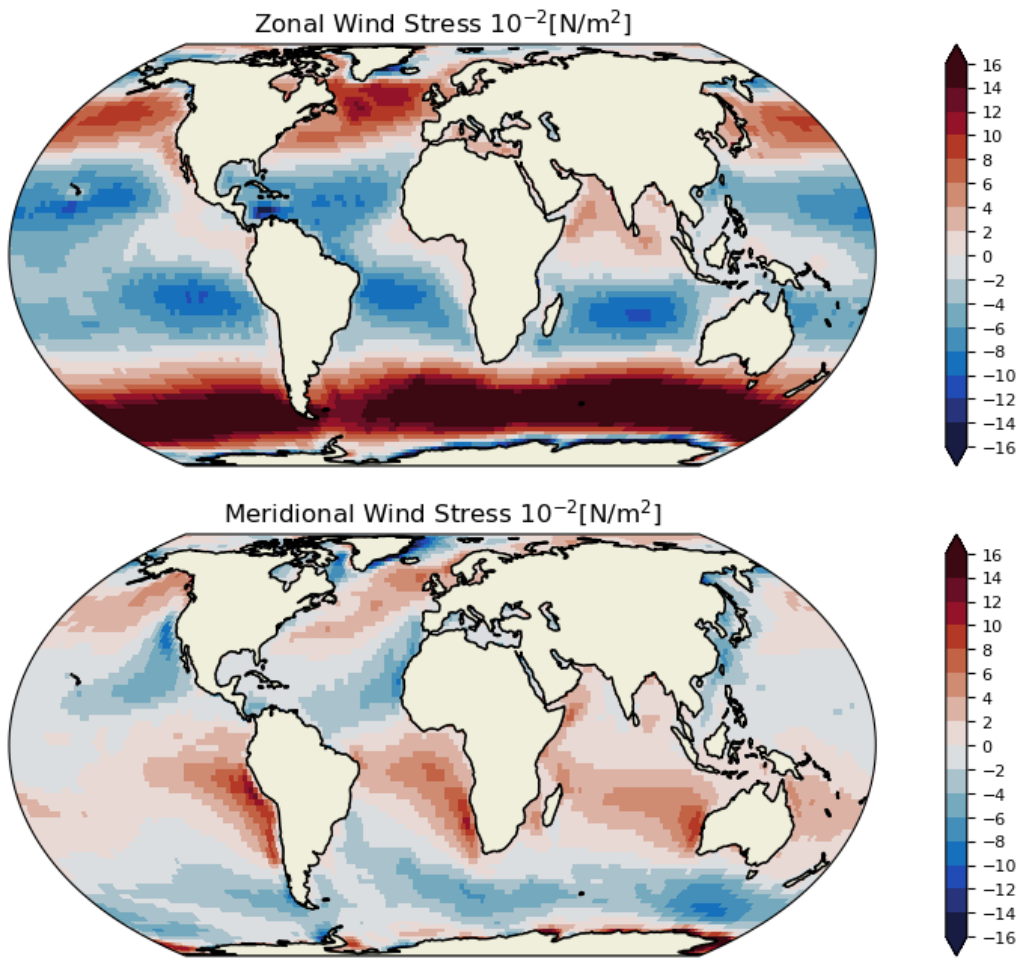
Figure 3.6: Surface zonal and meridional components of the wind stress computed from the NCEP/NCAR reanalysis for the period 2010-2019 *Kalnay et al.* (1996).

Chapter 4

Thermodynamics of Seawater

4.1 Thermodynamics of seawater

4.2 Temperature, Salinity, Density and Stratification
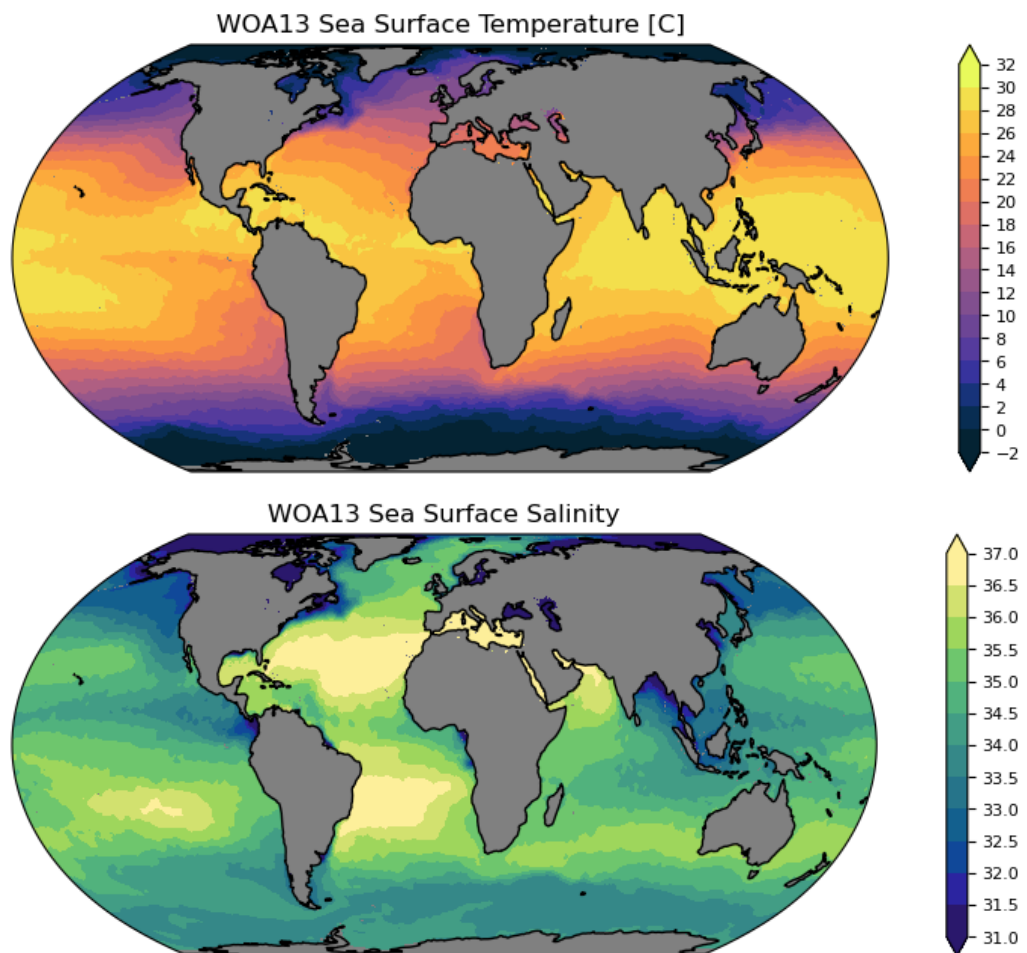
Figure 4.1: *Climatological mean (2005-2012) Sea Surface Temperature and Sea Surface Salinity for the global ocean from in situ profile data (World Ocean Atlas 2013 version 2) at 0.25 degree horizontal resolution.*
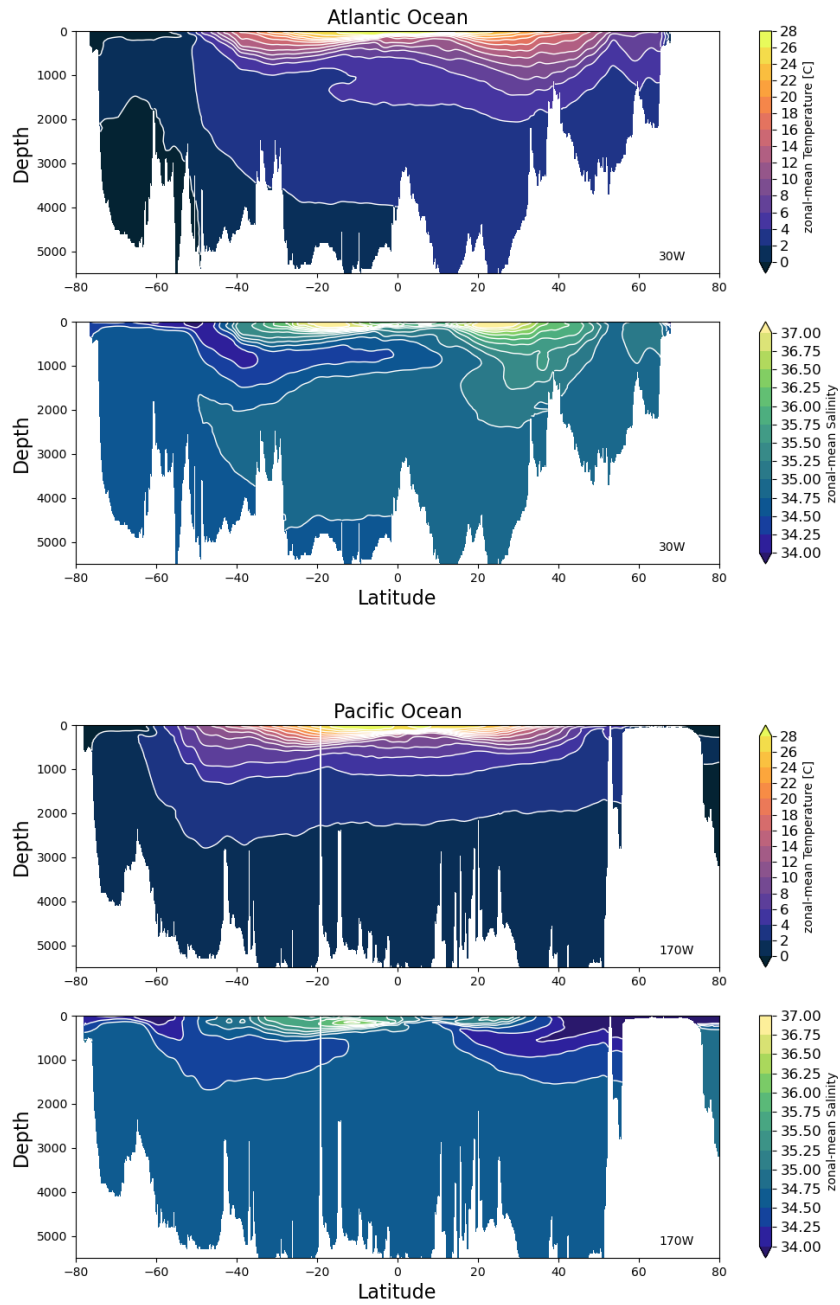
Figure 4.2: *Zonal-mean of the climatological (2005-2012) Temperature and Salinity for the Atlantic Ocean at 30W and Pacific Ocean at 170W from in situ profile data (World Ocean Atlas 2013 version 2) at 0.25 degree horizontal resolution.*

Page 53

4.2.1 Mixed layer Depth

The term 'mixed' refers to a given physical parameter of the ocean state (e.g. temperature, density, ...) that is assumed to be mixed and homogeneous to a certain level (e.g. regarding some space/time scales), from the surface down to the considered MLD. Here we want to estimate mixed layer over at least a daily cycle, and no more than a few days. This represents the depth over which surface fluxes have been recently mixed and integrated and is a characteristic timescale of air-sea interactions. The mixed layer depth is a thus a Density-Mixed Layer Depth, or Isopycnal Layer Depth.

The surface MLDs are estimated directly on individual profiles with data at observed levels. MLD is defined through the threshold method with a finite difference criterion from a near-surface reference value. A linear interpolation between levels is then used to estimate the exact depth at which the difference criterion is reached. The reference depth is set at 10 m to avoid a large part of the strong diurnal cycle in the top few meters of the ocean. The fixed criterion in density is 0.03 kg/m^3 difference from surface:

$$\text{MLD} = \text{depth where}(\sigma_0 = \sigma_0(10m) + 0.03 \quad \text{kg m}^{-3}). \qquad (4.1)$$

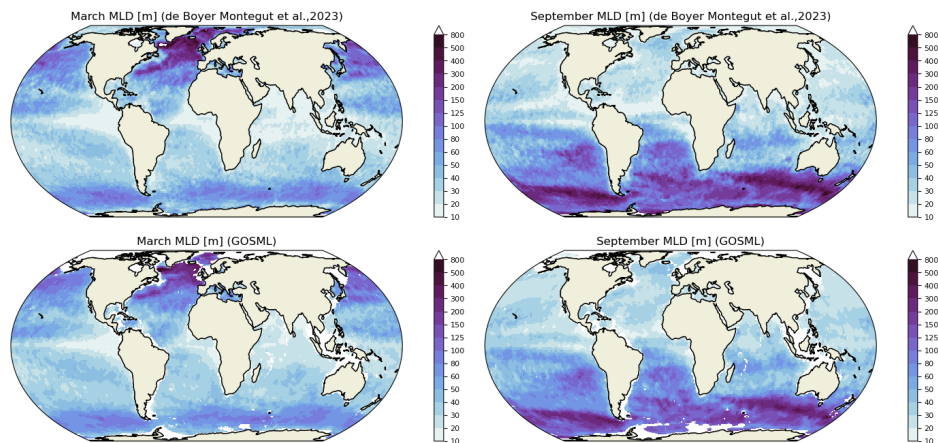See de Boyer Montegut et al. JGR 2004 for further details about the choice of the criterion).

Figure 4.3: *Mixed layer Depth (in m) computed from two different datasets for March and September.*

4.2.2 Static instability and Buoyancy frequency

Consider a stratified ocean and a parcel of fluid initially at rest, and therefore in hydrostatic balance. We will focus on vertical displacements and the restoring force is gravity. Consider a small adiabatic displacement of the parcel upward by δz, without altering the background pressure field. If the parcel is now lighter than the local environment, it will feel an upward pressure gradient force larger than the downward gravitational force, it will accelerate upwards and will become buoyant. In this case the fluid is statically unstable. If, instead, the parcel finds itself heavier than its sorroundings, the downward gravitational force will be greater than the upward pressure force, the fluid will sink back to its original position and will oscillate. This condition is statically stable.

Consider an incompressible fluid in which the density of the displaced parcel is conserved, $D\rho/Dt = 0$. If the environmental profile is $\tilde{\rho}(z)$ and the density of the parcel is ρ, a parcel displaced to a level $z + \delta z$ will show a change in density with respect to the local environement equal to

$$\delta\rho = \tilde{\rho}(z) - \tilde{\rho}(z + \delta z) = -\frac{\partial\tilde{\rho}}{\partial z}\delta z, \tag{4.2}$$

where the derivative on the right-hand side is the environmental gradient of density. If $\frac{\partial\tilde{\rho}}{\partial z} < 0$, the parcel will be heavier than its sorroundings and will sink back in a stable condition. Conversely, if $\frac{\partial\tilde{\rho}}{\partial z} > 0$, the parcel will be unstable. That is, the stability of a parcel of fluid is determined by the gradient of the environmental density. The upward force, per unit volume, on the displaced parcel is $F = -g\delta\rho$, and the equation of motion of the fluid parcel is thus

$$\rho(z)\frac{\partial^2\delta z}{\partial t^2} = g\frac{\partial\tilde{\rho}}{\partial z}\delta z, \tag{4.3}$$

or

$$\frac{\partial^2\delta z}{\partial t^2} = \frac{g}{\tilde{\rho}}\frac{\partial\tilde{\rho}}{\partial z}\delta z. \tag{4.4}$$

Static stability measures how quickly a water parcel is restored to its position in the water column if it is displaced vertically. If unstable, the water column has the potential to overturn. In stable water column conditions ($\frac{\partial\tilde{\rho}}{\partial z} < 0$), the parcel experiences a restoring force and will oscillate at a given frequency N:

$$\frac{\partial^2\delta z}{\partial t^2} = -N^2\delta z, \tag{4.5}$$
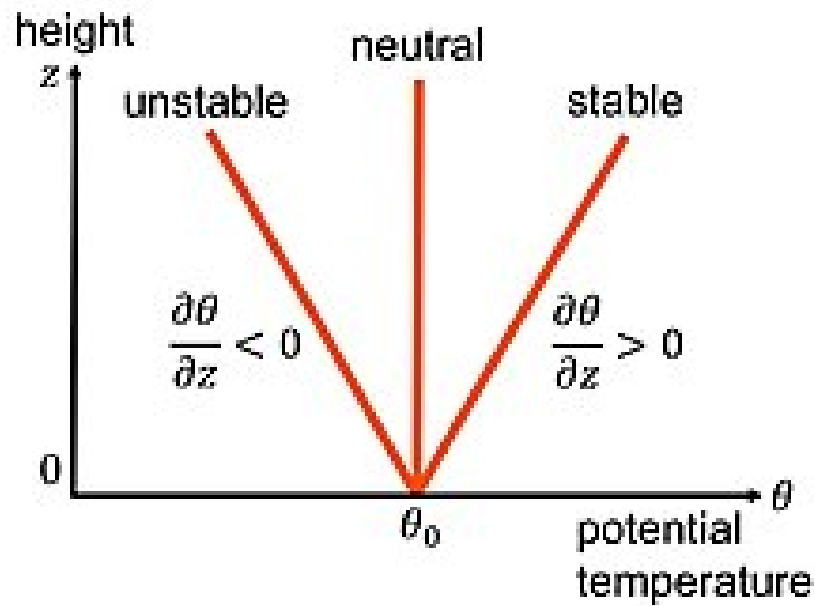
Figure 4.4: Possible temperature vertical profiles, in the atmosphere or ocean, giving rise to unstable, neutral or stable conditions.

where

$$N^2 = -\frac{g}{\tilde{\rho}}\frac{\partial \tilde{\rho}}{\partial z},$$ (4.6)

where N is the Brunt-Vaisala frequency. In liquids, it is a good approximation to replace $\tilde{\rho}$ by ρ_0.

If $N^2 < 0$, the density profile is unstable, the parcel continues to ascend and convection occurs. This is the condition for convective instability. Convection causes fluid parcels to mix and reduces an unstable profile to neutral stability.

> What is happening with global warming to the stratification of the
> ocean? How can you modify the stratification of the ocean? Which
> could be the implications?
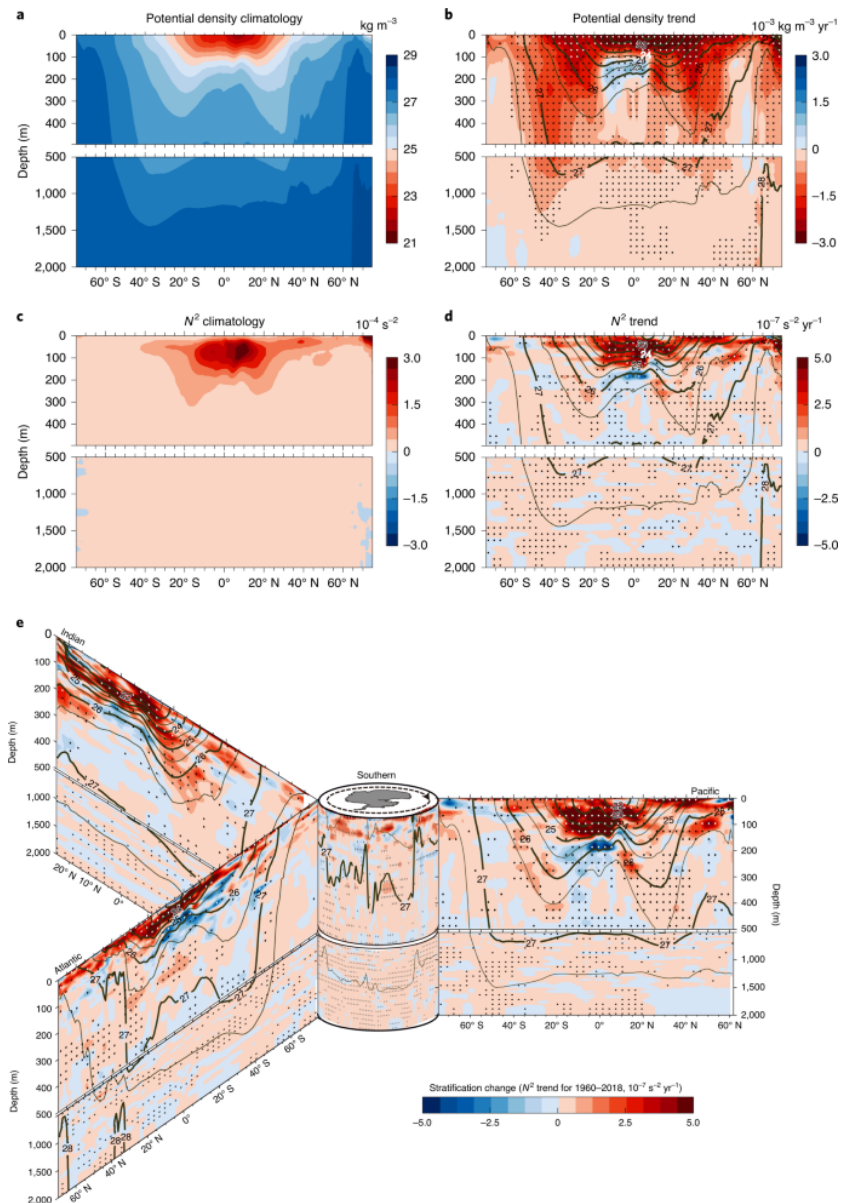
Figure 4.5: see *Li et al. Increasing ocean stratification over the past half-century. Nat. Clim. Chang. 10, 1116-1123 (2020).*

Chapter 5

Waves in the ocean

In this chapter we describe the general solution and dynamics of shallow-water waves and try to put them into a wider context, emphasizing their role in the ocean circulation and the coupled ocean-atmosphere system.

We will look for wave solutions of the shallow-water equations on the f-plane and β-plane. A few solutions will appear, some have already been discussed in different contexts, and some are new.

5.1   Poincaré Waves

We start by linearizing our shallow-water equations for a fluid $h = H + \eta$ over a state at rest

$$
\begin{aligned}
\boldsymbol{u} &= u' & (5.1)\\
h &= H + \eta & (5.2)
\end{aligned}
$$

so that our equations, after eliminating higher order terms, reduce to

$$
\begin{aligned}
\frac{\partial u}{\partial t} - f_0 v &= -g\frac{\partial \eta}{\partial x} & (5.3)\\
\frac{\partial v}{\partial t} + f_0 u &= -g\frac{\partial \eta}{\partial y} & (5.4)\\
\frac{\partial \eta}{\partial t} + H\nabla \cdot \boldsymbol{u} &= 0 & (5.5)
\end{aligned}
$$

A dispersion relation can now be obtained by looking for wave solutions of the type

$$
(u, v, \eta) = (u_0, v_0, \eta_0)e^{i(kx+ly-\omega t)} \tag{5.6}
$$

into our linearized equations:

$$-u_0 i\omega - f_0 v_0 = -g\eta_0 ik \tag{5.7}$$

$$-v_0 i\omega + f_0 u_0 = -g\eta_0 il \tag{5.8}$$

$$-\eta_0 i\omega + H(iku_0 + v_0 il) = 0 \tag{5.9}$$

Non-trivial solutions of the system exist only if the determinant is equal to zero, so that

$$\begin{vmatrix} -i\omega & -f_0 & gik \\ f_0 & -i\omega & gil \\ ikH & ilH & i\omega \end{vmatrix} = 0 \tag{5.10}$$

and this is true if

$$\omega[\omega^2 - f_0^2 - gH(k^2 + l^2)] = 0 \tag{5.11}$$

Now, there are a few interesting possible solutions for the frequency ω.

The first case is $\omega = 0$. This solution describes a time-independent flow and the equations describe a geostrophically balanced flow.

The second possible solution is if

$$\boxed{\omega^2 = f_0^2 + c^2(k^2 + l^2)} \tag{5.12}$$

where $c = (gH)^{1/2}$ is the gravity wave phase speed. The dispersion relation describes wave solutions of superinertial flow ($\omega > f_0$) which are called Poincaré waves. From this solution we can highlight three possible limiting cases (see Fig. 5.1).

First, the limit of no rotation, when $f_0 = 0$. The solution reduces to $\omega^2 = c^2 K^2$ and the frequency solutions are

$$\boxed{\omega = \pm Kc} \tag{5.13}$$

where $K = (k^2 + l^2)$, which describe a classical gravity wave.

Second, the short wave limit, when $K^2 \gg f_0^2/(gH)$, which gives

$$\boxed{\omega^2 = c^2 K^2} \tag{5.14}$$

again, the dispersion relation is that of the non-rotating case with phase speed c. This is because

$$\frac{2\pi^2}{\lambda^2} \gg \frac{f^2}{gH} \quad \frac{2\pi}{\lambda} \gg \frac{f}{c} \quad \lambda \ll \frac{(gH)^{1/2}}{f} 2\pi \tag{5.15}$$

so that $L_d \gg \lambda$, where L_d is the Rossby radius $L_d = (gH)^{1/2}/f$. Basically, this solution looks like a gravity wave in a rotating case.

Third, the long wave limit, when $K^2 \ll f_0^2/(gH)$. In this case we have

$$\boxed{\omega^2 = f_0^2} \tag{5.16}$$

and therefore the Rossby radius is much smaller than the wave length, $L_d \ll \lambda$. In this limiting case, there is no space dependency, $k = l = 0$, and the surface elevation anomaly is also zero $\eta = 0$. The solution is

$$\frac{\partial u}{\partial t} - fv = 0 \tag{5.17}$$

$$\frac{\partial v}{\partial t} + fu = 0 \tag{5.18}$$

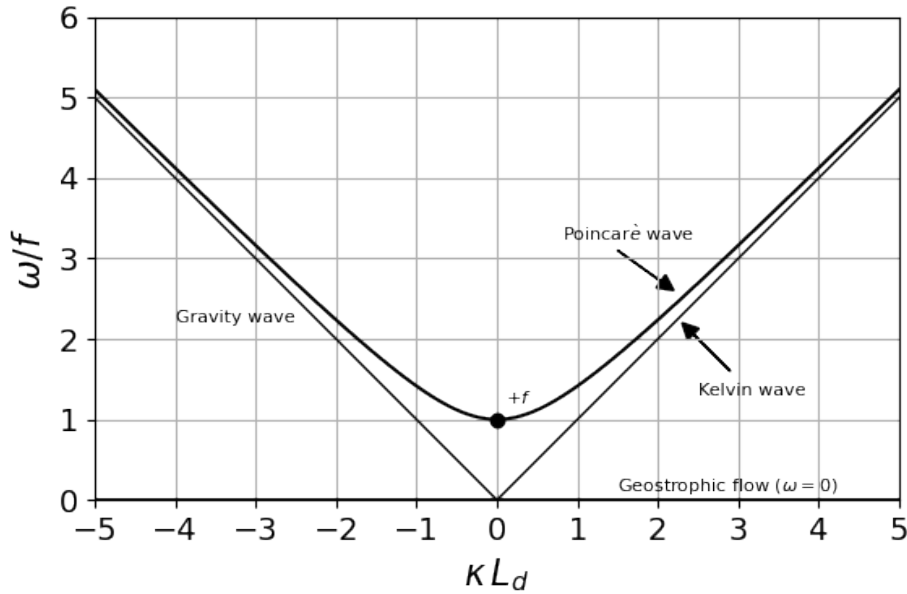and these are called inertial oscillations, circulating at the planetary frequency $\omega = f$.

Figure 5.1: *Dispersion relation for Poincarè and Kelvin waves. The frequency is scaled by f and the wavenumber by L_d. The black dot marks the inertial oscillations regime and the $\omega = 0$ is the geostrophic case.*

5.2 Kelvin Waves

Kelvin waves are a particular solution of the shallow water equations describing a gravity wave that exists in a rotating frame and with the help of lateral boundaries. We could show Kelvin waves propagating in a channel, with two parallel boundaries, but for a start we will consider the case of a single lateral boundary. The first assumption is that, if $u = 0$ at the boundary, we could simply consider the zonal component of the velocity zero everywhere. The meridional component is not zero at the boundary, because the flow is frictionless. The linearized shallow water equations are

$$-f_0 v = -g\frac{\partial \eta}{\partial x} \tag{5.19}$$

$$\frac{\partial v}{\partial t} = -g\frac{\partial \eta}{\partial y} \tag{5.20}$$

$$\frac{\partial \eta}{\partial t} + H\frac{\partial v}{\partial y} = 0 \tag{5.21}$$

Continuity becomes

$$\frac{\partial \eta}{\partial t \partial y} = -H\frac{\partial^2 v}{\partial y^2} \tag{5.22}$$

and using the momentum equation

$$\frac{\partial^2 v}{\partial t^2} = gH\frac{\partial^2 v}{\partial y^2} \tag{5.23}$$

which is the standard wave equation with phase speed $c = (gH)^{1/2}$. The solution to this is

$$v = V_1 \cos k(y - ct) + V_2 \cos k(y + ct) \tag{5.24}$$

and the wave propagates along the meridional boundary. Substituting this solution into the momentum equation we obtain a solution for η

$$\eta = V_1 \frac{c}{g} \cos k(y - ct) - V_2 \frac{c}{g} \cos k(y + ct) \tag{5.25}$$

which describes a propagating wave in terms of surface elevation. The solution has been found for both v and η with no Coriolis term: this has the characteristics of a non-rotating shallow water wave. The velocity is in geostrophic balance with the pressure field, although it is a wave and $\omega \sim f$.
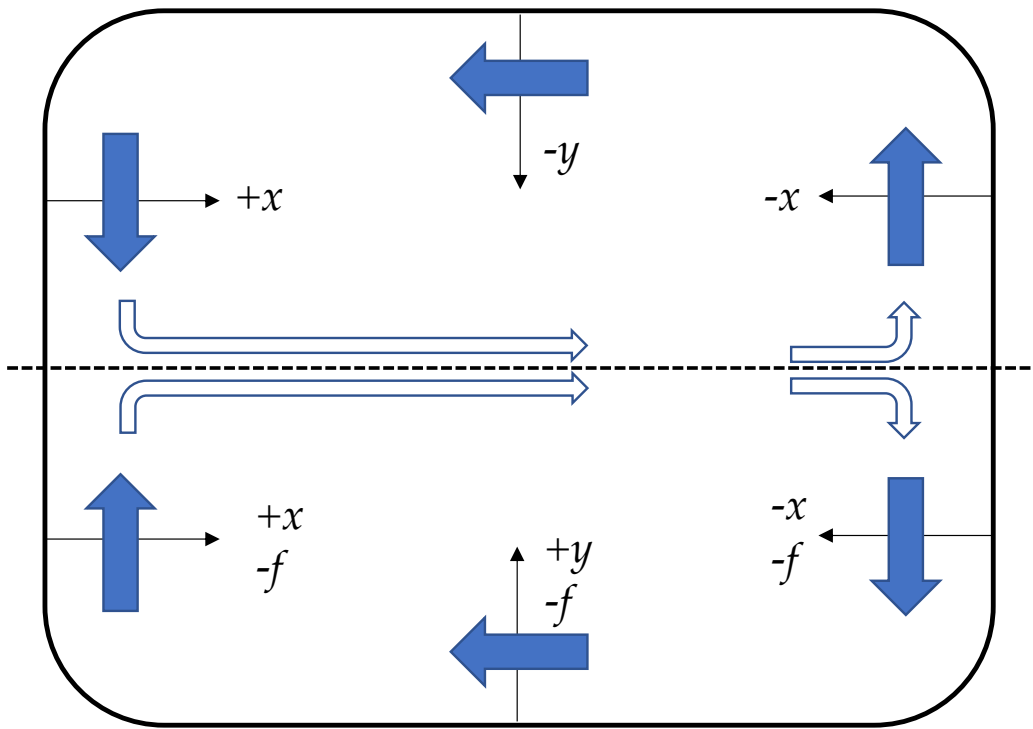
Figure 5.2: *For a system bounded to the west (x positive) the wave propagates in the negative y direction, i.e. to the south. If x is negative this reverses so on the eastern side of the basin the Kelvin wave propagates northwards. In the northern hemisphere a Kelvin wave will keep the coast to its right as it pushed against it by the Coriolis force.*

The solutions in the x-direction are

$$V_1 = e^{f_0/cx} \tag{5.26}$$

$$V_2 = e^{-f_0/cx} \tag{5.27}$$

and remember that $f_0/c = L_d^{-1}$. The first solution grows exponentially for positive x away from the meridional boundary, which is not physically possible. We are then left with the following set of solutions

$$v = e^{-x/L_d} \cos k(y + ct) \tag{5.28}$$

$$u = 0 \tag{5.29}$$

$$\eta = -e^{-x/L_d} \frac{c}{g} \cos k(y + ct) \tag{5.30}$$

$$= -(H/g)^{1/2} e^{-x/L_d} \cos k(y + ct) \tag{5.31}$$

These are Kelvin waves. They are trapped by the meridional boundary and decay exponentially away from it. The trapping spatial scale is given by the Rossby radius, and for f_0 positive the boundary is at the right of the wave propagation. Kelvin waves are balancing f against the wall, which could be a topographic boundary or a waveguide such as the equator (Fig. 5.2).

Barotropic Kelvin waves are also tidal waves, propagating around an amphidromic point .

5.3   Planetary, or Rossby, waves

The time-dependent ocean circulation has an important impact on our climate due to the ocean large heat capacity. Any abrupt change, the intrinsic variability and possible variations of the general circulation caused by the atmospheric influence is fundamental in climate studies. Moreover, the oceans are no longer considered passive in the atmosphere-ocean system, but contribute to the production of the climate low-frequency variability at interannual to decadal time scales (*Talley*, 1999; *Dewar*, 2001; *Pierce et al.*, 2001).

The oceans are forced at the surface by the wind frictional stress and Rossby waves appear to play a fundamental role in redistributing and dispersing large-scale time-varying energy in the ocean. The propagation of Rossby waves towards the ocean interior under the influence of wind stress results in establishing a Sverdrup balance in the basin, accumulating energy in the western boundaries and intensifying currents there (*Anderson and Gill*, 1975, 1979).

Due to the ubiquitous presence of Rossby waves in the world oceans they influence ocean gyres and air-sea fluxes at all latitudes, affecting in turn the atmospheric heat transport and circulation. They are believed to provide teleconnections between the equatorial and middle latitudes regions (*Galanti and Tziperman*, 2003) as well as transhemispheric and interbasin communications (*Cessi and Otheguy*, 2003). Other major effects are the maintenance and intensification of western boundary currents, transport of a large amount of heat and, because of their time-scale, they play a key role in the climate system.

Rossby waves are very long waves so that the f-plane is not a good approximation anymore and we will build our solutions on the β-plane. The frequency is going to be subinertial, $\omega \ll f$, and so they are close to geostrophy.

Our set of equations is

$$\frac{\partial u}{\partial t} - (f_0 + \beta y)\, v = -g\frac{\partial \eta}{\partial x} \tag{5.32}$$

$$\frac{\partial v}{\partial t} + (f_0 + \beta y)\, u = -g\frac{\partial \eta}{\partial y} \tag{5.33}$$

$$\frac{\partial \eta}{\partial t} + H\left(\frac{\partial u}{\partial x} + \frac{\partial v}{\partial y}\right) = 0 \tag{5.34}$$

Given that $\omega \ll f$, $\frac{\partial}{\partial t} \ll 1$ and $\beta L/f_0 \ll 1$ we can approximate the mo-

mentum equations to a geostrophic flow

$$-f_0 v = -g \frac{\partial \eta}{\partial x} \tag{5.35}$$

$$f_0 u = -g \frac{\partial \eta}{\partial y} \tag{5.36}$$

and adding these geostrophic solutions to the shallow water equations

$$-f_0 v = -g \frac{\partial \eta}{\partial x} + \beta y \frac{g}{f_0} \frac{\partial \eta}{\partial x} + \frac{g}{f_0} \frac{\partial^2 \eta}{\partial y \partial t} \tag{5.37}$$

$$f_0 u = -g \frac{\partial \eta}{\partial y} + \beta y \frac{g}{f_0} \frac{\partial \eta}{\partial y} - \frac{g}{f_0} \frac{\partial^2 \eta}{\partial x \partial t} \tag{5.38}$$

The first part of the momentum equations is that of a geostrophic flow and the remaining is the small contribution from variations induced by the ageostrophic component. The last terms will be responsible for the propagation of Rossby waves.

Using continuity and (5.37)-(5.38) we arrive to

$$\frac{\partial \eta}{\partial t} - L_d^2 \partial_t \nabla^2 \eta - \beta L_d^2 \frac{\partial \eta}{\partial x} = 0 \tag{5.39}$$

which is a leading order approximation to the potential vorticity equation describing a quasi-geostrophic flow

$$\partial_t \left(\nabla^2 \eta - L_d^{-2} \eta \right) + \beta \frac{\partial \eta}{\partial x} = 0 \tag{5.40}$$

Now we can look for Fourier type solutions in the form $\eta = \eta_0 e^{i(kx+ly-\omega t)}$

$$\boxed{\omega = -\frac{\beta k}{(k^2 + l^2) + L_d^{-2}}} \tag{5.41}$$

or alternatively

$$\omega = -\beta L_d^2 \frac{k}{1 + L_d^2 (k^2 + l^2)} \tag{5.42}$$

Evidently, on the f-plane ($\beta = 0$) the solution reduces to a geostrophic flow and no wave is allowed to propagate. The meridional gradient in f is thus the restoring force for Rossby waves.

Two possible cases can be envisaged, setting $l = 0$.

First, that of short waves, where $L \leq L_d$ and therefore $kL_d \geq 1$, for L a typical scale of the wave length and k a typical scale of the wave number. In this case the dispersion relation reduces to

$$\omega = -\beta L_d^2 \frac{k}{L_d^2(k^2)} = -\frac{\beta}{k} = -\beta L \tag{5.43}$$

Given that we are on the β-plane approximation, $\beta y \ll f_0 \rightarrow \beta L \ll f_0 \rightarrow \omega \ll f_0$, confirming the subinterial period.

Second, waves could have very long wave length $L \geq L_d$ or $kL_d \leq 1$

$$\omega = -\beta L_d^2 k = -\beta \frac{L_d k^2}{k} \ll -\frac{\beta}{k} = -\beta L \tag{5.44}$$

and therefore $\omega \ll f_0$. The period of Rossby waves is always subinertial.

Phase and group speeds

Keeping $l = 0$ and using the following scaling

$$\omega = \hat{\omega} \beta L_d \tag{5.45}$$

$$\kappa = \frac{\hat{\kappa}}{L_d} \tag{5.46}$$

The dispersion relation takes the form

$$\hat{\omega} \beta L_d = -\beta L_d^2 \frac{\hat{\kappa}/L_d}{1 + L_d^2 \frac{\hat{\kappa}^2}{L_d^2}} \tag{5.47}$$

$$\hat{\omega} = -L_d \frac{\hat{\kappa}/L_d}{1 + \hat{\kappa}^2} = -\frac{\hat{\kappa}}{1 + \hat{\kappa}^2} \tag{5.48}$$

and for $|\hat{\kappa}| = -1$ the frequency takes the value $|\hat{\omega}| = -0.5$ (see Fig. 5.3). The phase speed of Rossby waves is easily computed (with $l = 0$)

$$\boxed{c_p = \frac{\omega}{k} = \frac{-\beta}{k^2 + L_d^{-2}}} \tag{5.49}$$

it is always negative and larger for long waves .

For long Rossby waves, the phase velocity is approximated by

$$\boldsymbol{c_p} = \omega/\kappa = -\beta L_d^2 \tag{5.50}$$

which is strictly westward even if $l \neq 0$.

The phase speed is always negative but is the energy flux always directed westward? this does not seem possible.

The group velocity is obtained by differentiating the dispersion relation

$$c_g = (\frac{\partial \omega}{\partial \kappa}, \frac{\partial \omega}{\partial l}) = \beta(\kappa^2 - l^2 - L_d^{-2}, 2\kappa l) / (\kappa^2 + l^2 + L_d^{-2})^2 \qquad (5.51)$$

or, by setting $l = 0$

$$c_g = \frac{\beta \kappa^2 - \beta L_d^{-2}}{(\kappa^2 + L_d^{-2})^2} \qquad (5.52)$$

Set $k = 0$ and group and phase velocities are equal $c_p = c_g = -\beta L_d^2$ (see Fig. 5.3).

If $l \neq 0$ the dispersion relation takes the form of the dispersion diagram in Fig. 5.4. The group velocity, the gradient of the frequency in wavenumber space, is normal to the contours and inversely proportional to the spacing between contours. The hyperbola separating waves with eastward and

Figure 5.3: *Rossby wave dispersion relation, phase and group speeds.*
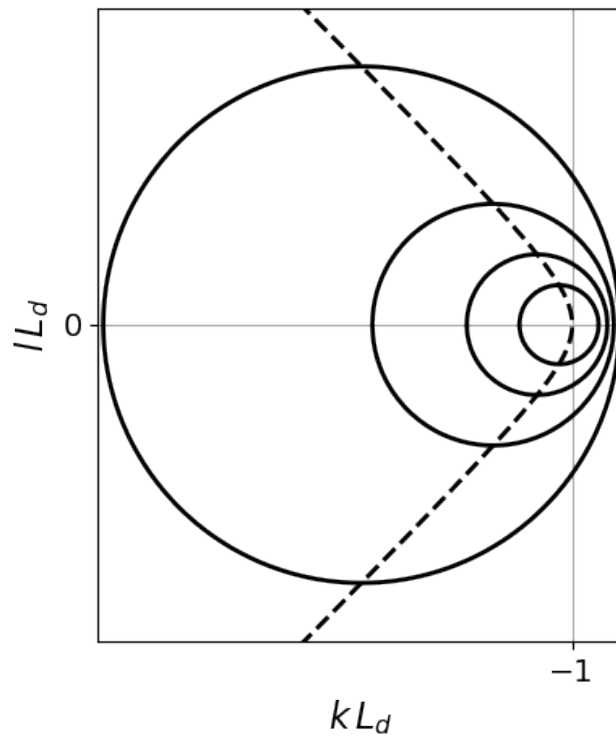
Figure 5.4: *Rossby wave dispersion diagram. Contours are of frequency in units of βL_d. The group velocity, the gradient of the frequency in wavenumber space, is normal to the contours and inversely proportional to the spacing between contours. The hyp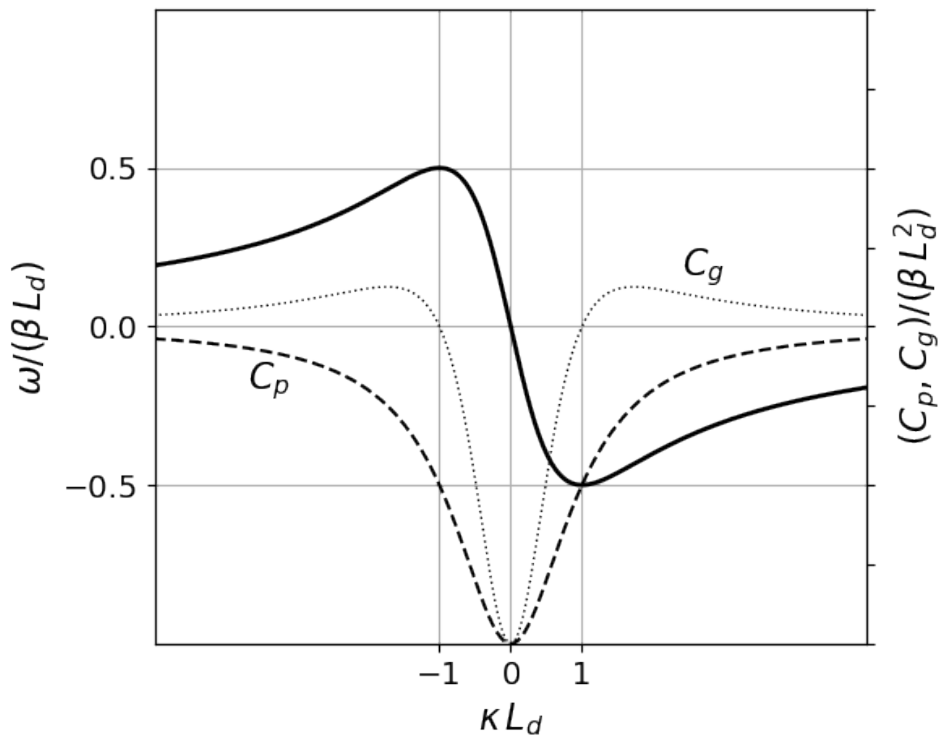erbola separating waves with eastward and westward group velocity is shown by the dashed line and is $\kappa^2 = l^2 + L_d^{-2}$. Frequency contours reduce to a single point when $\omega = 0.5\beta L_d$ and $\kappa = L_d$.*

westward group velocity is shown by the dashed line and is $\kappa^2 = l^2 + L_d^{-2}$. Frequency contours reduce to a single point when $\omega = 0.5\beta L_d$ and $\kappa = L_d$.

5.3.1 Quasi-geostrophic Rossby waves

The discovery of Planetary waves by the solution of Laplace's equation as the second class waves dates back to the late nineteenth century by *Hough* (1897). Later C.G. Rossby pointed out the characteristic of these waves, hence they carry his name and are also called Rossby waves.

Since then, Rossby wave theory is well known (*Gill*, 1982; *Dickinson*, 1978; *Leblond and Mysak*, 1981) and is usually applied to an ocean at rest with uniform depth.

Rossby waves owe their existence to the meridional variation of the Coriolis force (the β effect) and therefore propagate following an east-west waveguide, as the conservation of potential vorticity is their restoring force.

These kinds of waves, whose frequencies are considerably lower than those of gravity waves and are subinertial ($\omega \ll f$), are also sometimes called quasigeostrophic waves, with a dynamic evolution depending on the departure from geostrophy.

The generation of these waves is still not completely understood but the main forcing is wind stress and buoyancy forcing, though the latter is thought to act in a minor way, and upwelling-downwelling on the eastern boundary (*Leblond and Mysak*, 1981; *Gill*, 1982).

In order to obtain and describe the Rossby wave solutions, we consider the linearised quasi-geostrophic (QG) potential vorticity equation (*Pedlosky*, 1987):

$$\partial_t q_i + J(\psi_i, q_i) = 0, \tag{5.53}$$

where $J(a, b) = a_x b_y - a_y b_x$ is the Jacobian and ψ the stream function. Introducing a plane wave solution of the type $\psi = \Psi e^{i(kx+ly-\sigma t)}$ into (5.53) we naturally obtain the dispersion relation for Rossby waves, showing their basic characteristics (*Leblond and Mysak*, 1981; *Gill*, 1982)

$$\omega = -\frac{\beta k}{(k^2 + l^2) + L_d^{-2}},$$

where ω is the frequency, k and l are the horizontal wavenumber, β is the meridional variation of the Coriolis parameter and L_d the Rossby radius (C^2/f^2). It is clear that Rossby waves have westward phase velocities (of the order of a few cm/s) and that these are increasing toward the equator (where equatorial wave theory holds) with a maximum speed $c_x = \beta L_d^2$; the group velocities, C_g, in the case of long waves, are westward and the waves are nondispersive ($C_g = c_x$), while short waves propagate eastwards but with very slow speeds.

Another remarkable feature of the planetary wave dispersion relation is that not all frequencies exist, with a cutoff frequency at $\frac{1}{2}\beta L_d$.

Besides the horizontal problem, the vertical one is of great importance. Using a normal mode representation (*Leblond and Mysak*, 1981), separating the vertical and horizontal structure, we find an infinite set of solutions (or normal modes). The zeroth is the barotropic one, almost vertically independent and very rapid; the other solutions, or modes, are called baroclinic with decreasing phase speeds and increasing oscillation in the vertical. A first-mode baroclinic Rossby wave takes months to years to cross an ocean basin, depending on the latitude.

A 3-layer model

In the case of a 3-layer ocean, the potential vorticities are given by

$$
\begin{aligned}
q_1 &= \nabla \psi_1 + \beta y - F_{11}(\psi_1 - \psi_2) \\
q_2 &= \nabla \psi_2 + \beta y - F_{21}(\psi_2 - \psi_1) - F_{22}(\psi_2 - \psi_3) \\
q_3 &= \nabla \psi_3 + \beta y - F_{32}(\psi_3 - \psi_2),
\end{aligned}
$$

where $F_{m,n} = f_0^2 / (H_m g_n')$ and g_i' and H_i are the reduced gravities and layer depths respectively.

For this 3-layer system, substitution of a plane wave solution leads to a generalised eigenvalue problem of the form $A\Psi = \omega B\Psi$, or explicitly:

$$
\begin{bmatrix} \beta_1 & 0 & 0 \\ 0 & \beta_2 & 0 \\ 0 & 0 & \beta_3 \end{bmatrix} \begin{bmatrix} \psi_1 \\ \psi_2 \\ \psi_3 \end{bmatrix} = \omega \begin{bmatrix} -G_1 & 1 & 0 \\ G_2 & -G_3 & 1 \\ 0 & 1 & -G_4 \end{bmatrix} \begin{bmatrix} \psi_1 \\ \psi_2 \\ \psi_3 \end{bmatrix},
$$

where $\beta_1 = (k\beta)/F_{11}$, $\beta_2 = (k\beta)/F_{22}$, $\beta_3 = (k\beta)/F_{32}$ and $G_1 = (K^2 + F_{11})/F_{11}$, $G_2 = F_{21}/F_{22}$, $G_3 = (K^2 + F_{21} + F_{22})/F_{22}$, $G_4 = (K^2 + F_{32})/F_{32}$, where $K^2 = k^2 + l^2$.

The solution of the system is plotted in Fig.5.5 and it describes the basic properties of Rossby wave propagation. In fact, for the 3-layer system, the dispersion relation is found on the upper panel and both phase and group velocities on the bottom panel of Fig.5.5. We can distinguish the barotropic mode with increasing frequencies towards long wavelengths, very fast phase speeds and positive (eastward) group velocities. The baroclinic modes have smaller frequencies, their phase velocities are always westward but their group velocities turn from westward to eastward at the point of maximum frequency

$$
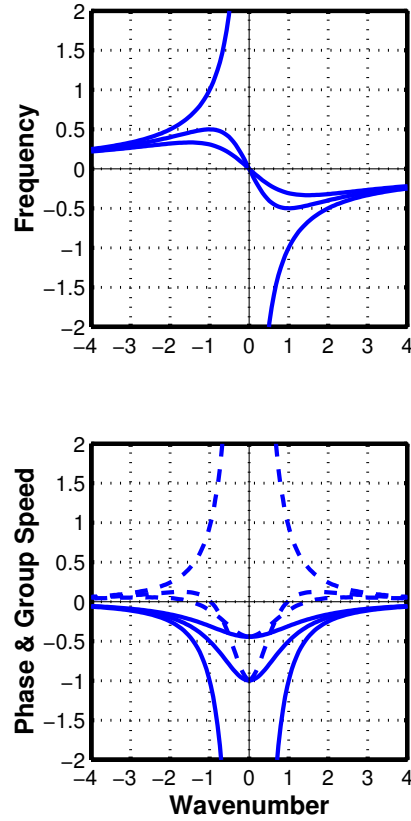kL_d = |1| \text{ and } \omega(\beta L_d)^{-1} = |0.5| \tag{5.54}
$$

Figure 5.5: Upper panel: the dispersion relation for the barotropic and first two baroclinic modes of the 3-layer QG ocean. Shown are values of both positive and negative wavenumbers. The wavenumber is scaled by the deformation radius L_d and the frequency by βL_d; the meridional wavenumber l is set to zero. The first baroclinic mode frequency reaches a maximum at $\omega_{max} = \beta L_d/2$, i.e. $\omega_{max} = |0.5|$. Lower panel: phase (solid lines, $c_x = \omega/k$) and group (dashed lines, $Cg_x = \partial\omega/\partial k$) velocities of the barotropic and first two baroclinic modes, scaled by βL_d^2.

where the group velocity is zero. Therefore, long baroclinic waves direct their energy westward while short waves direct it eastward. This means that, in the limit of long wavelengths, the phase and group speeds are the same and the waves are nondispersive. On the other hand, for short waves phase and group speeds differ and the waves are dispersive. The maximum group and phase velocity ($C_x = Cg_x = -\beta L_d^2$) are attained for long waves, they are to the west and can be found on the axis origin of the dispersion relation.

The system could be extended to an N-layer or even to a continuously stratified ocean. In every case, the solutions obtained are one barotropic and N-1 baroclinic modes of decreasing phase speeds. This method of analysis is called the *normal modes method*, in which the ocean is decomposed into an infinite set of solutions (or modes): one barotropic (or external) and the remaining baroclinic (or internal).

5.3.2 Rossby waves in observations and models

Chelton and Schlax (1996) presented for the first time the results of these observations identifying clear Rossby waves signals (Fig.5.6) and common features like the increase of phase speed in the western basin, the effect of bottom topography, eastward propagating equatorially trapped Kelvin waves and pulses related to El Niño events.

As anticipated, the advent of satellite altimetry brought a powerful tool to describe Rossby waves in the real ocean. The TOPEX/POSEIDON (T/P) altimeter is able to detect long baroclinic planetary waves unambiguously over the entire world ocean (Fig. 5.7).

The T/P altimetry data reveal the sea surface height anomalies (SSHA) and to analyse this data time-longitude plots, known as Hovmöller diagrams, are used, which clearly show Rossby waves as diagonal alignments of crests and troughs moving westward. An example of this is given in Fig.5.7, where SSHA data from the Indian Ocean are plotted for the latitude 20°S from 1993 till May 2005; in the left panel the row data are plotted while in the right panel the data have been filtered with a westward filter to better show Rossby wave propagation.

By this technique, Rossby waves are detected in all basins and altimetry has been used also in the Southern Ocean (*Hughes*, 1995) where two dynamical systems were found, a supercritical and a subcritical one with
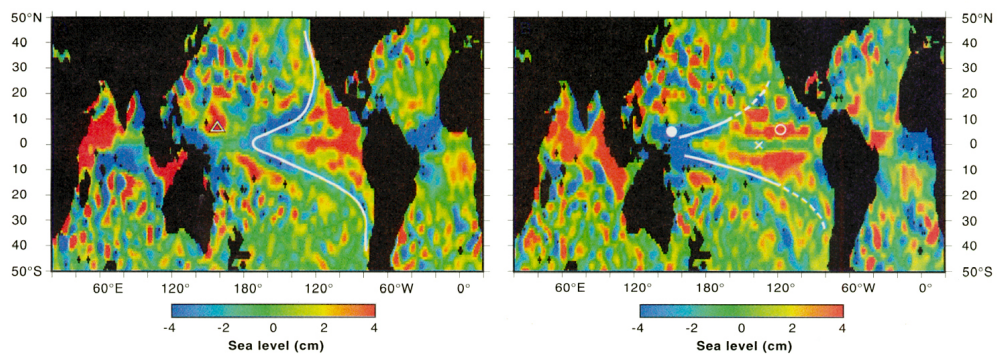
Fig. 4. Global maps of filtered sea level (*22*) on (**A**) 13 April 1993 (cycle 21) and 3.5 months later on (**B**) 31 July 1993 (cycle 32). White lines identify a westward-propagating, β-refracted Rossby wave trough. The time evolutions of the equatorial Kelvin wave trough (X), the Rossby wave crests (open triangle and open circle), and the Rossby wave trough (solid circle) can be traced from the times and locations of the matching symbols in Fig. 3. These two maps are frames from an animation of TOPEX/POSEIDON data that is available on the World Wide Web at http://topex-www.jpl.nasa.gov/contrib/chelton/rossby/.

Figure 5.6: Sea surface height anomalies showing the propagation of planetary waves in the Pacific Ocean. Also clear is the *β*-effect inducing larger phase speeds towards the equator [from *Chelton and Schlax* (1996)].
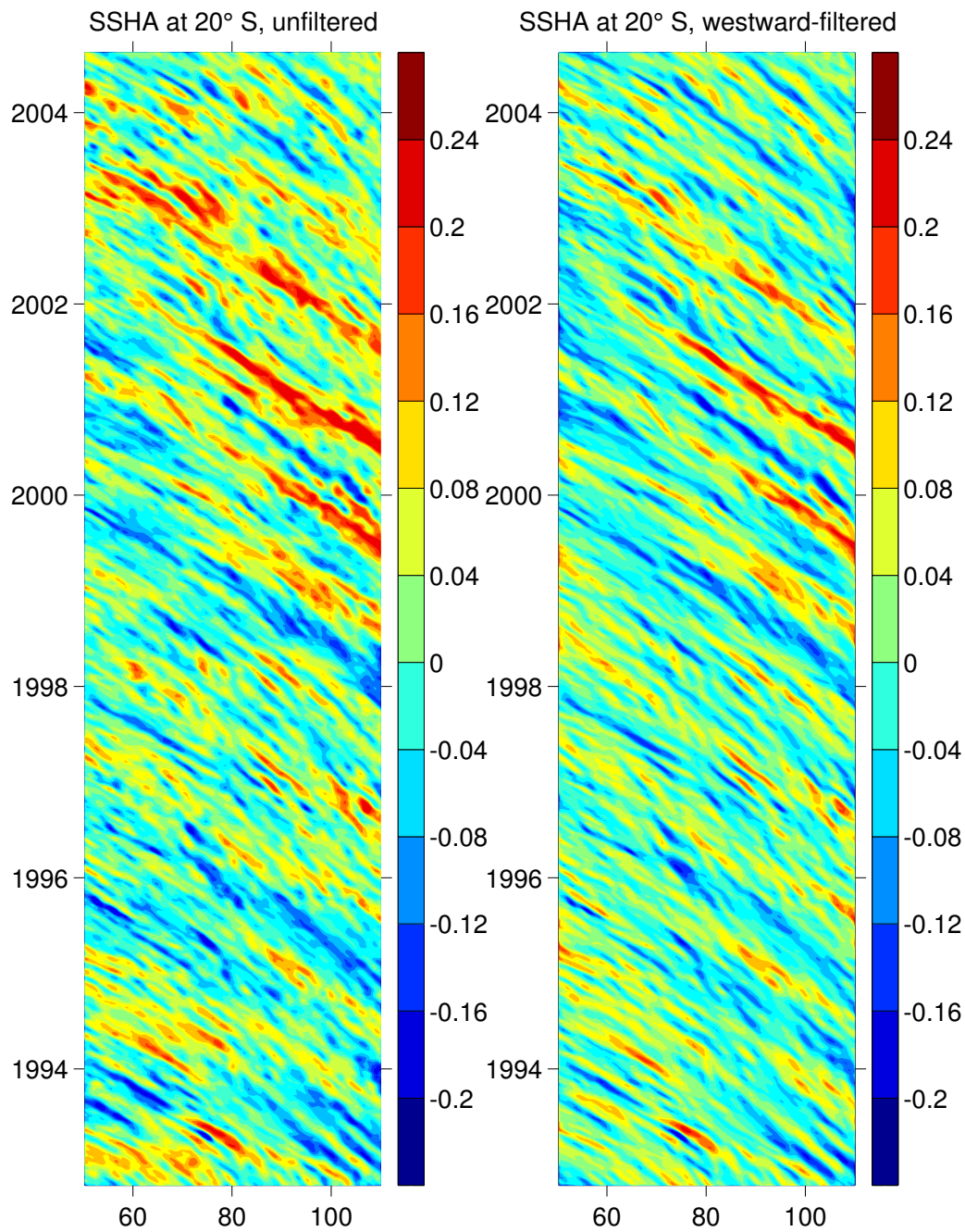
Figure 5.7: Time-longitude plot of the sea surface height anomalies (in meters) in the Indian Ocean at 20^oS. On the left panels, the original altimeter data. On the right panel, the corresponding westward-filtered signature. There is a clear evidence of crests and troughs propagating westward with a biannual period (Courtesy of P. Cipollini).

respect to Rossby waves, the first one being able to advect the waves eastward.

Rossby waves are also detected by other sensors like the Along-track Scanning Radiometer (ATSR) in sea surface temperature (SST) and, recently, SeaWiFS in ocean colour.

As an example, *Hill et al.* (2000) used a SST record to compute Rossby wave phase speeds finding good agreement with *Killworth et al.* (1997). They were also able to detect topographic effects such as those predicted by *Killworth and Blundell* (1999).

One of the latest applications has been using ocean colour. *Cipollini et al.* (2001) found for the first time Rossby waves in SeaWiFS datasets, although they are neither very clear nor ubiquitous. A preliminary explanation for this detectability was in term of the vertical displacements of the thermocline associated with the Rossby wave and subsequently changes in the nutrient upwelling.

Computing Rossby wave phase speeds

In order to compute the gravity wave phase speeds and Rossby radii of deformation we need to solve the generalized eigenvalue problem of Sturm-Liouville form:

$$\frac{d^2\phi}{dz^2} + \frac{N^2(z)}{C^2}\phi = 0 \tag{5.55}$$

subject to the following boundary conditions

$$\phi = 0 \qquad at \quad z = 0, -H \tag{5.56}$$

where H is the local mean water depth and N^2 is the Brunt-Väisälä frequency, computed from the potential density method as outlined in *Chelton et al.* (1998). Solution of the system (5.55)-(5.56) leads to an infinite set of eigenvalues C_m^{-2}, the baroclinic gravity wave phase speeds, and corresponding eigenfunctions ϕ_m.

However, *Chelton et al.* (1998) showed that a WKB approximation of the gravity wave speed is generally in good agreement with the solution given by the system (5.55)-(5.56), and this is:

$$C_m \approx C_m^{WKB} = (m\pi)^{-1} \int_{-H}^{0} N(z)\mathrm{d}z, \quad m \geq 1. \tag{5.57}$$

Then, within the extratropical regions, the Rossby radii of deformation are simply found by applying

$$L_d^m = \frac{C_m}{|f(\theta)|}. \tag{5.58}$$
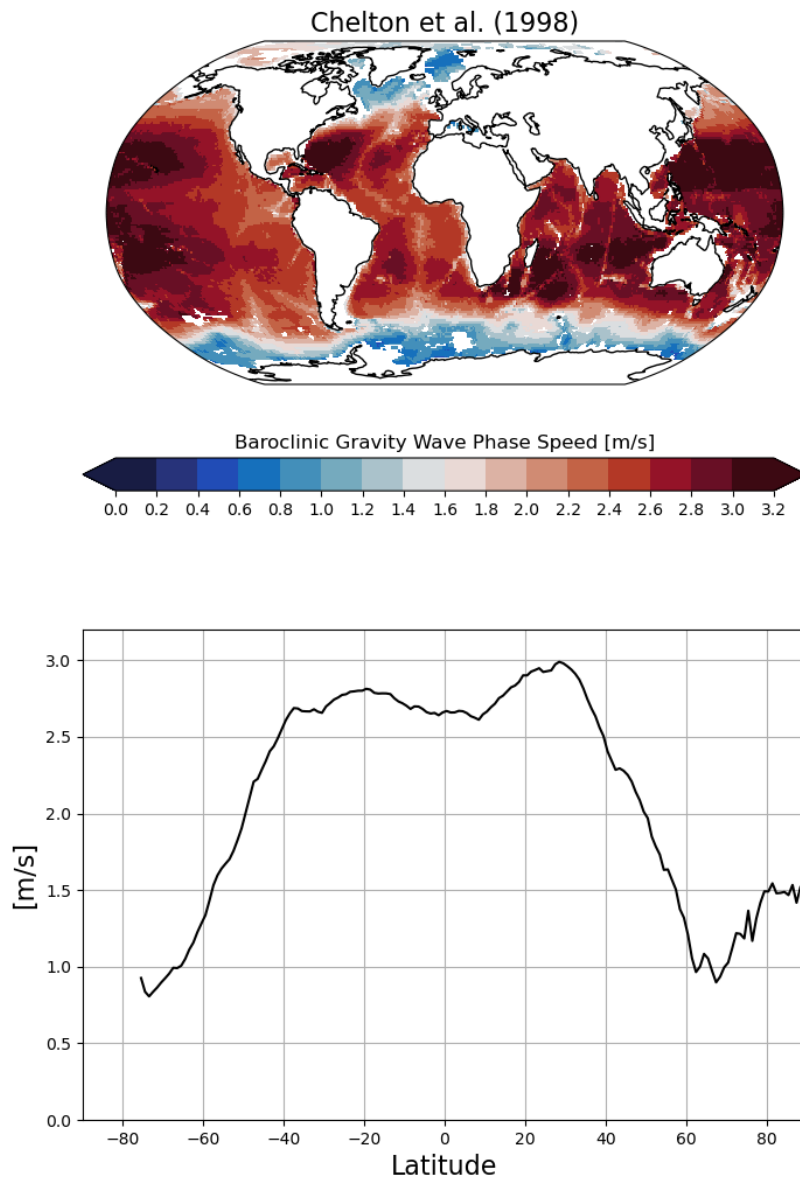
Figure 5.8: *A global contour map of the baroclinic gravity wave phase speed [from Chelton et al., 1998] and its zonal mean.*
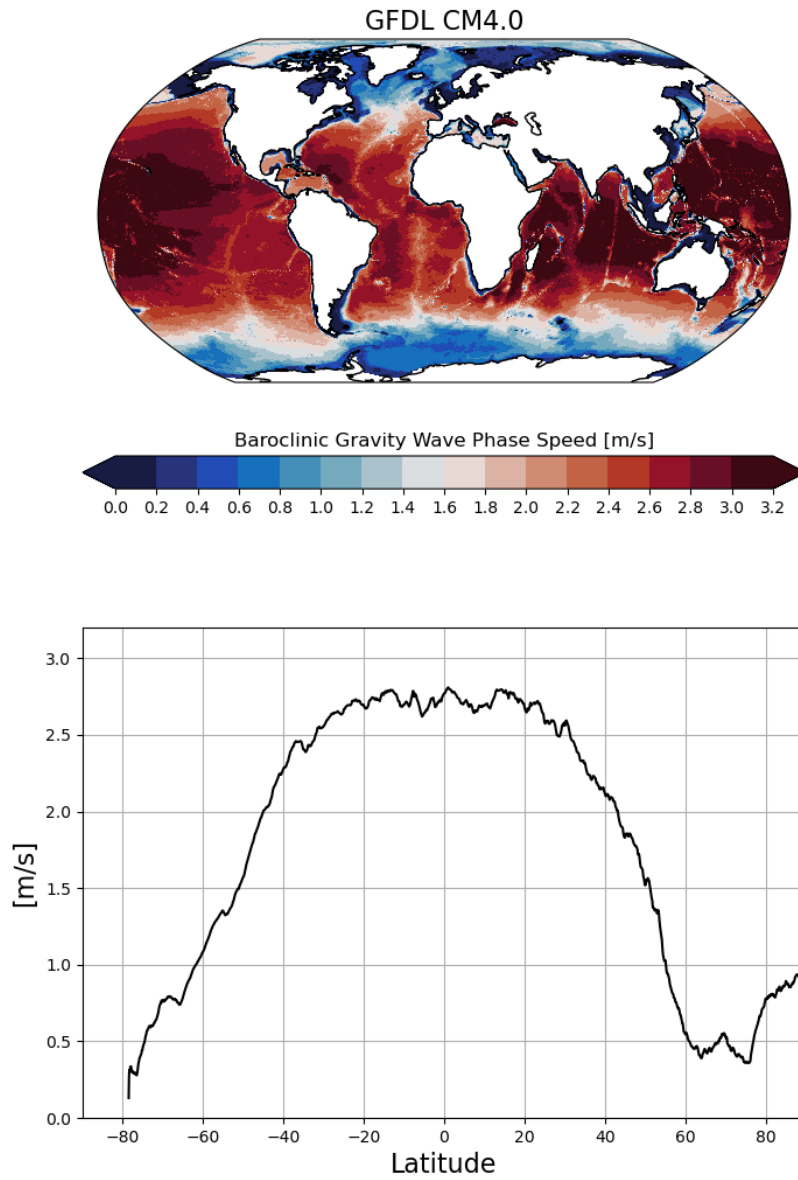
GFDL CM4.0

Baroclinic Gravity Wave Phase Speed [m/s]

Figure 5.9: *As in Fig.5.8 but from the GFDL-CM4.0 model under historical conditions for years 2010-2014.*

We will be focusing on extratropical regions only ($|\theta| \geq 10°$), leaving the equatorial wave dynamics response aside.

Now, we can compute the unperturbed long Rossby wave speeds $c_m = -\beta C_m^2 / f^2$.

Since model data provide potential density ρ_θ, we can compute the stratification directly from the potential density method of the non-equispaced vertical levels k:

$$N^2(z) = -g/\rho_0 \left[\rho_\theta(z) - \rho_\theta(z+1)/(\delta k(z) - \delta k(z+1)) \right] \tag{5.59}$$

The gravity wave speed can be obtained from two different method. First, as a good approximation, we can infer it from the WKB method as suggested in *Chelton et al.* (1998):

$$C_m = (m\pi)^{-1} \int_{-H}^{0} N(z)\mathrm{d}z, \quad m \geq 1. \tag{5.60}$$

After obtaining N^2 and C_m, the Rossby radii of deformation are readily computed as

$$L_d^m = \frac{C_m}{|f(\theta)|}, \quad |\theta| \geq 5° \tag{5.61}$$

$$L_d^m = \frac{C_m}{2|\beta(\theta)|}, \quad |\theta| \leq 5°. \tag{5.62}$$

or, for the extratropical band: $L_d^m = (|f| m\pi)^{-1} \int_{-H}^{0} N(z)\mathrm{d}z$

For the linear, long and extratropical waves, we can simply compute the Rossby wave phase speed as

$$c_m = -\beta (L_d^m)^2 \tag{5.63}$$
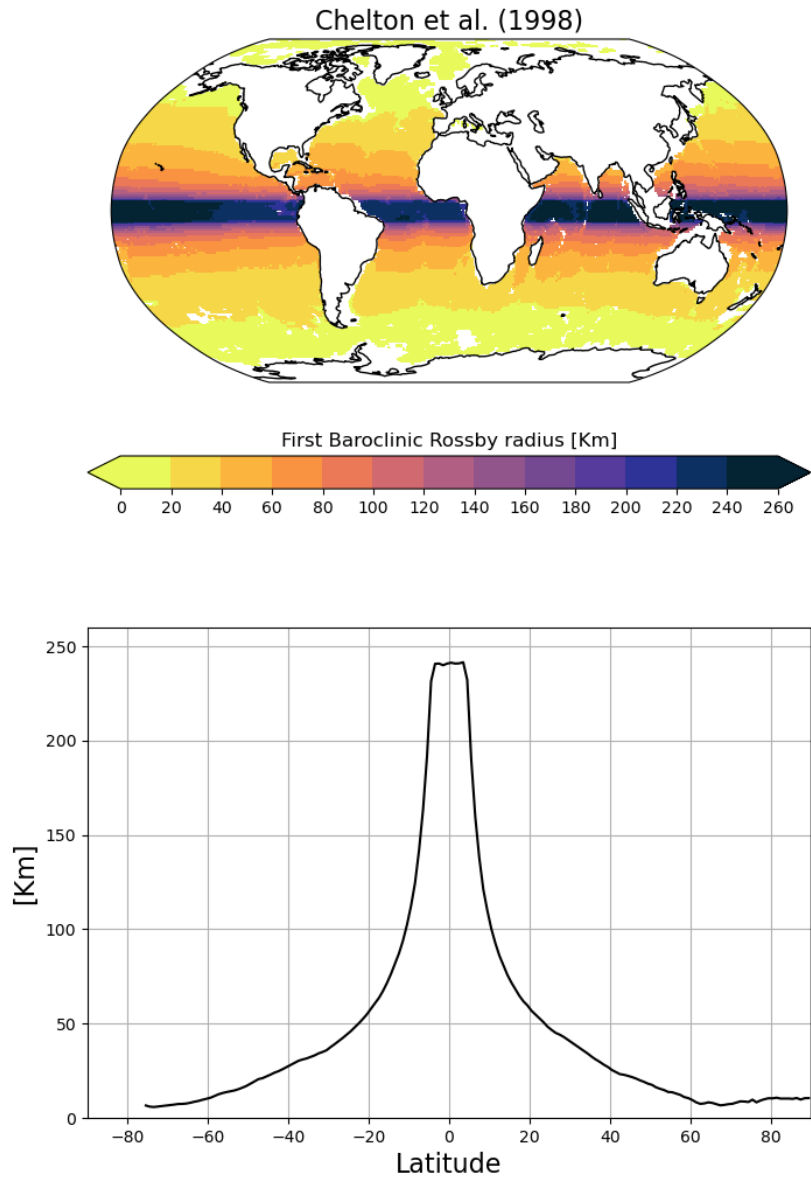
Figure 5.10: *A global contour map of the baroclinic Rossby radius of deformation and its zonal mean. [data from Chelton et al., 1998]*
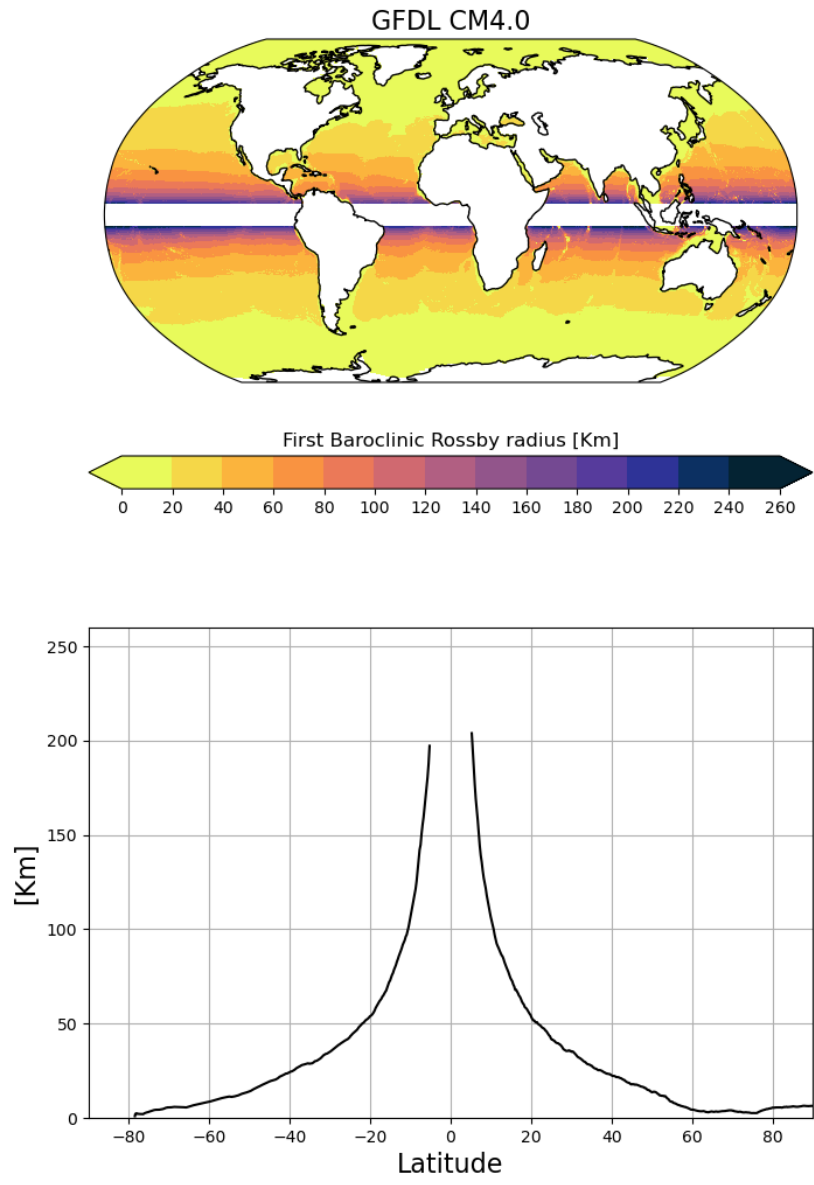
Figure 5.11: *As in Fig.5.10 but from the GFDL-CM4.0 model under historical conditions for years 2010-2014.*

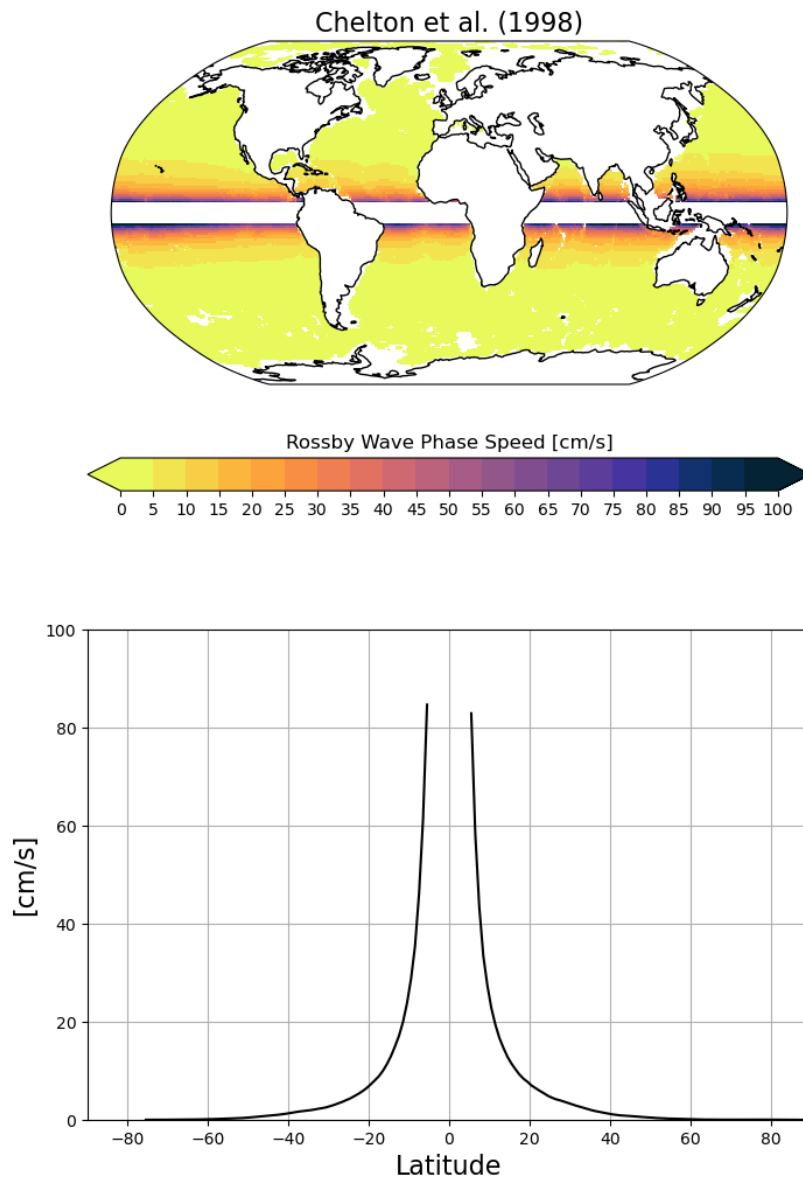Figure 5.12: *A global contour map of the baroclinic Rossby wave phase speed and its zonal mean. [data from Chelton et al., 1998]*
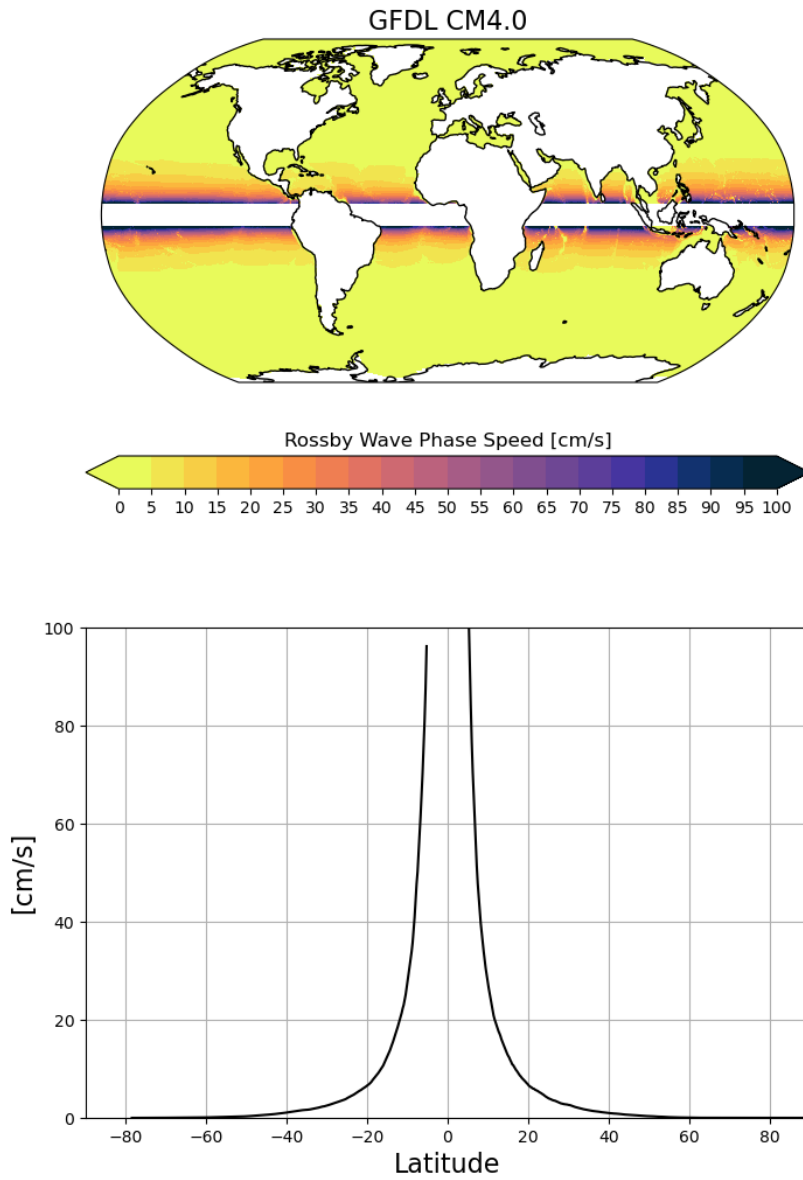
GFDL CM4.0

Figure 5.13: *As in Fig.5.12 but from the GFDL-CM4.0 model under historical conditions for years 2010-2014.*

Kelvin and Rossby waves in the general oceanic adjustment

The importance of Rossby waves in the spinup of the ocean and in the adjustment of the ocean interior was also recently shown by *Johnson and Marshall* (2002). They proposed a theory for surface Atlantic response to thermohaline variability; in their work they study the reaction of the ocean to a perturbation of the rate of deep water formation at high latitudes. These changes initiate Kelvin waves which propagate along the western boundary, in a similar response of that demonstrated by *Kawase* (1987), and then cross the basin as equatorial Kelvin waves until they reach the eastern boundary where they propagate northwards and southwards. The final part of the response is the radiation of Rossby waves from the eastern boundary, communicating the thermocline displacement to the ocean interior which is clearly illustrated with a series of snapshots (Fig. 5.14).
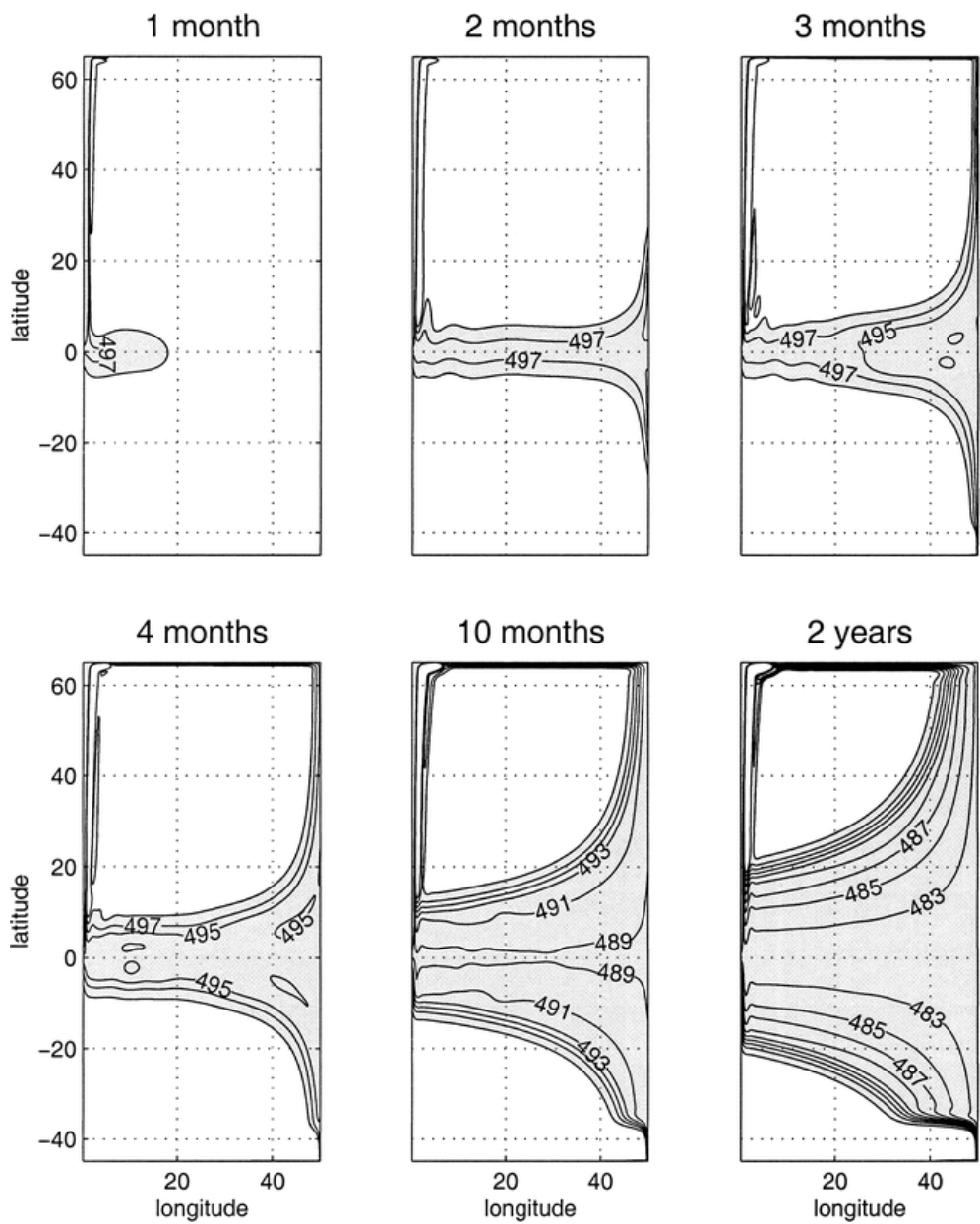
Figure 5.14: *Surface layer thickness after a thermohaline overturning of 10 Sv is switched on at time t = 0 in the northwest corner of an ocean initially at rest. There is no wind forcing, and the surface layer is initially 500 m deep. The contour interval is 2 m, and thicknesses less than 499 m are shaded. Note that the thickness anomaly on the western boundary is much greater than that in the interior. [from Johnson and Marshall, JPO2022]*

What will happen in the future?

Saenko (2006) recently showed that, within the IPCC models, there is clear evidence of an increase of the first baroclinic Rossby radius with increasing oceanic stratification in the warmer climate. The changes range from 15 to 20% depending on the model and latitude. This would imply a greater length scale for mesoscale eddies and modified characteristics for oceanic Rossby waves, whose speed is proportional to the squared baroclinic Rossby radius of deformation. Also, the adjustment time scale in the ocean would decrease as well as in any ocean-atmosphere climate variability process where Rossby waves set the dominant period. Equally important, if not more in certain basins, is the change in the background baroclinic mean flow and its subsequent effect on the propagation of Rossby waves. This effect was not considered in *Saenko* (2006).

Modifications to the background stratification and mean flows are observed between pre-industrial and climate-change runs in the GFDL CM4 model (Fig.5.15 and Fig.5.16).

The effects of an increased stratification on the Rossby radius of deformation and gravity wave speed have been the subject of recent studies (*Saenko*, 2006). However, the question of the quantification of these effects on the Rossby wave activity, as well as the changes induced by a modified background mean flow, is still unanswered.

We expect to show considerable alterations to the Rossby wave phase speeds at different latitudes, leading to important changes in the ocean adjustment time-scale and coupled ocean-atmosphere interactions where Rossby waves set the clock (Fig.5.19 and Fig.5.20).

Figure 5.15: *The baroclinic gravity wave phase speed computed from the GFDL-CM4.0 model under historical conditions for years 2010-2014.*

Figure 5.16: *The baroclinic gravity wave phase speed computed from the GFDL-CM4.0 model for the future scenario SSP585.*

Figure 5.17: *The Rossby radius computed from the GFDL-CM4.0 model under historical conditions for years 2010-2014.*

Figure 5.18: *The Rossby radius computed from the GFDL-CM4.0 model for the future scenario SSP585.*
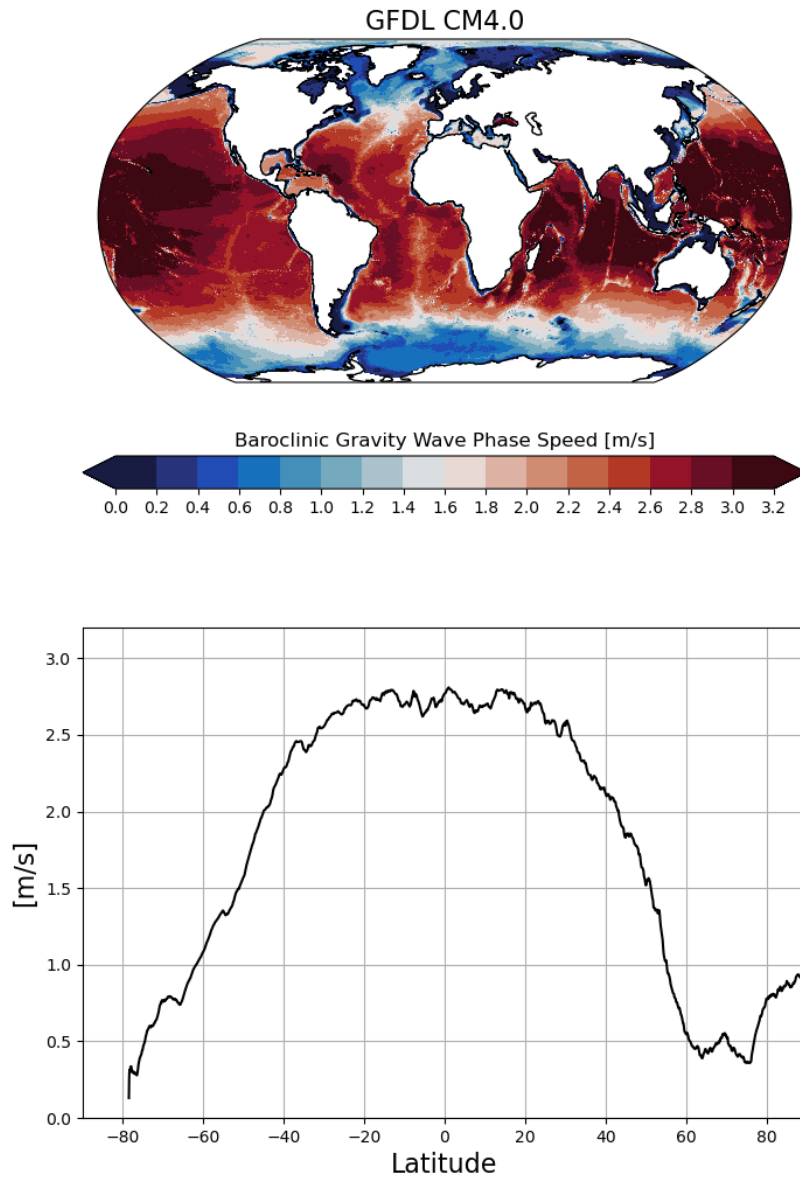
Figure 5.19: *The baroclinic Rossby wave phase speed computed from the GFDL-CM4.0 model under historical conditions for years 2010-2014.*
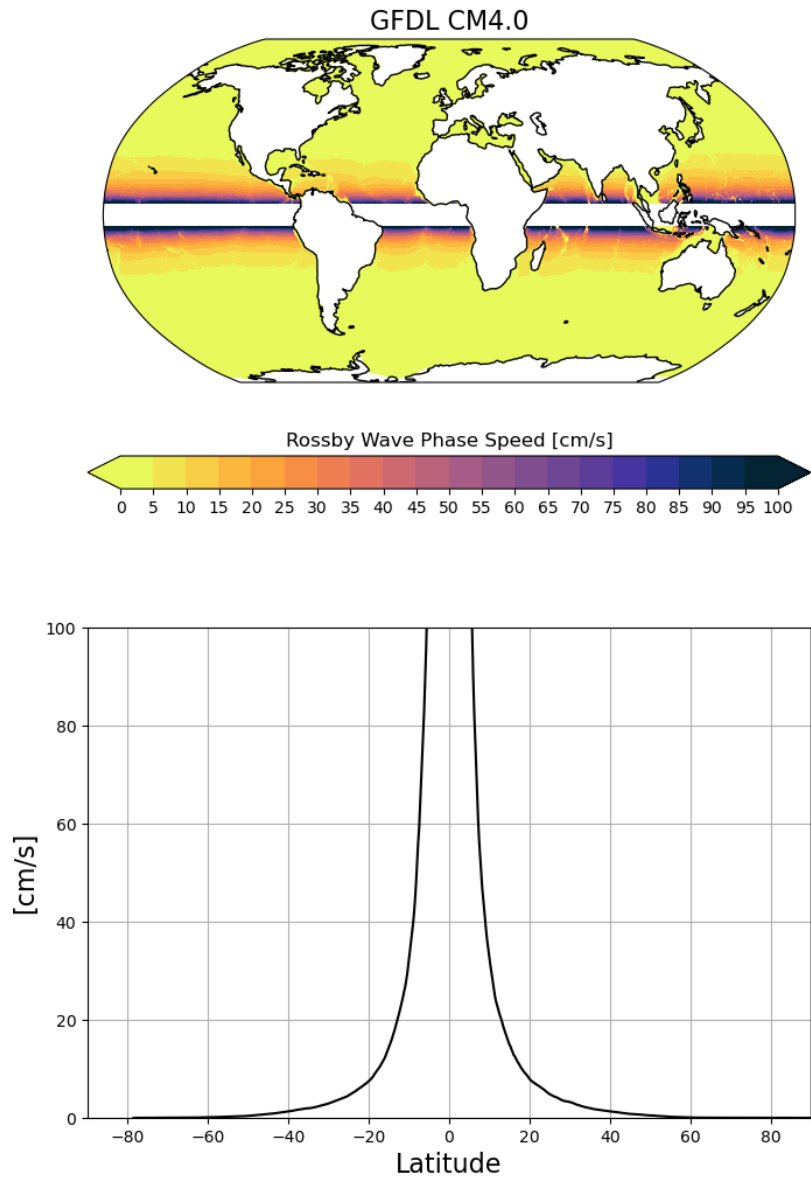
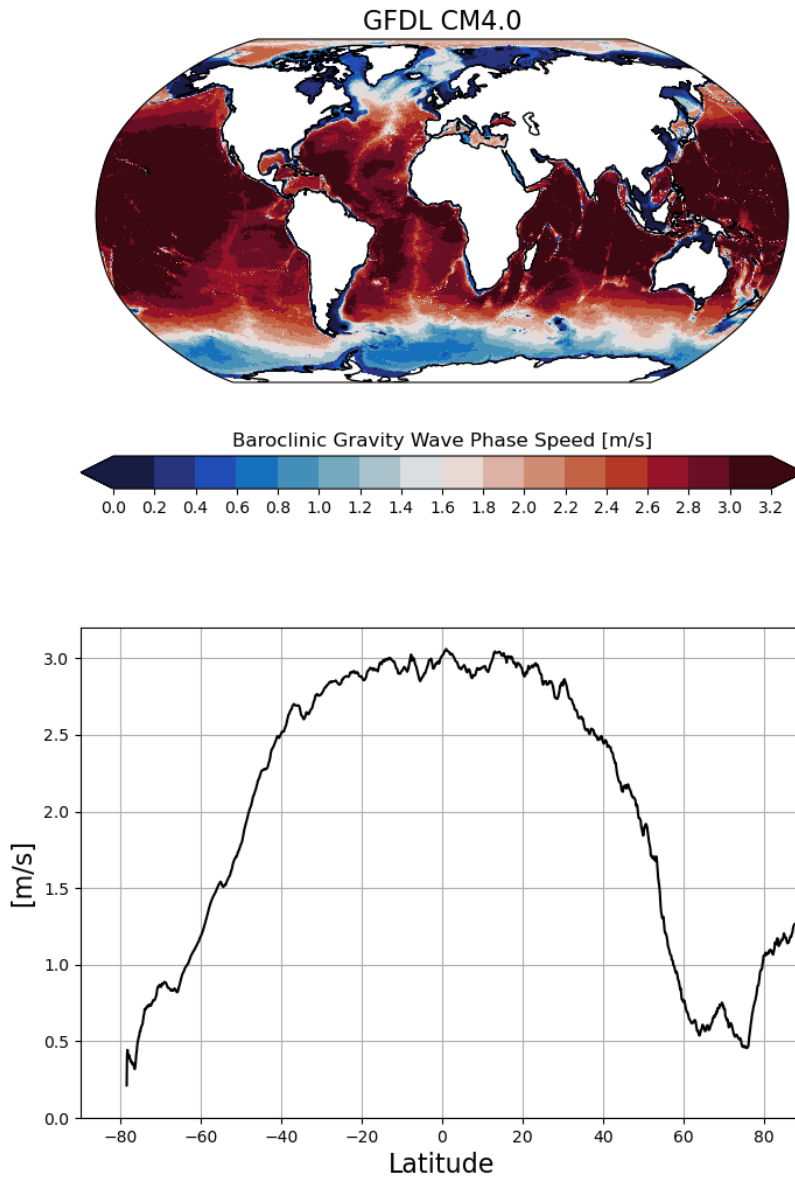**GFDL CM4.0**

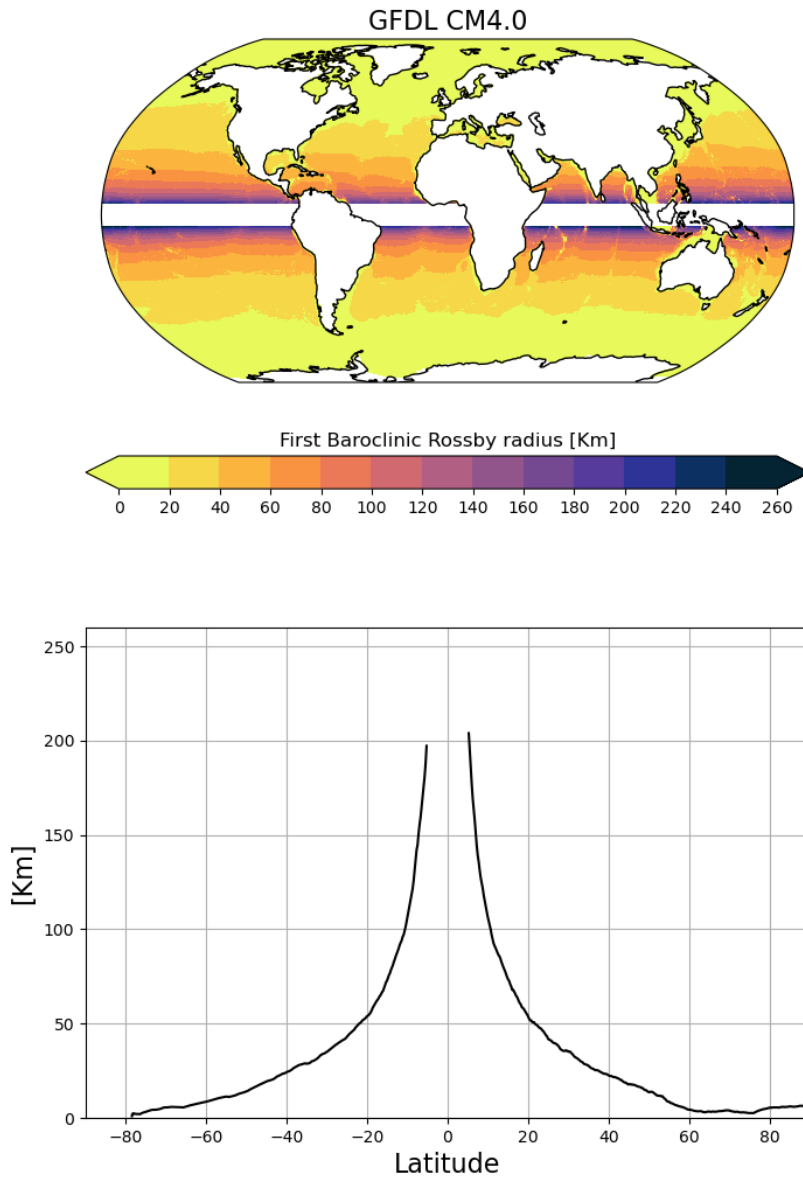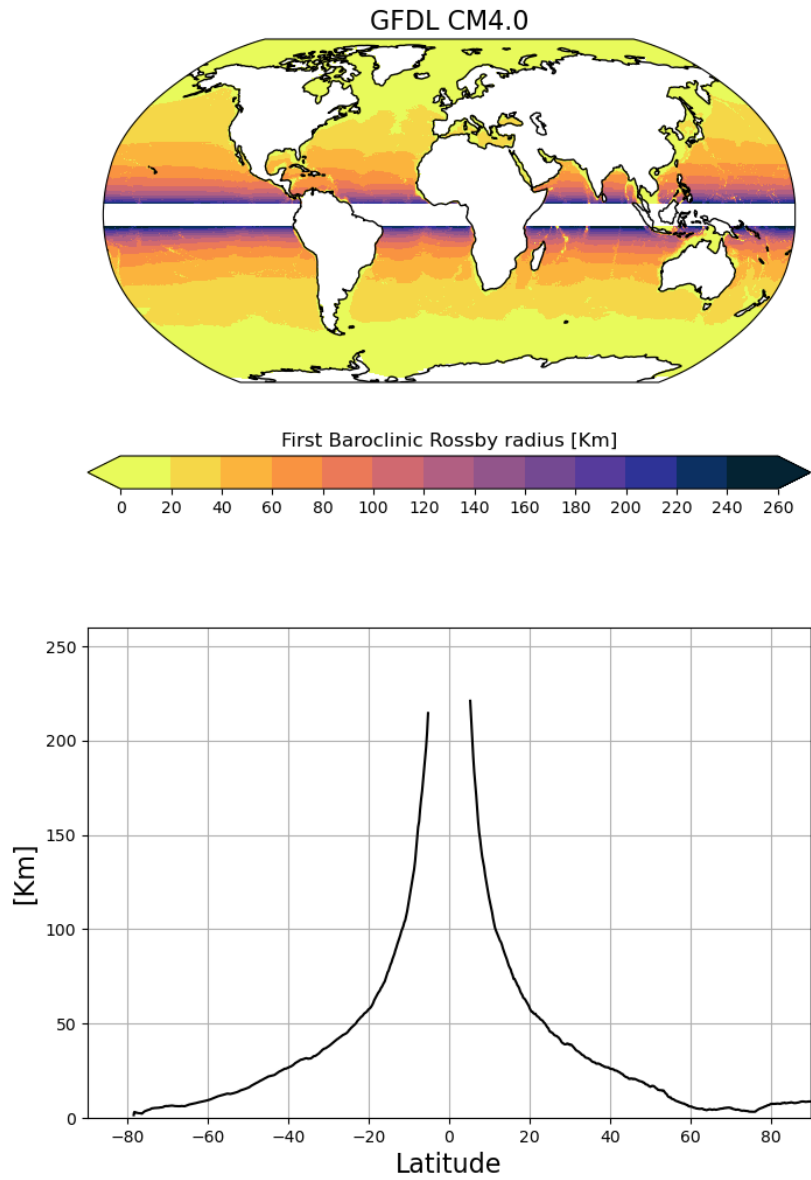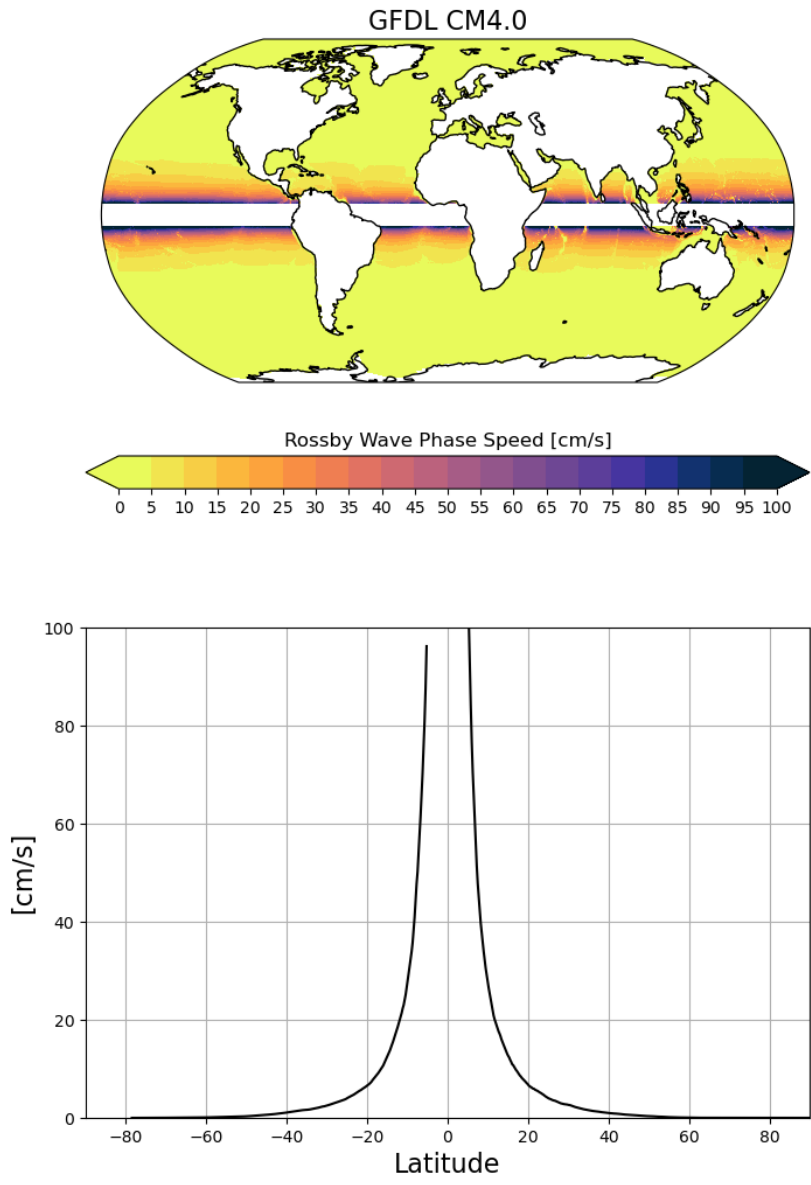Figure 5.20: *The baroclinic Rossby wave phase speed computed from the GFDL-CM4.0 model for the future scenario SSP585.*

Chapter 6

Frictional Dynamics

So far we have dealt with frictionless flows, where the dominant balance is between the Coriolis and pressure gradient forces. That was shown to be a rather good approximation for flows away from boundaries (topography, surface of the ocean, side boundaries, etc.) but this balance does not hold anymore when a boundary is approached, and frictional forces become important. The region where frictional terms have to be taken into account is called a *boundary layer* (see Fig.6.1). Here we will consider the following:

- The boundary layer is Boussinesq.

- The boundary layer has a finite depth, δ, that is less than the total depth of the fluid, H. The depth is given by the level at which frictional stresses vanish. Within the boundary layer, frictional terms are important, whereas geostrophic balance holds beyond it.

- Nonlinear time-dependent terms in the equations of motion are negligible, hydrostasy holds in the vertical, and buoyancy is constant, not varying in the horizontal.

In atmosphere and ocean dynamics, where the focus is on rapidly rotating turbulent fluids, this boundary layer is called *Ekman layer*.
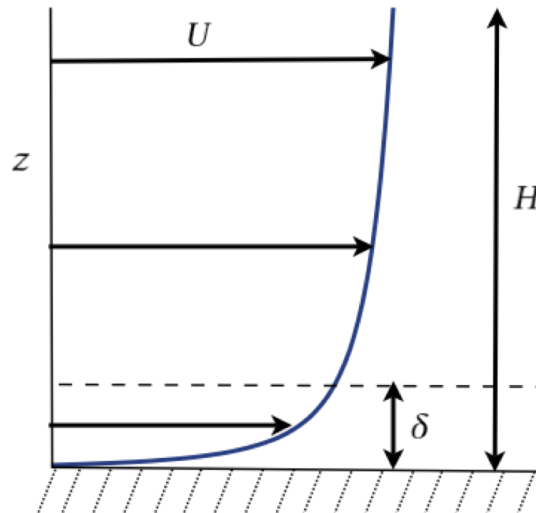
Figure 6.1: *An idealized boundary layer. The boundary layer has thickness δ, within a typical vertical scale H and typical velocity U, which varies rapidly within the boundary layer in order to satisfy the rigid lid boundary condition. [from Vallis (2006)]*

The Ekman Layer
The development of the theories for the wind-driven circulation actually has as a foundation the discovery of the so-called Ekman layer and its circulation. In 1898, the polar explorer Nansen observed that icebergs in the Arctic drifted in a direction to the right of the direction of the surface winds, roughly bewteen 20° and 40° to right of the wind stress. This qualitative observation can be explained by the presence of frictional forces. In fact, wind force applied to the surface of the ocean will try to transmit momentum in the same direction. However, as soon as the fluid starts to move, the Coriolis force will come into action deflecting its movement to the right. Importantly, there is also a frictional force within the fluid that will exert some resistance to this movement, and its direction is opposite to the direction of the fluid. The final balance between wind force, Coriolis and frictional forces, will determine the actual direction and velocity of the fluid, which will be to the right of the wind direction in the northern hemisphere.
As we shall see later, Ekman explained quantitatively how the rotation of the earth was responsible for the deflection of the current which Nansen observed.

6.1 Equations of motion

Let us now include frictional effects in our equations of motion

$$\frac{\mathrm{D}u}{\mathrm{D}t} - fv = -\frac{1}{\rho_0}\frac{\partial p}{\partial x} + F_x \tag{6.1}$$

$$\frac{\mathrm{D}v}{\mathrm{D}t} + fu = -\frac{1}{\rho_0}\frac{\partial p}{\partial y} + F_y \tag{6.2}$$

$$\tag{6.3}$$

Here, F_x and F_y are the friction components per unit mass. Assuming no accelerations in the fluid we are left with a balance between three forces

$$-fv = -\frac{1}{\rho_0}\frac{\partial p}{\partial x} + F_x \tag{6.4}$$

$$fu = -\frac{1}{\rho_0}\frac{\partial p}{\partial y} + F_y. \tag{6.5}$$

We can now make progress on the frictional terms. For a geophysical fluid, the vertical component dominates. The Newton's law of friction states that the friction stress τ, which is the force per unit area, is given by

$$\tau = \mu\frac{\partial \mathbf{u}}{\partial z} = \rho_0 \nu \frac{\partial \mathbf{u}}{\partial z} = \rho_0 A_z \frac{\partial \mathbf{u}}{\partial z}, \tag{6.6}$$

where μ is the dynamic viscosity and $\nu = \mu/\rho_0$ the kinematic viscosity. For a turbulent fluid such as the ocean, eddy viscosity A_z (coming about from the Reynolds stresses $-\overline{u'w'} = A_z \partial u/\partial z$) has a value $\sim 10^{-1}\ \mathrm{m^2\ s^{-1}}$.

The eddy friction stress can be expressed in terms of a mass of fluid, where for the vertical component leads to frictional force per unit mass

$$\frac{1}{\rho_0}\frac{\partial \tau}{\partial z} = \frac{1}{\rho_0}\frac{\partial}{\partial z}\left(\rho_0 A_z \frac{\partial u}{\partial z}\right) = A_z \frac{\partial^2 u}{\partial z^2}. \tag{6.7}$$

Our equations of motion thus reduce to

$$-fv = -\frac{1}{\rho_0}\frac{\partial p}{\partial x} + A_z\frac{\partial^2 u}{\partial z^2} \tag{6.8}$$

$$fu = -\frac{1}{\rho_0}\frac{\partial p}{\partial y} + A_z\frac{\partial^2 v}{\partial z^2}. \tag{6.9}$$

Or simply

$$\boxed{\mathbf{f} \times \mathbf{u} = -\frac{1}{\rho_0}\nabla_z p + A\frac{\partial^2 \mathbf{u}}{\partial z^2}}. \tag{6.10}$$

The momentum equation in the vertical is the hydrostatic balance, and the set is completed with mass continuity, $\nabla \cdot \mathbf{u} = 0$.

The Ekman number

We now apply the usual scaling arguments to the equations and obtain the Ekman number

$$\text{Ek} = \left(\frac{A}{f_0 H^2}\right), \tag{6.11}$$

which determines the importance of frictional terms in the horizontal equations. For interior flows, $Ek < 1$, and the flow is geostrophic. Within the Ekman layer, $Ek \geq 1$, and friction is important. The difference between the geostrophic equations and the equations of motion when frictional effects are retained is thus clear.

This implies that the vertical velocities w are not negligible within the boundary layer, near the sea surface and bottom. Friction terms are small enough to be neglected only in the interior of the ocean. If we do not neglect the friction term in the momentum equation this means that the friction term is comparable in size to the Coriolis term

$$A_z \frac{\partial^2 u}{\partial z^2} \simeq fu \tag{6.12}$$

A scaling analysis reveals that

$$A_z(U/H^2) \simeq fU \tag{6.13}$$

For typical values $A_z = 10^{-1}$ m^2 s^{-1} and $f = 10^{-4}s^{-1}$ we get

$$H^2 \simeq \frac{A_z U}{fU} = 10^{-1}/10^{-4} = 10^3 \text{m}^2. \tag{6.14}$$

A typical boundary layer is in the order of $H \simeq 30$ m and frictional effects can be felt up to a 100 m or so.

Momentum balance

We write the velocity field and the pressure field as the sum of interior geostrophic part and a boundary layer correction:

$$\mathbf{u} = \mathbf{u_g} + \mathbf{u_E}, \qquad p = p_g + p_E, \tag{6.15}$$

where the Ekman layer corrections are negligible away from the boundary layer. In the fluid interior we have, by hydrostatic balance, $\frac{\partial p_g}{\partial z} = 0$, because we have considered the fluid to have constant buoyancy $b = -g\rho'/\rho_0$. In the boundary layer, we still have $\frac{\partial p_g}{\partial z} = 0$ and, to satisfy

hydrostasy, $\frac{\partial p_E}{\partial z} = 0$. But because p_E vanishes away from the boundary, $p_E = 0$ everywhere. This implies that there is no boundary layer in the pressure field. For the Ekman layer then, the horizontal momentum equation becomes

$$\mathbf{f} \times \mathbf{u_E} = A_z \frac{\partial^2 \mathbf{u}}{\partial z^2}, \tag{6.16}$$

the dominant force balance in the Ekman layer is thus between the Coriolis force and friction.

We can now estimate the depth over which the Ekman layer extends. Recalling the Ekman number:

$$\mathrm{Ek} = \frac{A_z}{\Omega d^2} \simeq 1, \tag{6.17}$$

this implies that $d = (A_z/\Omega)^{1/2}$. With typical values $A = 10^{-1}\ \mathrm{m^2\ s^{-1}}$ and $\Omega = 10^{-4}\ \mathrm{s^{-1}}$, we get a boundary layer of the order of 30 m.

6.2 Integral properties of the Ekman layer

Let's now deduce the properties of the Ekman layer without specifying the frictional stress tensor τ_{ij}.

The Ekman mass transport

The frictional-geostrophic balance is

$$\mathbf{f} \times \mathbf{u} = -\frac{1}{\rho_0} \nabla_z p + \frac{1}{\rho_0} \frac{\partial \boldsymbol{\tau}}{\partial z}, \tag{6.18}$$

where $\boldsymbol{\tau}$ is zero at the edge of the Ekman layer. In the Ekman layer we have

$$\mathbf{f} \times \mathbf{u_E} = \frac{1}{\rho_0} \frac{\partial \boldsymbol{\tau}}{\partial z}. \tag{6.19}$$

As we seek properties for the entire boundary layer, let's integrate over its thickness

$$\mathbf{f} \times \int_{Ek} \rho_0 \mathbf{u_E}\, \mathrm{d}z = \boldsymbol{\tau}_T - \boldsymbol{\tau}_B, \tag{6.20}$$

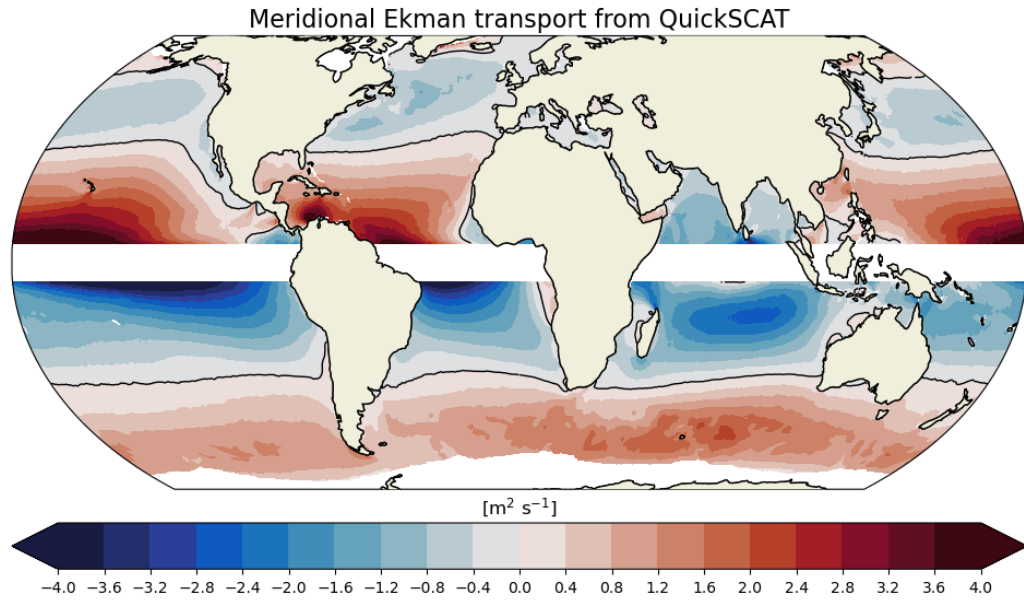where subscripts T and B are for the stresses at the top and bottom of the Ekman boundary layer.

Figure 6.2: *Meridional Ekman volume transport, $-\tau^x/(f\rho_0)$, from QuickSCAT.*

We now define the ageostrophic mass transport in the Ekman layer as

$$\mathbf{M}_E = \int_{Ek} \rho_0 \mathbf{u_E} \, \mathrm{d}z. \tag{6.21}$$

For a bottom Ekman layer, stress at the top will be zero. For a top Ekman layer, stress at the bottom will be zero:

$$Top: \quad \mathbf{f} \times \mathbf{M}_E = \boldsymbol{\tau}_T \tag{6.22}$$

$$Bottom: \quad \mathbf{f} \times \mathbf{M}_E = -\boldsymbol{\tau}_B \tag{6.23}$$

which is equivalent to writing

$$\boxed{Top: \quad \mathbf{M}_E = -\frac{1}{f} \mathbf{k} \times \boldsymbol{\tau}_T} \tag{6.24}$$

$$\boxed{Bottom: \quad \mathbf{M}_E = \frac{1}{f} \mathbf{k} \times \boldsymbol{\tau}_B.} \tag{6.25}$$

Take a situation in which $\tau_x = 0$ and therefore $M_{yE} = \int_{Ek} \rho_0 v_E \, \mathrm{d}z = 0$ but $M_{xE} > 0$ with $\tau^y > 0$. **The net transport is thus at right angles to the stress at the surface (to the right for $f > 0$), and proportional to the magnitude of the stress.**
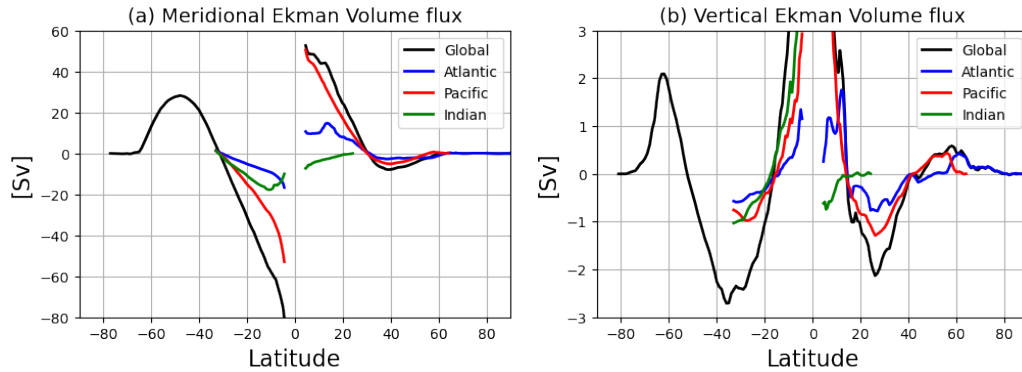
Figure 6.3: *(a) Meridional Ekman volume flux, $-\tau^x/(f\rho_0)$, for each of the world oceans as a function of latitude. Note the maximum of V_E at about $45°N$ and the changeover between westerlies and easterlies at about $30°N$. (b) Vertical Ekman volume flux, w_e, for the world's oceans (see also Levitus, 1988).*

Integrated over the depth of the Ekman layer, the surface stress must be balanced by the Coriolis force, which in turn acts at right angles to the mass transport. **Mass transports in a top oceanic and bottom atmospheric Ekman layers are equal and opposite, because the stress is continuous across the ocean-atmosphere interface (see Fig.6.4).**

The Ekman vertical velocity: Ekman Pumping

We now obtain an expression for the vertical velocity induced by an Ekman layer. We start from the mass conservation equation

$$\frac{\partial u}{\partial x} + \frac{\partial v}{\partial y} + \frac{\partial w}{\partial z} = 0 \tag{6.26}$$

and we integrate this over the Ekman layer

$$\int_{Ek} \left(\frac{\partial u}{\partial x} + \frac{\partial v}{\partial y} \right) dz = - \int_{Ek} \frac{\partial w}{\partial z} dz. \tag{6.27}$$

Remembering that we have defined $\mathbf{M}_E = \int_{Ek} \rho_0 \mathbf{u_E} \, dz$,

$$\frac{1}{\rho_0} \nabla \cdot \mathbf{M}_E = - \int_{Ek} \frac{\partial w}{\partial z} dz \tag{6.28}$$

$$\frac{1}{\rho_0} \nabla \cdot \mathbf{M}_E = -(w_T - w_B). \tag{6.29}$$
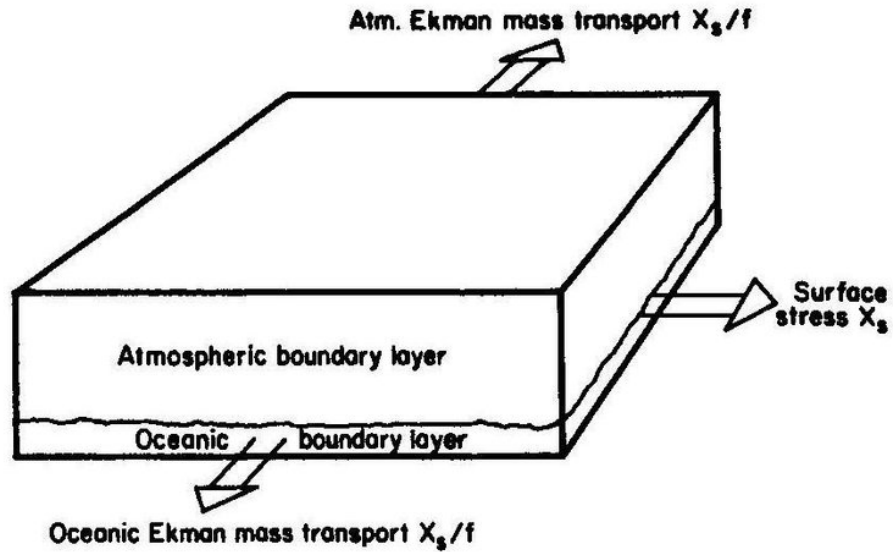
Page 99

Figure 6.4: *The directions, for the northern hemisphere, and magnitude of the steady Ekman mass transports in the atmosphere and oceanic boundary layers when stress at the surface has the direction shown. Note that the sum of the atmospheric and oceanic Ekman mass transports is zero. When there is no pressure gradient, the force per unit area exerted by the surface stress on each boundary layer is equal to the product of mass per unit area and the Coriolis acceleration of the layer. The latter quantity is f times the Ekman mass transport and is directed at right angles to the stress. [from Gill (1982)]*

Using Eq.6.20:
$$\mathbf{f} \times \mathbf{M}_E = \boldsymbol{\tau}_T - \boldsymbol{\tau}_B, \tag{6.30}$$

and taking its curl we find

$$\nabla \cdot \mathbf{M}_E = \mathrm{curl}_z[(\boldsymbol{\tau}_T - \boldsymbol{\tau}_B)/f] \tag{6.31}$$

where we have used the curl_z operator on a vector $\mathbf{A}$ defined as $\mathrm{curl}_z\mathbf{A} \equiv \partial_x A_y - \partial_y A_x$.

We now make use of Eq.6.29 and we obtain

$$\frac{1}{\rho_0}\nabla \cdot \mathbf{M}_E = -(w_T - w_B) = \frac{1}{\rho_0}\mathrm{curl}_z[(\boldsymbol{\tau}_T - \boldsymbol{\tau}_B)/f]. \tag{6.32}$$

For a top Ekman layer we have:

$$\boxed{w_B = \frac{1}{\rho_0}\mathrm{curl}_z\left(\boldsymbol{\tau}_T/f\right)} \tag{6.33}$$

For a bottom Ekman layer we have:

$$w_T = \frac{1}{\rho_0} \operatorname{curl}_z \left(\boldsymbol{\tau}_B / f \right) \tag{6.34}$$

Friction induces a vertical velocity in the Ekman layer, proportional to the curl of the stress at the surface. This vertical velocity is called *Ekman pumping* (see Fig.6.3). The production of a vertical velocity at the edge of the Ekman layer is one of the most important effects of the layer, especially with regard to the large-scale circulation, for it provides an efficient means whereby surface fluxes are communicated to the interior flow.

6.3 A bottom boundary layer

We now derive the properties for the bottom boundary layer. If you are more atmospherically inclined, think of this bottom boundary layer as the one generated by the wind over some topography.

Our momentum equations (Eq.6.10) are completed by the mass conservation equation

$$\frac{\partial u}{\partial x} + \frac{\partial v}{\partial y} + \frac{\partial w}{\partial z} = 0 \tag{6.35}$$

and hydrostatic balance in the vertical

$$0 = -\frac{1}{\rho_0} \frac{\partial p}{\partial z}. \tag{6.36}$$

Remember we are in a Boussinesq fluid. The flow can be divided into an interior geostrophic part

$$-f v_g = -\frac{1}{\rho_0} \frac{\partial p}{\partial x} \tag{6.37}$$

$$f u_g = -\frac{1}{\rho_0} \frac{\partial p}{\partial y}, \tag{6.38}$$

$$\tag{6.39}$$

or

$$f(u_g, v_g) = \left(-\frac{\partial \phi}{\partial y}, \frac{\partial \phi}{\partial x}\right) \tag{6.40}$$

where $\phi \equiv p/\rho_0$. And a boundary layer correction

$$-fv = -\frac{1}{\rho_0}\frac{\partial p}{\partial x} + A\frac{\partial^2 u}{\partial z^2} \tag{6.41}$$

$$fu = -\frac{1}{\rho_0}\frac{\partial p}{\partial y} + A\frac{\partial^2 v}{\partial z^2}. \tag{6.42}$$

$$\tag{6.43}$$

Given Eq.6.40, the frictional-geostrophic balance can be written as

$$-f(v - v_g) = A\frac{\partial^2 u}{\partial z^2} \tag{6.44}$$

$$f(u - u_g) = A\frac{\partial^2 v}{\partial z^2}, \tag{6.45}$$

or even better as

$$\mathbf{f} \times (\mathbf{u} - \mathbf{u_g}) = A\frac{\partial^2 \mathbf{u}}{\partial z^2}. \tag{6.46}$$

Our boundary conditions will be

$$\text{at z=0:} \quad u = 0, v = 0 \quad \text{(no slip boundary condition)} \tag{6.47}$$

$$\text{as z} \to \infty: \quad u = u_g, v = v_g \quad \text{(a geostrophic interior).} \tag{6.48}$$

We seek solutions of the form

$$u = u_g + A_0 e^{\alpha z}, \quad v = v_g + B_0 e^{\alpha z}, \tag{6.49}$$

where A_0 and B_0 are constants. Substituting into Eq.6.46 leads to

$$fA_0 - AB_0\alpha^2 = 0, \quad -fB_0 - AA_0\alpha^2 = 0. \tag{6.50}$$

Remember that, given the absence of temperature horizontal gradients, via thermal wind, $\partial_z u_g = \partial_z v_g = 0$.

For non-trivial solutions we have $\alpha^4 = -f^2/A^2$, from which we find $\alpha = \pm(1 \pm i)(1/d)$, where $d = (2A/f)^{1/2}$. Using the boundary conditions we obtain the solution

$$u = u_g - e^{-z/d}\left[u_g cos(z/d) + v_g sin(z/d)\right] \tag{6.51}$$

$$v = v_g + e^{-z/d}\left[u_g sin(z/d) - v_g cos(z/d)\right]. \tag{6.52}$$

We have used $d = (2A/f)^{1/2}$, the depth of the Ekman layer. It is apparent that the solution decays exponentially from the surface with an e-folding scale equal to d.

Now let's suppose a flow that is directed eastward and has zero meridional component ($u_g > 0$, $v_g = 0$). Velocities reduce to

$$u \;=\; u_g[1 - e^{-z/d}cos(z/d)] \tag{6.53}$$

$$v \;=\; u_g \; e^{-z/d}sin(z/d). \tag{6.54}$$

This is already telling us that the meridional velocity within the boundary layer is not zero. As $z \to 0$[1] we have

$$u \;=\; u_g[1 - (1 - z/d)] = u_g z/d \tag{6.55}$$

$$v \;=\; u_g \; (1 - z/d)z/d = u_g z/d - \underline{u_g z^2/d^2}.^{\,0} \tag{6.56}$$

Hence, u and v are equal and generate a flow that is 45° to the left of the direction of the interior flow (to the right when $f < 0$).

We can find a local maximum for the velocity in the boundary layer

$$\frac{\partial u}{\partial z} = 0 \to \partial_z[u_g - u_g e^{-z/d}cos(z/d)] = 0 \tag{6.57}$$

$$\frac{1}{d}u_g e^{-z/d}cos(z/d) + \frac{1}{d}u_g e^{-z/d}sin(z/d) = 0$$

$$cos(z/d) + sin(z/d) = 0$$

$$tan(z/d) = -1$$

And so the depth of maximum velocity is

$$z = \frac{3\pi}{4}d.$$

At this depth

$$u = u_g\left(1 - e^{\frac{3\pi}{4}}cos(\frac{3\pi}{4})\right) = 1.07 u_g. \tag{6.58}$$

Hence, the theoretical value of u reaches values larger then the interior geostrophic flow because of frictional effects and redistribution of momentum within the boundary layer.

The bottom Ekman layer can be seen in Fig.6.5, where the Ekman spiral is depicted. At the bottom, the flow is at 45° to the left of the interior geostrophic flow. The maximum u is obtained at $z/d = \frac{3\pi}{4}$

---

[1]Taylor expanding and neglecting higher order terms $e^{-z/d} = 1 - z/d + \underline{z^2/(2d^2)}$; $cos(z/d) = 1 - \underline{z^2/(2d^2)}$; $sin(z/d) = z/d - \underline{z^3/(3d^3)}$
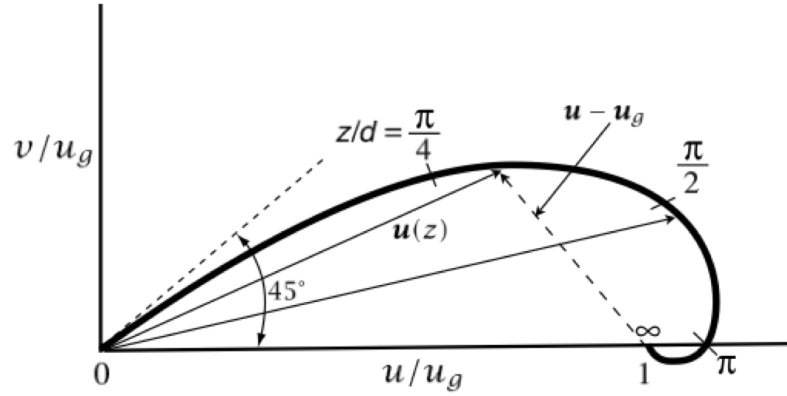
Figure 6.5: *The idealized Ekman layer solution at the bottom for $v_g = 0$. [from Vallis (2006)]*

Transport and vertical velocity

We now find an expression for the (cross-isobaric) transport produced by frictional effects. For $v_g = 0$, we have

$$V = \int_0^\infty v\,dz = \int_0^\infty u_g e^{-z/d} sin(z/d)\,dz \;=\; \frac{d}{2}u_g \qquad (6.59)$$

$$U = \int_0^\infty (u - u_g)\,dz = -\int_0^\infty u_g e^{-z/d} sin(z/d)\,dz \;=\; -\frac{d}{2}u_g, \quad (6.60)$$

and the general case with $v_g \neq 0$ is simply

$$V \;=\; \frac{d}{2}(u_g - v_g) \qquad\qquad\qquad (6.61)$$

$$U \;=\; -\frac{d}{2}(u_g + v_g). \qquad\qquad\quad (6.62)$$

The total mass transport caused by frictional forces is thus

$$\mathbf{M}_E = \frac{\rho_0 d}{2}\Big[-\mathbf{i}(u_g + v_g) + \mathbf{j}(u_g - v_g)\Big]. \qquad (6.63)$$

Recalling that the frictionally induced transport in the Ekman layer is related to the stress at the surface by $\mathbf{M}_E = (\mathbf{k} \times \boldsymbol{\tau}_B)/f$, a full picture of stress, cross-isobaric velocity and total transport is given in Fig.6.6.
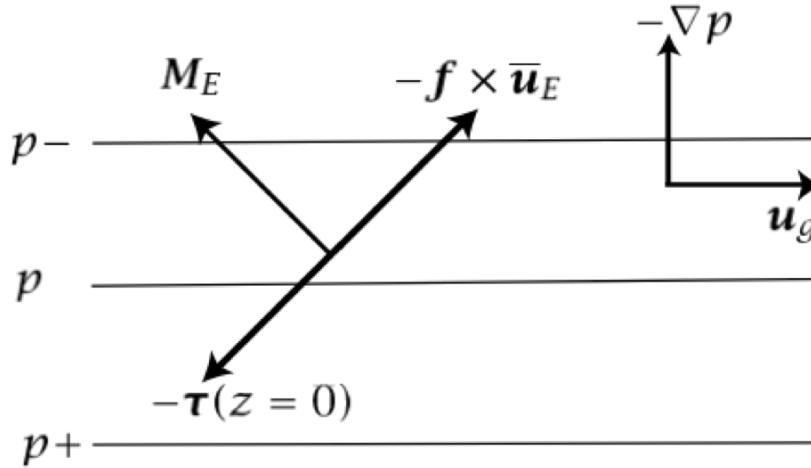
Figure 6.6: *A bottom Ekman layer, generated from an eastward geostrophic flow above. An overbar denotes a vertical integral over the Ekman layer. so that $-f \times \overline{u}_E$ is the Coriolis force on the vertically integrated Ekman velocity. $\mathbf{M}_E$ is the frictionally induced boundary layer transport, and $\boldsymbol{\tau}$ is the stress. [from Vallis (2006)]*

The flow within the Ekman layer has a nonzero divergence, indeed:

$$\frac{\partial U}{\partial x} + \frac{\partial V}{\partial y} = -\frac{d}{2}\left[\partial_x(u_g + v_g) - \partial_y(u_g - v_g)\right] \tag{6.64}$$

$$= \frac{d}{2}\left[-(\partial_x u_g + \partial_y v_g) - \partial_x v_g + \partial_y u_g\right]. \tag{6.65}$$

The first term on the r.h.s. is zero because the interior flow is non-divergent, hence:

$$\frac{\partial U}{\partial x} + \frac{\partial V}{\partial y} = -\frac{d}{2}(\partial_x v_g - \partial_y u_g) = -\frac{d}{2}\zeta_g \tag{6.66}$$

The vertical velocity at the top of the Ekman layer is, for a constant f (and using Eq.6.34)

$$\boxed{w_E = -\frac{1}{\rho_0}\nabla \cdot \mathbf{M}_E = \frac{1}{\rho_0}\text{curl}_z\left(\boldsymbol{\tau}_B/f\right) = \frac{d}{2}\zeta_g} \tag{6.67}$$

There will be divergence if the interior geostrophic flow presents vorticity. **The vertical velocity at the top of the bottom Ekman layer, which**

arises because of the frictionally-induced divergence of the flow in the Ekman layer, is proportional to the geostrophic vorticity and to the Ekman layer height.

6.4 A surface boundary layer

We now look for solutions for a surface Ekman layer. In this case, the wind provides a stress on the upper ocean, and the Ekman layer serves to communicate this to the ocean interior.

We start again with our momentum equations, which for the interior geostrophic flow are

$$-f v_g = -\frac{1}{\rho_0} \frac{\partial p}{\partial x} \tag{6.68}$$

$$f u_g = -\frac{1}{\rho_0} \frac{\partial p}{\partial y}, \tag{6.69}$$

or

$$f(u_g, v_g) = \left(-\frac{\partial \phi}{\partial y}, \frac{\partial \phi}{\partial x}\right) \tag{6.70}$$

where $\phi \equiv p/\rho_0$. And for the Ekman layer

$$-f v = -\frac{1}{\rho_0} \frac{\partial p}{\partial x} + A \frac{\partial^2 u}{\partial z^2} \tag{6.71}$$

$$f u = -\frac{1}{\rho_0} \frac{\partial p}{\partial y} + A \frac{\partial^2 v}{\partial z^2}. \tag{6.72}$$

$$\tag{6.73}$$

The frictional-geostrophic balance can be written again as

$$-f(v - v_g) = A \frac{\partial^2 u}{\partial z^2} \tag{6.74}$$

$$f(u - u_g) = A \frac{\partial^2 v}{\partial z^2}, \tag{6.75}$$

or even better as

$$\boxed{\mathbf{f} \times (\mathbf{u} - \mathbf{u_g}) = A \frac{\partial^2 \mathbf{u}}{\partial z^2}} \tag{6.76}$$

Our boundary conditions will be

$$\text{at } z=0: \quad \tau^x = \rho_0 A \frac{\partial^2 u}{\partial z^2}, \text{ (a given surface stress)} \qquad (6.77)$$

$$\tau^y = \rho_0 A \frac{\partial^2 v}{\partial z^2} \qquad (6.78)$$

$$\text{as } z \to -\infty: \quad u = u_g \text{ (a geostrophic interior)} \qquad (6.79)$$

$$v = v_g \qquad (6.80)$$

We now introduce the kinematic wind stress at the surface, $\tilde{\tau} = \tau/\rho_0$, and seek solutions by the same method we used for the bottom layer:

$$u = u_g + \frac{\sqrt{2}}{fd} e^{z/d} \left[\tilde{\tau}^x cos(z/d - \pi/4) - \tilde{\tau}^y sin(z/d - \pi/4) \right], \quad (6.81)$$

$$v = v_g + \frac{\sqrt{2}}{fd} e^{z/d} \left[\tilde{\tau}^x sin(z/d - \pi/4) + \tilde{\tau}^y cos(z/d - \pi/4) \right]. \quad (6.82)$$

Note that the boundary layer correction depends only on the imposed surface stress, and not on the interior flow. In the absence of an imposed stress the boundary layer correction is zero, and $\mathbf{u} = \mathbf{u}_g$. Similar to the bottom boundary layer, the velocity vector traces a diminishing spiral as it descend into the interior (Fig.6.7). The velocity within the boundary depends on its depth, $d = \sqrt{\frac{2A}{f}}$, which depends on the eddy viscosity A. If the fluid is not very viscous, it will generate a small Ekman layer, and the velocity within the layer can be large for small stresses.

What is the value and direction of the surface velocity? at $z = 0$ we have

$$u(0) = u_g + \frac{\sqrt{2}}{fd} \left[\tilde{\tau}^x cos(-\pi/4) - \tilde{\tau}^y sin(-\pi/4) \right], \qquad (6.83)$$

$$v(0) = v_g + \frac{\sqrt{2}}{fd} \left[\tilde{\tau}^x sin(-\pi/4) + \tilde{\tau}^y cos(-\pi/4) \right]. \qquad (6.84)$$

Since $cos(-\pi/4) = \sqrt{2}/2$ and $sin(-\pi/4) = -\sqrt{2}/2$, the solution is

$$u(0) = u_g + \frac{\sqrt{2}}{fd} \left[\tilde{\tau}^x \frac{\sqrt{2}}{2} + \tilde{\tau}^y \frac{\sqrt{2}}{2} \right], \qquad (6.85)$$

$$v(0) = v_g + \frac{\sqrt{2}}{fd} \left[-\tilde{\tau}^x \frac{\sqrt{2}}{2} + \tilde{\tau}^y \frac{\sqrt{2}}{2} \right]. \qquad (6.86)$$
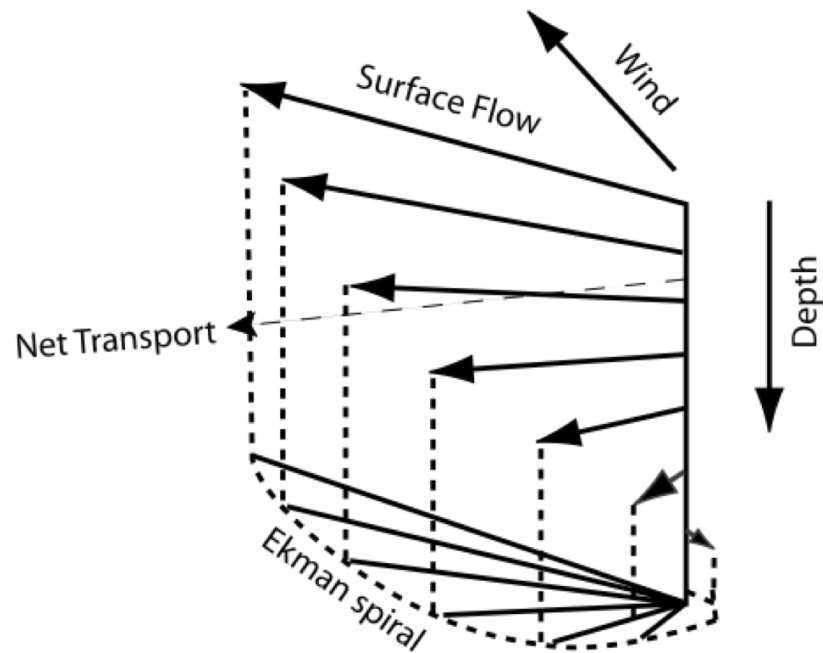
Page 107

Figure 6.7: *An idealized Ekman spiral in the southern hemisphere ocean, driven by an imposed wind stress. The net transport is at right angles to the wind, independent of the detailed form of the friction. The angle of the surface flow is at 45° to the wind (only for a Newtonian viscosity). [from Vallis (2006)]*

Suppose the surface wind is eastward. In this case $\tilde{\tau}^y = 0$ and the solutions reduce to

$$u(0) = u_g + \frac{\sqrt{2}}{fd}\left[\tilde{\tau}^x \frac{\sqrt{2}}{2}\right], \tag{6.87}$$

$$v(0) = v_g - \frac{\sqrt{2}}{fd}\left[\tilde{\tau}^x \frac{\sqrt{2}}{2}\right]. \tag{6.88}$$

The velocity at the surface of the Ekman layer are simply

$$u(0) - u_g = \frac{\tilde{\tau}^x}{fd}, \tag{6.89}$$

$$v(0) - v_g = -\frac{\tilde{\tau}^x}{fd}. \tag{6.90}$$

Therefore the magnitudes of the frictional flow in the x and y directions are equal to each other, and the ageostrophic flow is 45° to the right (for $f > 0$) of the wind. This result does not depend on the size of the viscosity.

Transport and vertical velocity (or Ekman pumping / suction)

The transport induced by the surface stress is obtained by integrating (6.81) and (6.82)

$$U = \int_{-\infty}^{0} (u - u_g)\,\mathrm{d}z = \frac{\tilde{\tau}^y}{f} \tag{6.91}$$

$$V = \int_{-\infty}^{0} (v - v_g)\,\mathrm{d}z = -\frac{\tilde{\tau}^x}{f}, \tag{6.92}$$

which indicates that **the ageostrophic transport is perpendicular to the wind stress**, as previously noted (see Fig.6.8). It should be noted that these results are correct even if the details of the Ekman spiral are not.

Again the ageostrophic flow will be divergent

$$\frac{\partial U}{\partial x} + \frac{\partial V}{\partial y} = \int_{-\infty}^{0} \mathrm{d}z \Big(\frac{\partial U}{\partial x} + \frac{\partial V}{\partial y}\Big) = \frac{1}{f}\Big(\partial_x \tilde{\tau}^y - \partial_y \tilde{\tau}^x\Big) = \tag{6.93}$$

$$w_E = \frac{1}{f}\,\mathrm{curl}_z \tilde{\tau}. \tag{6.94}$$

As previously noted in (6.33). At the edge of the Ekman layer the vertical velocity (*Ekman pumping*) is proportional to the curl of the wind stress.

The Ekman pumping is associated with the frictionally induced vertical velocity w_E. This vertical Ekman velocity starts with zero due to
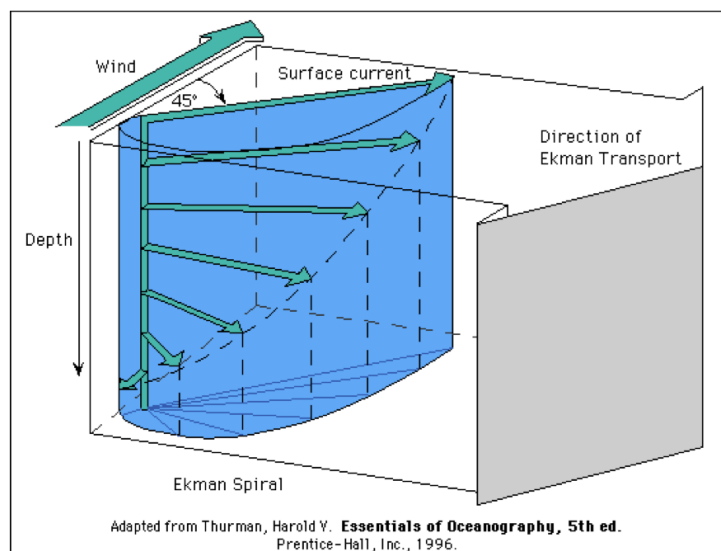

Figure 6.8: An idealized Ekman velocity spiral.

the boundary condition at the surface, followed by an exponential pattern within the top Ekman layer, and approaches a constant below.

It is quite hard to observe Ekman spirals both in the ocean and atmosphere (but not in a laboratory where you can control viscosity and background conditions!). The theory does not take into account stratification, gravity waves and assumes a steady wind. Nevertheless both the Ekman mass transport and vertical velocity are independent of details of the Ekman layer, and only depend on the imposed stress (Fig. 6.9 and Fig. 6.11).
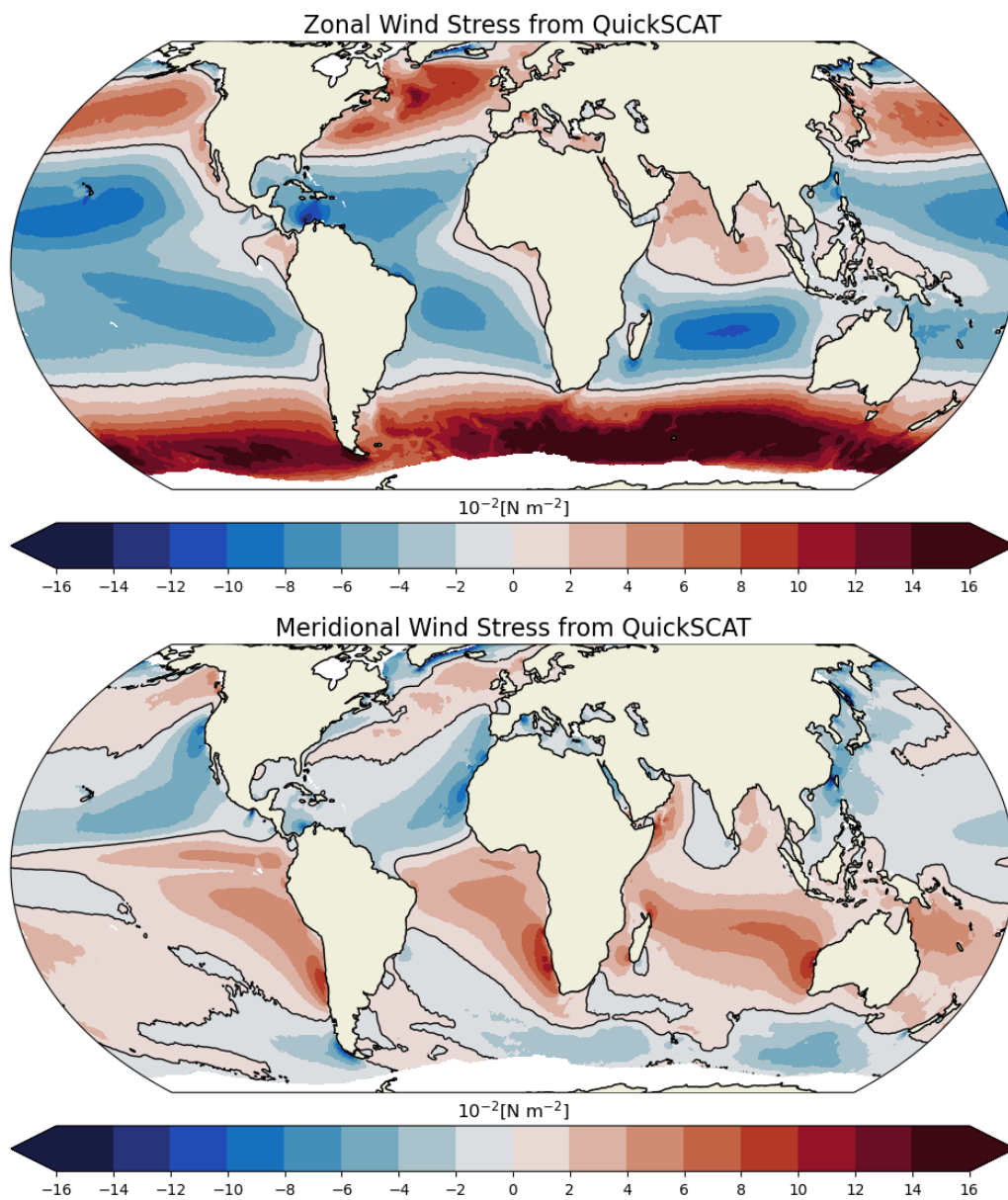
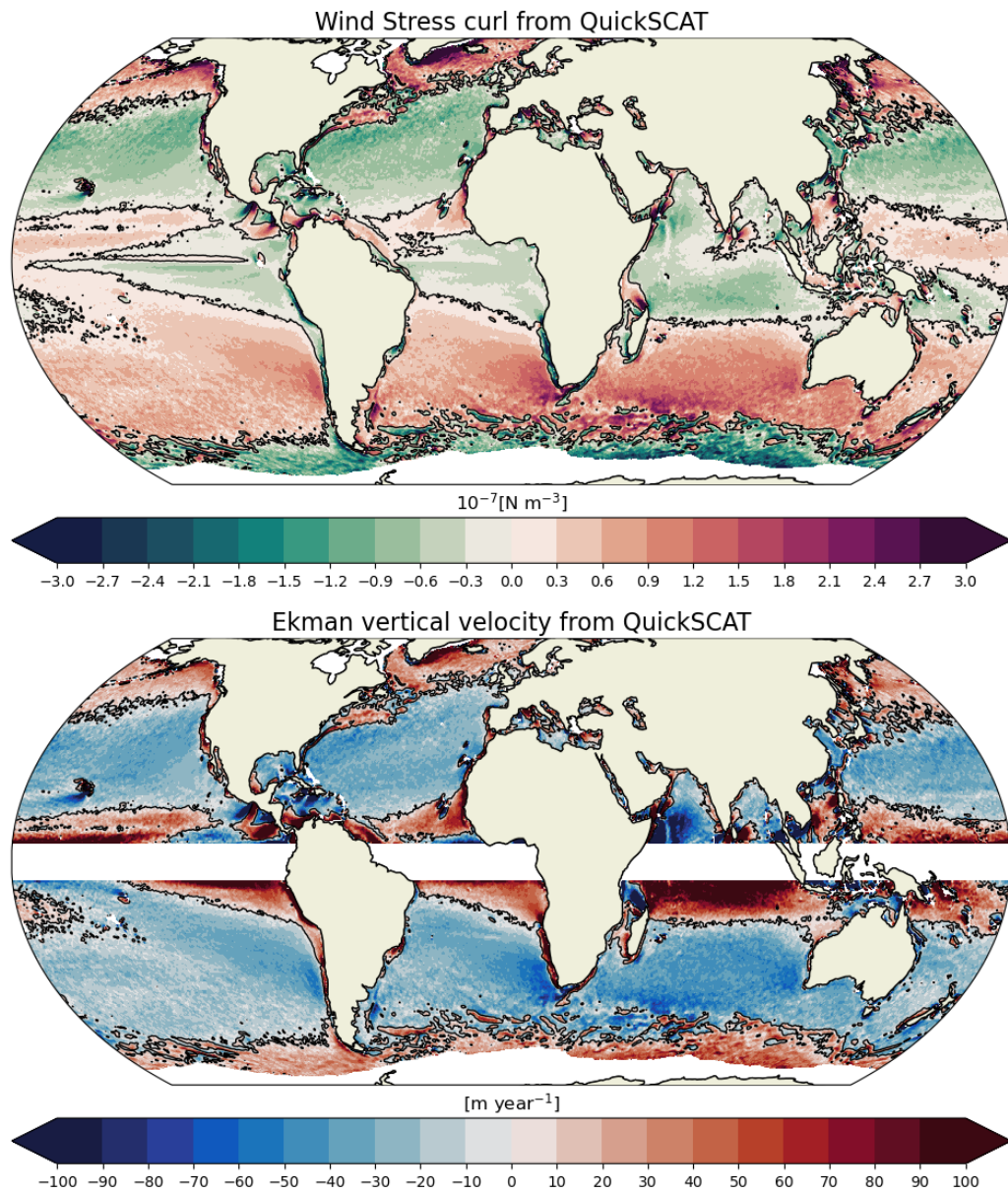Figure 6.9: *Climatological zonal and meridional wind stress from QuickSCAT.*

Figure 6.10: *Climatological wind stress curl and Ekman pumping velocity, w_e (m/year), from QuickSCAT. It is positive in the subtropical regions on the order of 20-50 m per year and mostly negative over the subpolar regions. Towards the equator, f goes to zero, and Ekman pumping and Ekman transport become ill-defined.*
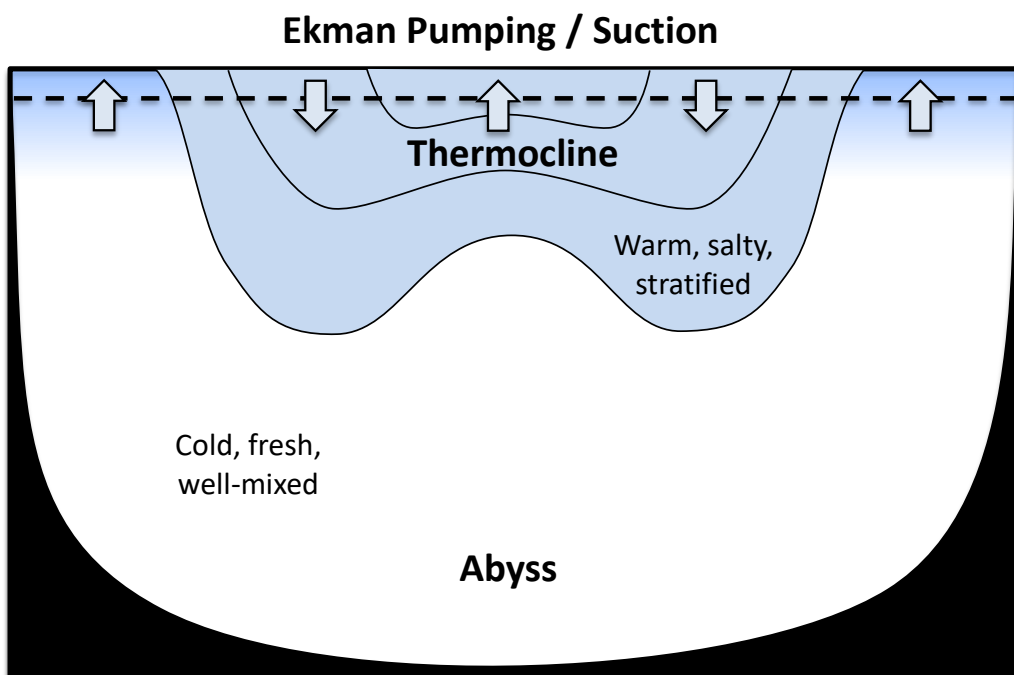
Ekman Pumping / Suction

Thermocline

Warm, salty,
stratified

Cold, fresh,
well-mixed

Abyss

Figure 6.11: *The direction of Ekman pumping and suction is responsible for the odd bi-modal shape of the ocean's density anomaly.*
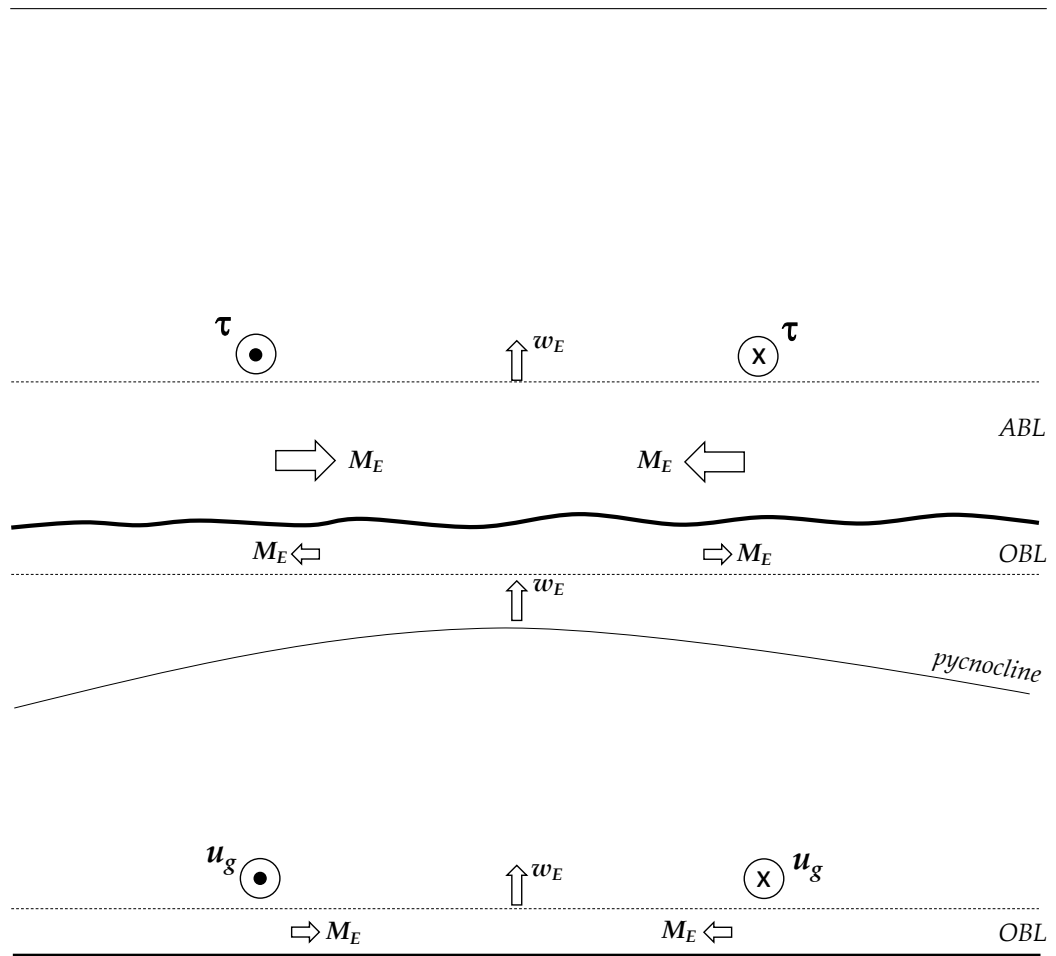
Figure 6.12: *Section through a cyclonic wind over the ocean. The geostrophic wind gives a cyclonic rotation around the low-pressure center. The Ekman mass transport in the atmospheric boundary layer is inward, bringing mass to fill the low, and the associated vertical pumping velocity is therefore upward. The Ekman mass transport in the oceanic boundary layer is equal and opposite to that in the atmosphere, so there is an outward mass transport and upward pumping velocity in the ocean. This tends to raise the thermocline. The upper Ekman layer in the ocean is primarily driven by an imposed wind stress, whereas the lower Ekman layer in the ocean largely results from the interaction of interior geostrophic velocity and a rigid lower surface [from Vallis (2006) and Gill (1982)].*

Ekman velocity Spiral

- Frictionally induced surface velocity to the right of the wind (for $f > 0$, due to Coriolis)

- Surface layer pushes next layer down slightly to the right, generating a slightly weaker current

- Next layer pushes next layer, slightly to right and generating a slightly weaker current

- Producing a "spiral" of the current vectors, to the right in the northern hemisphere, with decreasing speed as depth increases

- Details of the spiral depend on the vertical viscosity (how frictional the flow is, and also whether friction depends on depth)

- The total transport only depends on the imposed wind stress

- Typical transport size: for a wind stress 0.1 N m^{-2}, $M_E = \tau/(\rho f)$ =1 m^2 s^{-1}. Integrate this over 'width' of the ocean, say 5000 km, we get a total transport of 5×10^6 m^3 s^{-1}= 5 Sv (1 $Sv \equiv 10^6$ m^3 s^{-1})

6.5 Upwelling

6.5.1 Coastal Upwelling

Suppose we have a wind which is entirely meridional, $\tau^x = 0$, and therefore $M_E^y = 0$ and $M_E^x > 0$ for $\tau^y > 0$. The net transport will be to the left of and at right angles to the wind direction (for $f < 0$). Continuity requires that there must be inflow from the right of the wind direction. If the wind is blowing parallel to a coastline which is on the right of the wind, as the wind causes an Ekman frictionally induced transport to the left away from the coast, water is replaced from below, generating a so-called *coastal upwelling* near the region of divergence along the coast.

Coastal upwelling is accompanied by a rise in upper ocean isopycnals toward the coast. This creates an equatorward geostrophic surface flow, the *eastern boundary current*. Poleward undercurrents are observed at about 200 m depth beneath the equatorward surface currents (Fig.6.13c). Poleward undercurrents are created mainly by the alongshore pressure gradient that drives the onshore subsurface geostrophic flow that feeds the upwelling.

Given the prevailing wind directions, the largest coastal upwelling regions happen to be on eastern boundaries of ocean basins. Eastern boundary upwelling systems (EBUS) cover less than 3% of the world ocean surface yet they have a significant role in the climate system, and are home to the largest contribution of ocean biological productivity with up to 40% of the reported global fish catch (Fig.6.14). The upwelled water does not come from great depths. Observations and models show that upwelled water comes from depths not greater than 200-300 m. Usually the upwelled water has high nutrient content, and plankton production may be promoted with important biological consequences when photosynthesis is activated in the photic zone.

Coupled with the vast coastal human populations, these regions play key biological and socio-economical roles. There are common features to eastern boundary upwelling regions: wind-driven flows, alongshore currents, steep shelves and large vertical and offshore nutrient transports. Despite the commonality, each of the main upwelling systems (California, Humboldt, Canary and Benguela Current Systems), exhibits substantial differences in primary productivity, phytoplankton biomass, and community structures. The reasons for these differences are not fully understood.

Many coupled climate models generate very large sea surface temperature (SST) biases in the coastal upwelling regions of the California Current System, the Humboldt Current system and the Benguela Current System,
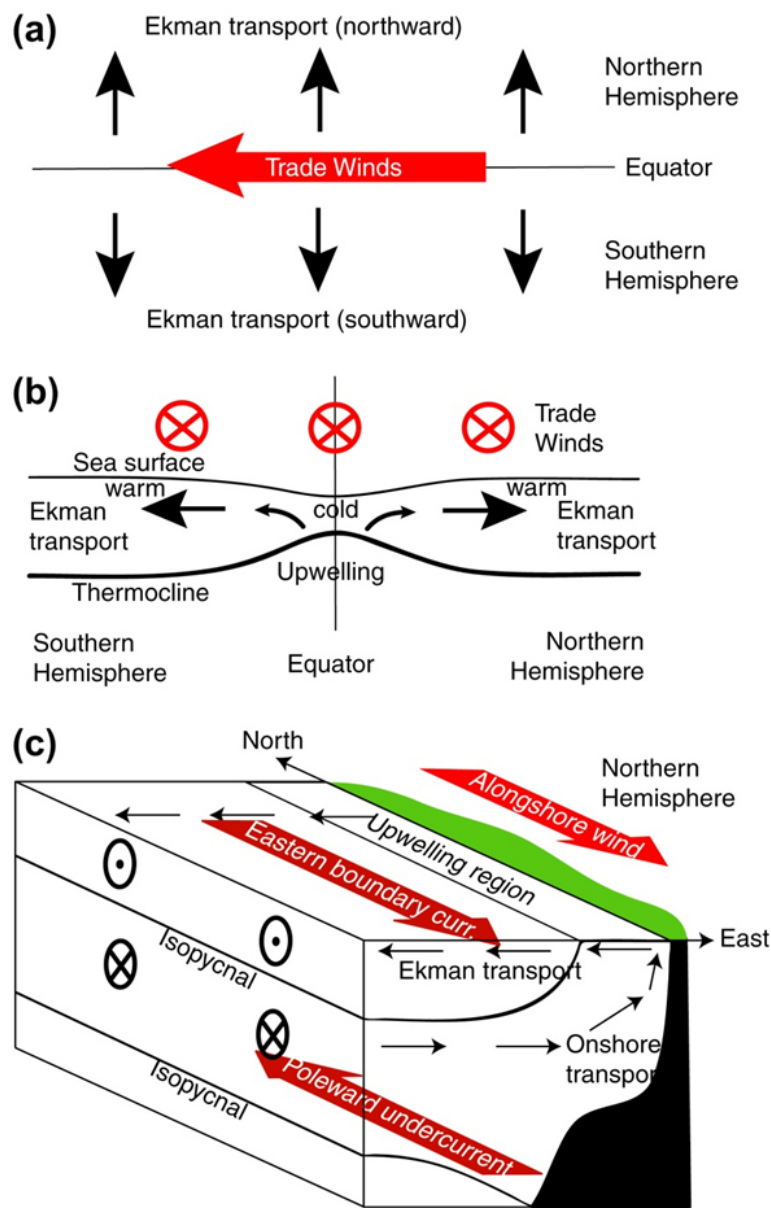
Figure 6.13: *Ekman transport divergence near the equator driven by easterly trade winds. (a) Ekman transports. (b) Meridional cross-section showing effect on the thermocline and surface temperature. (c) Coastal upwelling system due to an alongshore wind with offshore Ekman transport ($f > 0$). The accompanying isopycnal deformations and equatorward eastern boundary current and poleward undercurrent are also shown. [from Talley et al. (2011)]*
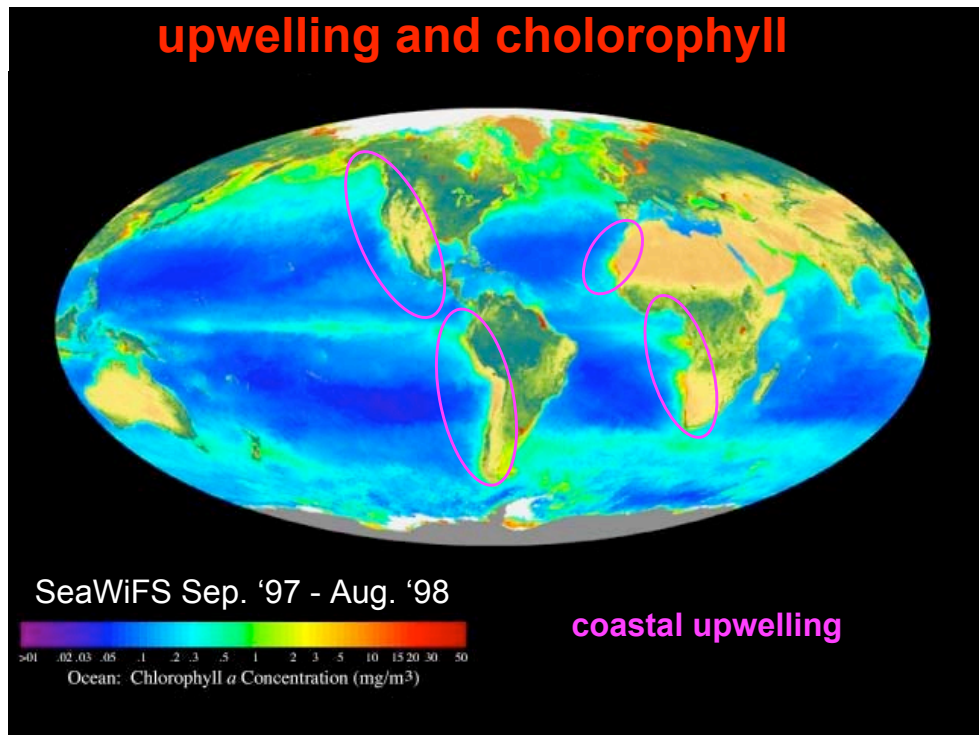
Figure 6.14: *A false-color image depicting chlorophyll-a concentration as measured from the SeaWIFS satellite data. Eastern Boundary Upwelling systems (EBUS) regions (California, Peru, Canary and Benguela) are shown by the pink ovals.*

where simulated mean SSTs are much warmer than observed (typically in excess of 3°C and as high as 10°C; see Fig.6.15). Furthermore, these SST biases have significant remote effects on surface and subsurface temperature and salinity, and on precipitation and hence atmospheric heating and circulation. The warm temperature biases associated with upwelling regions strongly limit the prediction of future evolution of these regions. Increased model resolution, achieved via nesting or adaptive gridding, improves simulations of the regional climate and affects the large-scale climate system through feedbacks.
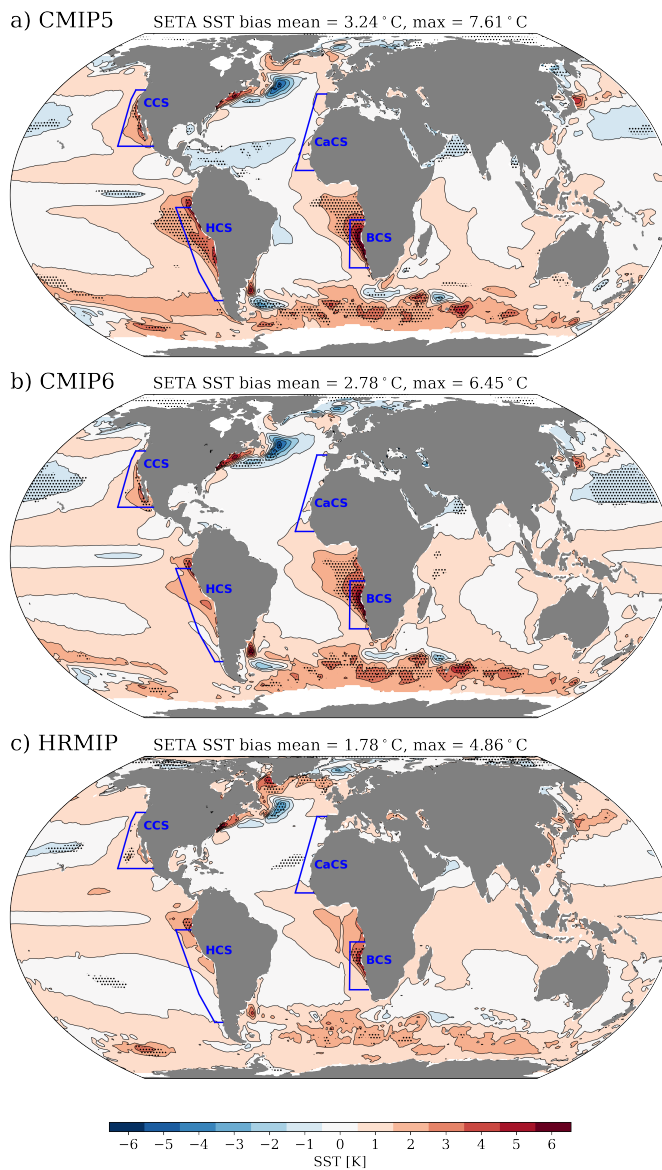
Figure 6.15: *Time-mean (1985-2004) SST bias for (a) CMIP5, (b) CMIP6 and (c) HighResMIP multi-model mean relative to OISST. Every contour represents an SST bias of 1 K. Black dots show regions where all models agree on the sign of the bias. The poles are excluded in order to highlight the biases in the EBUS regions, which present the highest SST anomalies. The 4 major EBUS are: the California Current System (CCS), the Canary Current System (CaCS), the Humboldt Current system (HCS) and the Benguela Current System (BCS). [from Farneti et al. (2022)]*

6.5.2 Equatorial Upwelling

Equatorial upwelling due to Ekman transport results from the westward wind stress (trade winds). These cause northward Ekman transport north of the equator and southward Ekman transport south of the equator. This results in upwelling along the equator, even though the wind stress curl is small because of the Coriolis parameter dependence in (6.33).

At the equator, where the Coriolis parameter changes sign, zonal (east-west) winds can cause Ekman convergence or divergence even without any variation in the wind (Fig.6.13a). Right on the equator, there is no Ekman layer since the Coriolis force that would create it is zero ($f = 0$). If the equatorial wind is westward (a trade wind), then the Ekman transport just north of the equator is northward, and the Ekman transport just south of the equator is southward, and there must be upwelling into the surface layer on the equator.

Trade winds are relatively steady easterlies. They are driven by warm waters in the western region and cooler waters in the east, which creates rising air in the west and sinking air in the east, and a thermally direct flow from east to west to feed this (Walker cell). In the ocean the true equatorial region is much narrower - about 2 degrees wide. Easterly trade winds at the equator drive (1) poleward Ekman transport and (2) westward surface flow, as follows. The easterly trade winds cause northward Ekman transport just to the north of the equator and southward Ekman transport just to the south of the equator. This causes upwelling at the equator. As a result, the pycnocline shoals towards the equator (Fig.6.13b). **This drives a westward geostrophic flow at the sea surface.**

Directly on the equator, the effect of rotation on the circulation vanishes, and so the concepts of geostrophic and Ekman flow do not apply. At the equator, the easterly trade winds push the surface water directly (frictionally) from east to west. This water piles up gently in the western Pacific (0.5 meters higher there than in the eastern Pacific). The pycnocline is deeper in the west also as a result, and much warmer water is found there (so-called **"warm pool"**). Upwelling in the east draws cool water to the surface because of the shallow pycnocline there, but intense eastward-flowing upwelling in the west cannot create cold water at the surface there because of the thickness of the warm pool.

Because the sea surface is higher in the west than in the east, there is a pressure difference that causes the flow just beneath the surface layer to be eastward. This strong eastward flow is the Equatorial Undercurrent. It is centered at about 150 to 200 m depth. EUC speeds are in excess of 100 cm/sec. The current is exceptionally thin vertically (about 150 m

thick). The Equatorial Undercurrent shoals towards the east, as does the pycnocline. The shoaling is associated with upwelling of cool water in the central/eastern Pacific, giving rise to the "cold tongue" (in non-El Niño years). Steady trade winds, which cause equatorial upwelling, are more prevalent in the east than in the west. When the trade winds weaken or even reverse, the flow of water westward at the equator weakens or reverses and upwelling weakens or stops. Surface waters in the eastern Pacific warm significantly since upwelling is no longer bringing the cool waters to the surface. The deep warm pool in the western Pacific thins as its water sloshes eastward along the equator in the absence of the trade winds which maintain it.

Exercices

1. For $A = 10^{-1}$ m^2 s^{-1} and $f = 10^{-4}$ s^{-1}, what would be the typical depth of an Ekman layer?

2. Assume that the atmospheric Ekman layer over the earth's surface at latitude 45°N can be modeled with a turbulent kinematic viscosity $\nu = 10$m^2 s^{-1}. If the geostrophic velocity above the layer is 10 m s^{-1} and is uniform, what is the vertically integrated flow across the isobars (pressure contours)? Is there any vertical velocity?

3. Meteorological observations above New York City (41°N) reveal a neutral atmospheric boundary layer (no convection and no stratification) and a westerly geostrophic wind of 12 m s^{-1} at 1000 m above street level. Under neutral conditions, Ekman layer dynamics apply. Using an eddy viscosity of 10 m^2 s^{-1}, determine the wind speed and direction atop the World Trade Center (height: 411 m).

4. Between 15°N and 45°N, the winds over the North Pacific consist mostly of the easterly trades (15°N to 30°N) and the westerlies (30°N to 45°N. An adequate representation is

$$\tau^x = \tau_0 sin\left(\frac{\pi y}{2L}\right), \quad \tau^y = 0, \quad -L \leq y \leq L, \qquad (6.95)$$

where $\tau_0 = 0.15 \, N/m^2$ is the maximum wind stress and $L = 1670 \, km$. Taking $\rho_0 = 1028 \, kg/m^3$ and the value of the Coriolis parameter corresponding to 30°N, calculate the Ekman pumping. Which way is it directed? Calculate the vertical volume flux over the entire 15°N-45°N strip of the North Pacific (width = 8700 km). Express your answer in Sverdrup units (1 Sverdrup = 1 Sv $\equiv 10^6$ m^3 s^{-1}).

Bibliography

Anderson, D. L. T., and A. E. Gill, Spin-up of a stratified ocean, with application to upwelling, *Deep-Sea Res.*, *22*, 583–596, 1975.

Anderson, D. L. T., and A. E. Gill, Beta-dispersion of inertial waves, *J. Geophys. Res.*, *84*, 1836–1842, 1979.

Cessi, P., and P. Otheguy, Oceanic teleconnections: Remote response to decadal wind forcing, *J. Phys. Oceanogr.*, *33*, 1604–1617, 2003.

Chelton, D. B., and M. G. Schlax, Global observations of oceanic rossby waves, *Science*, **272**, 234–238, 1996.

Chelton, D. B., R. A. deSzoeke, M. G. Schlax, K. E. Naggar, and N. Siwertz, Geographical variability of the first baroclinic rossby radius of deformation, *J. Phys. Oceanogr.*, **28**, 433–460, 1998.

Cipollini, P., D. Cromwell, P. G. Challenor, and S. Raffaglio, Rossby waves detected in global ocean colour data, *Geophys. Res. Lett.*, **28**, 323–326, 2001.

Dewar, W., On ocean dynamics in midlatitude climate, *J. Climate*, **14**, 4380–4397, 2001.

Dickinson, R. E., Rossby waves-long period oscillations of oceans and atmosphere, *Annu. Rev. Fluid Mech.*, **10**, 159–195, 1978.

Farneti, R., A. Stiz, and J. Ssebandeke, Improvements and persistent biases in the southeast tropical Atlantic in CMIP models, *npj Climate and Atmospheric Science*, *x*, xx–xx, 2022.

Galanti, E., and E. Tziperman, A midlatitude-enso teleconnection mechanism via baroclinically unstable long rossby waves, *J. Phys. Oceanogr.*, *33*, 1877–1888, 2003.

Gill, A. E., *Atmosphere-Ocean Dynamics*, *International Geophysics Series*, vol. **30**, 662 pp., Academic Press, 1982.

Hill, K. L., I. Robinson, and P. Cipollini, Propagation characteristics of extratropical planetary waves observed in the atsr global sea surface temperature record, *J. Geophys. Res.*, **105**, 21,927–21,945, 2000.

Hough, S., On the application of harmonic analysis to the dynamical theory of the tides, part i, on laplace's oscillations of the first species, and on the dynamics of ocean currents, *Phil. Trans. Roy. Soc. Lond.*, *189*, 201–257, 1897.

Hughes, C. W., Rossby waves in the southern ocean: A comparison of topex/poseidon altimetry with model predictions, *J. Geophys. Res.*, **100**, 15,933–15,950, 1995.

Johnson, H. L., and P. Marshall, A theory for the surface atlantic response to thermohaline variability, *J. Phys. Oceanogr.*, *32*, 1121–1132, 2002.

Kalnay, E., M. Kanamitsu, R. Kistler, W. Collins, D. Deaven, L. Gandin, M. Iredell, S. Saha, G. White, J. Woollen, Y. Zhu, M. Chelliah, W. Ebisuzaki, W. Higgins, J. Janowiak, K. Mo, C. Ropelewski, J. Wang, A. Leetmaa, R. Reynolds, R. Jenne, and D. Joseph, The NCEP/NCAR 40-year reanalysis project, *Bull. Amer. Meteor. Soc.*, *77*, 437–471, 1996.

Kawase, M., Establishment of deep ocean circulation driven by deepwater production, *J. Phys. Oceanogr.*, *17*, 2294–2317, 1987.

Killworth, P. D., and J. R. Blundell, The effect of bottom topography on the speed of long extratropical planetary waves, *J. Phys. Oceanogr.*, *29*, 2689–2710, 1999.

Killworth, P. D., D. B. Chelton, and R. A. de Szoeke, The speed of observed and theoretical long extratropical planetary waves, *J. Phys. Oceanogr.*, *27*, 1946–1966, 1997.

Kuhlbrodt, T., A. Griesel, M. Montoya, A. Levermann, A. Hofmann, and S. Rahmstorf, On the driving processes of the atlantic meridional overturning circulation, *Reviews of Geophysics, 45*, RG2001.10.1029/2004RG000,166, 2007.

Leblond, P. H., and L. A. Mysak, *Waves in the Ocean*, 1st ed., 602 pp., Elsevier Oceanography Series, 1981.

Levitus, S., Ekman volume fluxes for the World Ocean and individual ocean basins, *J. Phys. Oceanogr.*, *18*, 271–279, 1988.

Olbers, D., J. Willebrand, and C. Eden, *Ocean Dynamics*, Springer-Verlag, 704 pp, 2012.

Pedlosky, J., *Geophysical Fluid Dynamics*, 2nd ed., Springer-Verlag, 724 pp, 1987.

Pierce, D., T. P. Barnett, N. Schneider, R. Saravanan, D. Dommenget, and M. Latif, The role of ocean dynamics in producing decadal climate variability in the north pacific, *Climate Dyn.*, *18*, 51–70, 2001.

Saenko, O. A., Influence of global warming on baroclinic rossby radius in the ocean: a model intercomparison, *J. Climate*, *19*, 1354–1360, 2006.

Talley, L., Simple coupled midlatitude climate models, *J. Phys. Oceanogr.*, *29*, 2016–2037, 1999.

Talley, L., G. L. Pickard, W. J. Emery, and J. H. Swift, *Descriptive Physical Oceanography*, Academic Press, 560 pp, 2011.

Vallis, G. K., *Atmospheric and Oceanic Fluid Dynamics*, Cambridge Univ. Press, 745 pp, 2006.

Vallis, G. K., *Essentials of Atmospheric and Oceanic Dynamics*, Cambridge Univ. Press, 356 pp, 2019.